OPTICAL CHARACTERIZATION AND RAMAN SPECTROSCOPY OF AFLATOXIN B1 AND AFLATOXIN-CONTAMINATED MAIZE

By

Sr. Simiyu Mary Taabu (H.H.C.J.)

B.Ed (Hons)

I56/70569/2013

Thesis submitted in partial fulfilment for the award of Master of Science degree in

Physics, University of Nairobi.

2015

Declaration

This thesis is my original work and has not been submitted elsewhere for an award of a degree at any university

Simiyu Taabu Mary Sr.

I56/70569/2014

Department of Physics

University of Nairobi

Signature…… .. Date……..

This Thesis is submitted with our approval as University of Nairobi supervisors.

Dr. Zephania Birech

Department of Physics, University of Nairobi

Signature…… Date……..…

Dr. Kenneth Kaduki

Department of Physics, University of Nairobi

Signature…… Date…….

Dedication

I dedicate this work to my lovely mom (Maayi Victorina Nekesa), my late dad (Papa Maurice Simiyu Khisa), my beloved sisters and brother (the Simiyus) and my religious sisters of Handmaids of the Holy Child Jesus in Kenya Region.

Acknowledgement

I thank the Almighty God and father of our Lord Jesus Christ for the gift of good health of mind and body during this research period. I wish to appreciate my supervisors, Dr. Zephania Birech and Dr. Kenneth Kaduki, for being patient with me and more so for the supervision they offered me throughout the journey of my research. I am highly indebted to the International Science Program for the full scholarship that was given to me to study for my masters degree. My sincere gratitude go to the Chairman, lecturers, students and support staff of the Department of Physics, University of Nairobi for the provision of a good learning environment for research. I also acknowledge my colleagues in a special way; Jacinta Okwako, Isaac Obegi, Newton Akech, Patrick Musumba, Thormas Nyang'onda and Elijah Cheruiyot for all the help they granted me during my entire research period. Further appreciations go to Fr Martin Mtai (SCA), Dr. Robinson Musembi and Dr. Joseph N. Mutemi of Department of Metrology. Though not my supervisors these noble people were always attentive to my educational needs and were always willing to lend me a helping hand.

This work would not have been a reality without the help of my regional superior (Sr. Rosemary Chiemeke) and her council (Sr. Louise Onyeanusi, Sr. Stella Cherobom and Maryann Agulana the Bursar). Thank you sisters for your financial support and for your endless encouragement that made me to persevere to this end. My community members in Lang'ata community, thanks a lot for enduring my absence in the community during the long hours of research. May God bless Sr. Magdaline Chepkemei for all the house chores she did on my behalf. Thank you too for doing my laundry. Please God bless my brother Zakayo Sifuna and my niece Naomi Sifuna for providing the samples for research. May God bless all who contributed to the success of this research and their names have not been mentioned here.

ABSTRACT

Aflatoxins are toxic and carcinogenic chemicals produced by several fungi grown in many farm produce and food spices. The naturally produced aflatoxins by fungi *Aspergillus flavus* and *Aspergilus parasiticus* are aflatoxin B1, aflatoxin B2, aflatoxin G1 and aflatoxin G2. Aflatoxin B1 (AFB1), investigated in this work, is the most toxic, highly carcinogenic and the most widespread contaminant. The existing detection techniques are slow, expensive, involve use of chemicals, tedious sample preparation and some devices are complicated. This work reports on application of Raman spectroscopy in detecting the presence of AFB1 in maize kernels and flour. The technique promises to be rapid, non-invasive, requires no sample preparation and can be modified to be deployed in the fields. It uses laser light (here of wavelengths centred at 532 nm and 785 nm) to excite vibrational bands in the AFB1 molecules and the scattered radiation detected and measured. Maize kernels and ground samples were intentionally contaminated with AFB1 with concentrations ranging from 0 ppb to $1.1x10^6$ ppb. Twenty two Raman peaks were identified with the most intense centred at 1552 cm^{-1} and 1593 cm^{-1}. Classification and quantification of AFB1 concentrations in maize kernels and flour was achieved using the following chemometric tools: Principal Component Analysis (PCA), Partial Least Squares Regression (PLSR) and Multiple Linear Regression (MLR). PCA classified AFB1 contaminated samples based on concentration ranges (variance of > 59%). Of the models for predicting concentration PLSR performed better than MLR with $R^2 > 0.9$. Predicted concentration values from Raman spectroscopy were found to correlate well with reference values from ELISA ($P > 0.9$ for 785 nm laser). Maize samples from Nairobi open markets were found to have AFB1 concentration levels of 12 ppb to 869 ppb which were higher than the permissible limits of 10 ppb in Kenya. The absorption and fluorescence spectra of AFB1 in methanol were centred and

peaked at 340 nm and 440 nm respectively and with some small maxima ascribed to vibrational bands in the first excited and ground state.

TABLE OF CONTENTS

LIST OF TABLES

LIST OF FIGURES

LIST OF ABREVIATIONS

ae	amutant extender
AFB1	Aflatoxin B1,
AFB2	Aflatoxin B2
AFG1	Aflatoxin G1
AFG2	Aflatoxin G2
AFM	Aflatoxin M
AFM1	Aflatoxin M1
AFM2	Aflatoxin M2
A_p	Mass of aflatoxin powder
A_{sol}	Mass of aflatoxin solution
$A_{sol}+B_e+M$	Mass of aflatoxin solution and the bottle containing it.
B	Matrix of regression coefficient
B_e	Mass of empty bottle
B_e+M	Mass of empty bottle and methanol
BGYF	Bright Greenish-Yellow Fluorescence
CCD	Charge Coupled Device
CDC	Centre for Diseases
CIMMYT	International Maize and Wheat Improvement Centre
Conc.	Concentration

ELISA	Enzyme-linked Immunosorbent assay
EM	Electromagnetic
HPLC	High Power Liquid Chromatography
ICA	Immunoaffinity Column Assay
IR	Infrared
LC	Liquid Chromatography
LDA	Linear Discriminant Analysis
LED	Light Emitting Diode
LOD	Limit of Detection
LOQ	Limit of Quantification
LSD	Laser Spot Diameter
M	Mass of methanol
M_{AFB1}	Mass of Aflatoxin B1 powder
ML	Machine Learning
MLP	Multi-layer Perceptron
MLR	Multiple Linear Regression
MSI	Mass Spectrometry Imaging
M_{sol}	Mass of Aflatoxin B1 solution
NDF	Neutral Density Filters

PBS	Phosphate buffer solution
PCA	Principal Component Analysis
PCR	Principal Component Regression
PCs	Principal Components
PC 1	1st Principal Component
PC 2	2nd Principal Component
PLS	Partial Least Squares
PLS-DA	Partial Least Squares Discriminant Analysis
PLSR	Partial Least Squares Regression
ppb	parts per billion
RIA	Radioimmunoassay
RS	Raman Spectroscopy
SEC	Standard Error of Calibration
SERS	Surface Enhanced Raman Spectroscopy
SEP	Standard Error of Prediction
RMSEC	Root Mean Square Error of Calibration
RMSEP	Root Mean Square Error of Prediction
SNR	Signal to Noise Ratio
TLC	Thin layer Chromatography

USB	Universal Serial Bars
UV	Ultraviolet
UV-VIS-NIR	Ultraviolet-Visible Near Infrared
VIS	Visible

CHAPTER 1: INTRODUCTION

1.1 Aflatoxin

Aflatoxins are toxic chemicals produced by fungi species *Aspergillus flavus*, *Aspergillus parasiticu*s and the rare type *Aspergillus nomius* (Ali *et al.*, 2005). These fungi produce several similar compounds of aflatoxin (around 20) but only four are naturally found in food stuffs: aflatoxin B1 (AFB1), aflatoxin B2 (AFB2), aflatoxin G1 (AFG1) and aflatoxin G2 (AFG2) (Cary *et al.*, 2005). All aflatoxins absorb maximally at a wavelength centred at 360 nm (Dirr, 1987; Pestka and Chu, 1984). Under ultraviolent (UV) light illumination they fluoresce around 425 nm (blue light hence the B designation in aflatoxins B types) and around 450 nm (green-blue light for aflatoxins G types). It should be noted that the designations '1' and '2' only show the major and minor compounds. Both the moulds *Aspergillus flavus* and *Aspergillus parasiticus* produce aflatoxin B (AFB) but aflatoxin G (AFG) is mainly produced by the latter (Alcaide-Molina *et al.*, 2009). This happens when there is warm and humid weather together with poor after harvest storage or damaged seeds and stress conditions like drought and insect infections on the seeds (Zöllner and Mayer-Helm, 2006; Alcaide-Molina *et al.*, 2009).

Aflatoxin M1 (AFM1) and aflatoxin M2 (AFM2) are found in milk from dairy animals that ingest feed stuff contaminated with AFB1 and AFB2 respectively. Consequently cheese and yoghurt derived from them are also contaminated. Their existence in milk led to the M designation of aflatoxin M (AFM) (Stroka and Anklam, 2002). Feed and food stuffs in warmer and humid regions of the world experience more contamination due to ideal conditions for culprit fungi growth (Alcaide-Molina *et al.*, 2009).

AFB1 has the highest acute and chronic toxicity followed by AFG1, AFB2 and AFG2 respectively (Ali *et al.*, 2005). Table 1.1 presents chemical formulas and physical properties including molar weights and melting points of the four aflatoxins; B1, B2, G1 and G2 (Pitt *et al.*, 2009). Figure 1.1 on the other hand shows the molecular structures of the four aflatoxins.

Table 1.1: A presentation of melting point, molecular formula and weight of Aflatoxins B1, B2, G1 and G2 adopted from (Pitt *et al.*, 2009)

Aflatoxin	Molecular formula	Molecular weight (g)	Melting point (^{0}C)
B1	$C_{17}H_{12}O_6$	268-269	268-269
B2	$C_{17}H_{14}O_6$	286-289	286-289
G1	$C_{17}H_{12}O_7$	328	244-246
G2	$C_{17}H_{14}O_7$	330	237-240
M1	$C_{17}H_{12}O_7$	328	299
M2	$C_{17}H_{14}O_7$	330	298

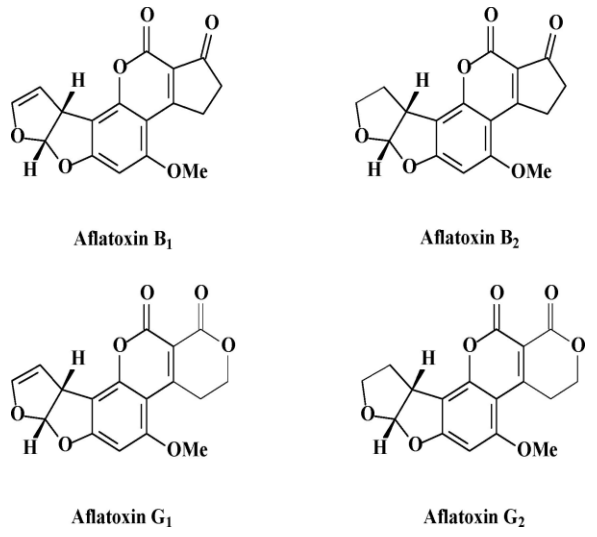

Figure 2.1: Molecular structures of aflatoxin B1, B2, G1, and G2 (Netto-Ferreira et al., 2011). The only structural difference between aflatoxin B and G is the inclusion of oxygen in the cyclopentanone ring

AFB1 has been recognized as a potent carcinogen which causes liver cancer in humans and animals after prolonged exposure (Thirumala-Devi *et al.*, 2001; Fung and Clark, 2004). Due to the health dangers posed by aflatoxins, extreme care must be observed during handling contaminated stuff. Disposable gloves, mouth masks, aprons or overalls and boots should be worn when handling contaminated samples (see appendix I).

Health risks and economic losses posed by aflatoxin contaminated food and feed stuff has forced various countries to go a great length in detecting the presence of these toxins (Robens and Cardwell, 2003). Limits of allowable toxin concentration in various products have been set in different regions and countries as summarized in Table 1.2. Due to this, farmers with highly contaminated farm produce often incur immense financial loses. To avoid infestation by aflatoxin producing fungi, food and feed stuff should be stored in less humid conditions and for cereals like maize with moisture content below 14 % at 20^0C. A method that can provide fast reliable aflatoxin detection and quantification is therefore welcome since appropriate action can be taken before widespread contamination and poisoning takes place.

In Kenya, cases of aflatoxin poisoning leading to a number of fatalities were first reported in the year 1981 and several other cases followed with the worst incident reported in April 2004 in Eastern province (Daniel *et al.*, 2011; Lewis *et al.*, 2005). This case claimed the lives of one hundred and twenty five people with three hundred and seventeen reported cases despite the country having allowed aflatoxin set limits in food stuff at 10 ppb (Daniel *et al.*, 2011). The incident was termed as the most severe outbreaks of acute aflatoxicosis ever documented worldwide (Lewis *et al.*, 2005).

The conventional methods of detecting and quantifying the amount of aflatoxin contamination often employ expensive equipment requiring trained personnel to operate. A lot of time is also required in preparing the samples besides using large amounts of chemicals in terms of reagents. These methods include: Chromatography methods like Thin layer chromatography (TLC) (Hoeltz *et al.*, 2010), Liquid chromatography (LC) and Immunochemical methods such as Radioimmunoassay (RIA), Enzyme-linked immunosorbent assay (ELISA) and immunoaffinity column assay (ICA), Mass Spectrometry Imaging (MSI) (Norris and Caprioli, 2013; Ivanova and Spiteller, 2014). In developing countries where risks of contamination are high, the above mentioned techniques are scarce due to their costs (Bhat *et al.*, 1997). For this reason, fast, sensitive, simple to operate and inexpensive detection methods need to be developed.

Table 1.2: Aflatoxin set limits in human food products of different countries (Frelka and Harris, 2014). For the presence of all aflatoxins, the term Total has been used while those of AFB1 only have been indicated

COUNTRY	AFLATOXIN	TYPE OF FOOD
United states of America	20 Total	Human food
Kenya	10 ppb	Human food
European union members	4-15 Total	Subject to the type of food and the level of production
Saudi Arabia	0.05 Total	Children and infant food
South Africa	10 Total (5 AFB1)	All food

Fluorescence spectroscopy with UV light excitation (wavelength ~ 360 nm) would have provided a cheap and fast detection process but the spectral overlap of signals from aflatoxins and the bright greenish-yellow fluorescence (BGYF) emanating from kojic acid make it unfavourable (Yao *et al.*, 2006); Yao *et al.*, 2010). Kojic acid (see Figure 1.2 for its molecular

structure) is another metabolite of *Aspergillus flavus* (Yao *et al.*, 2010). Fluorescence from food or feed samples exposed to UV light is therefore only used as preliminary inspection signature for samples requiring further tests. This spectral overlap renders definitive distinction between aflatoxins and BGYF compounds impossible (Afoakwa and Sefa-Dedeh, 2001).

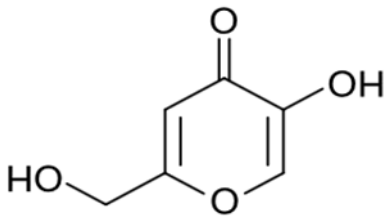

Figure 1.3: Molecular structure of kojic acid (May et al., 1931). Kojic acid is one of the compounds produced together with AFB1 and has similar characteristics of fluorescence with AFB1

This work shows that Raman spectroscopy can be a plausible alternative to the above mentioned methods. Maize kernels and flour intentionally laced with AFB1 are used. Its application in detection of mycotoxins in cereals, in particular maize is rare in literature. A recent report by Lee and his companions showed a great potential in this direction (Lee *et al.*, 2013). It is for this reason that we explored it further here. The technique involves irradiation of a sample with a monochromatic light (laser light) in the UV or VIS or Infrared regimes of the electromagnetic spectrum and the wavelength shifted scattered light dispersed in a spectrometer equipped with a Charge Coupled Device (CCD) camera. The energy (or frequencies) of the scattered light corresponds to the vibrational motions of the molecules under study (Demtröder, 2011). Both the Raman and infrared spectroscopic techniques provide information about vibrational motions of the molecule. The latter technique however, does not work well in situations where aflatoxins levels are very low due to spectrum overlap and interference from other functional groups with active modes in the spectral region (Lee *et al.*, 2013). Besides, distortions emanating from HOH

bending mode of water molecules are common (Medders and Paesani, 2015; Falk and Ford, 1966). Raman spectroscopy on the other hand is insensitive to water and hence can also be used for aqueous samples.

In this work chemometric techniques (Partial Least Squares Regression (PLSR) and Multiple Linear Regression (MLR)) have been trained to predict the concentration of AFB1 in unsuspected samples of maize kernels and flour from Nairobi open markets. Principal component analysis (PCA) has been employed in pattern recognition based on the information from spectral signatures from maize samples. The results obtained indicate the possibility of using Raman Spectroscopy and chemometrics to qualify and quantitative AFB1 in maize.

1.2 Problem statement

Conventional methods used in the detection of aflatoxin are labour intensive, time consuming, require highly qualified personnel and the results can be subjective. This is because some aspects of these techniques can depend on the expertise of the analyser. Optical methods offer the safest and fastest means of detecting aflatoxins. However, the existing optical methods such as fluorescence, infrared transmittance and reflectance spectroscopies which would have come in handy to solve these problems have shortcomings of spectral overlapping with other molecules including kojic acid. Raman spectroscopy on the other hand does not need sample preparation, is more sensitive to the symmetrical vibrations of the covalent bonds and is a better option for aqueous samples as it is insensitive to water. In this study, Raman spectroscopy is adopted because it is non-invasive, non-subjective and can be easily modified for deployment in the field for detection and quantification of AFB1.

1.3 Objectives

1.3.1 Main objective

The broad objective of this work was to be able to employ Raman spectroscopy in providing a fast, accurate detection and quantification of aflatoxins, in particular the potent aflatoxin B1, in maize kernels and flour.

1.3.2 Specific objectives

1 To measure the absorption spectrum of AFB1 dissolved in methanol solvents using a UV-VIS-IR spectrophotometer.

2 To obtain fluorescence spectrum of AFB1 solutions after 375 nm excitation with an LED diode light source and a USB Ocean Optics spectrometer.

3 To obtain the specific Raman spectra of AFB1 using a confocal Raman spectrometer at 532 and 785 nm excitations.

4 To interpret and make assignments on the Raman peaks in the spectra.

5 To obtain Raman spectra on the AFB1 spiked and clean maize kernels and flour excited at 532 and 785 nm.

6 Use chemometric techniques such as Principal Component Analysis (PCA), Multiple Linear Regression (MLR) and Partial Least Squares Regression (PLSR) in developing calibration models for aflatoxin quantification.

7 Compare the concentration results obtained from Raman spectroscopy and chemometrics with those obtained from analysis of the same samples using ELISA.

1.4 Justification

From 1960, when aflatoxin claimed the lives of 100,000 turkeys in England to date aflatoxin poisoning has claimed the lives of both human and domestic animals. Kenya is not exceptional to this problem. During the year 1981, Kenya reported its first case of aflatoxin poisoning and in 2004 it recorded the highest number of casualties worldwide among which were 125 deaths. Farmers have also suffered enormous losses caused by aflatoxin contaminated feeds. These problems have even escalated in our modern times because of the change in weather that cause prolonged droughts and excessive rain during rainy seasons. The high cost of living has also made pesticides and fertilizers very expensive not to mention the conventional aflatoxin detection methods. The few who can afford these detection techniques have to go through long and tedious hours of sample preparations. Coupled to these is the lack of streamlined aflatoxin regulatory limits in developing countries that exposes so many people and domestic animals to aflatoxin poisoning. It is for these reasons that we explore an alternative detection and quantification technique using Raman spectroscopy. The most common and most toxic aflatoxin B1 is chosen as a prototype. Investigation of aflatoxin B1 contaminated maize is done and PCA employed for classification of samples. In order to detect and quantify AFB1 levels in maize consumed in Nairobi PLSR and MLR are applied.

CHAPTER 2: LITERATURE REVIEW

This chapter reviews the most common techniques used in aflatoxin detection and annihilation ranging from the current conventional methods to optical methods with myriad applications of Raman Spectroscopy in various research works. Data pre-processing and chemometrics used by various researchers in aflatoxin classification and quantification using Raman spectroscopy are also discussed.

2.1 Conventional methods

Aflatoxins as earlier indicated in this work are first class carcinogenic metabolites of *Aspergillus* fungi that grow on myriads of food crops ranging from cereals, nuts to processed food stuffs provided the conditions are favourable (Rocha *et al.*, 2014; Egmond *et al.*, 2007). Conditions responsible for the presence of aflatoxins in both processed and unprocessed foods and animal feeds can be various including cultural practices, biotic and abiotic alongside weather conditions.

Aflatoxicosis which refers to poisoning resulting from ingestion of food or feed contaminated with aflatoxins was first reported during the year 1960 in England on aflatoxin contaminated feeds. Thisclaimed the lives of more than a hundred thousand turkeys. Over the years Aflatoxicosis has frequently been reported in India and Kenya. In 2004 Kenya recorded the worst aflatoxicosis characterized by one hundred and twenty deaths with three hundred and seventeen reported cases (Center for Disease Control and Prevention (CDC), 2004; Lewis *et al.*, 2005). Because aflatoxins pose a threat to animal/human health and life, researchers have been working endlessly to eliminate their presence in food and feeds by educating farmers on good farming methods with pre-harvest and post-harvest techniques being emphasized. In cases where prevention of aflatoxins in harvested produce has failed farmers tend to physically sort

infected/mouldy seeds (cereals) from healthy looking ones.

However not all aflatoxin infected seeds show physical presence of the fungi for farmers to physically eliminate them from the food chain. Thus researchers have adopted the application of chemicals and electromagnetic beams to destroy aflatoxin and its fungi or reduce the level of aflatoxin in food samples (Ribeiro *et al.*, 2011). Various chemicals are used to destroy aflatoxin and their fungi. Some of these chemicals include bleach, borax, vinegar, ammonia, hydrogen peroxide, baking soda, tea, oils from some trees and grapefruit seed extracts (Ribeiro *et al.*, 2011; Torbert, 2002). At the same time aflatoxin contaminated samples can be exposed to a laser beam of appropriate intensity, microwaves and pressure cooking (Herzallah *et al.*, 2008), gamma radiation (Ghanem *et al.*, 2008; Ribeiro *et al.*, 2011) and to solar radiation (Herzallah *et al.*, 2008; Netto-Ferreira *et al.*, 2011) in order to annihilate the contaminants.

Although the above procedures seem promising, quick and cheap, they do not offer a solution for detection of the presence of aflatoxin in food and feed stuff. Since aflatoxins are poisonous carcinogen substances early detection methods are urgently needed in order to take precautions against its spread in human food and animal feeds. Moreover, there have been no reported cases where aflatoxins were totally eliminated from food and feeds. Rather the use of chemicals even makes human food and animal feed unfit for consumption. It is for this reason that researchers have resorted to more sensitive chromatographic techniques like Thin Layer Chromatography (TLC) and High Power Liquid Chromatography (HPLC) in detection of aflatoxins (Bacaloni *et al.*, 2008; (Khayoon *et al.*, 2010). The use of assay is as sensitive as chromatography. Perhaps this is why several methods involving assay have been employed recently: Radioimmunoaffinity assay (RIA) and Enzyme-linked Immunosorbent assay (ELISA) and Immunoaffinity Column assay (ICA) among others (Wang *et al.*, 2014). However, these techniques and procedures

therein are expensive, laborious, time consuming and require very highly qualified personnel to use them.

2.2 Optical methods

2.2.1 Introduction

Optical based methods are increasingly being pursued as potential alternatives due to their portability and rapidity in delivering results combined with the fact that they require little or no sample preparation. Such techniques have been demonstrated in groundnut and groundnut cakes, pistachios (Pearson and Schatzki, 1998), oil (Mirghani *et al.*, 2002), figs (Kalkan *et al.*, 2014; (Gunes *et al.*, 2013), peanuts (Kaya-Celiker *et al.*, 2014), chili powder (Tripathi and Mishra, 2009) and in single corn kernels (Yao *et al.*, 2010). The optical characteristics of interest include transmittance (Pearson *et al.*, 2001), reflectance (Mirghani *et al.*, 2002; Pearson *et al*., 2001) and fluorescence (Hruska *et al*., 2009; Yao *et al.*, 2010). Molecular vibrational motions initiated by optical excitation with wavelengths in the infrared (infrared spectroscopy) (Tripathi and Mishra, 2009) or in the ultraviolet or visible (Raman spectroscopy) (Lee *et al.*, 2014; Wu *et al.*, 2012) regime of the electromagnetic spectrum are also gaining interest in aflatoxin detection and quantification.

2.2.2 Fluorescence spectroscopy

As earlier mentioned in the introduction, aflatoxins readily fluorescence with spectra centred around a wavelength of 425 nm for the B aflatoxins and around 450 nm for the G aflatoxins upon irradiation with an ultra-violet light centred at around 360 nm (Ononye *et al.*, 2010; Yao *et al.*, 2010; Netto-Ferreira *et al.*, 2011; Fujita *et al.*, 2013). This property has been employed in the characterization of aflatoxins in nutmeg (Fujita *et al.*, 2013) and maize (Hruska *et al.*, 2014).

Fluorescence and machine learning techniques have also been used successfully to detect and quantify aflatoxins (Yao *et al.,* 2010; Kalkan *et al.,* 2014). However, this method faces challenges especially in distinguishing the fluorescence signal of aflatoxins from those of the kojic acid (also produced by *Aspergillus Flavus*) which is associated with the bright greenish-yellow fluorescence substance (BGYF) (Basappa, 1970). This is why Fluorescence Spectroscopy is known for false positive results (Alcaide-Molina *et al.,* 2009).

2.2.3 Absorbance spectroscopy

Absorbance spectroscopy is another optical technique that has been used in detection of aflatoxin detections. However, this technique has not been used independently in the study of aflatoxins but it is usually combined with other methods. Pearson and companions for example combined it with reflectance and transmittance to study single corn kernels and found that the 750 nm band is capable of detecting discoloration in fungal infested kernels while the 1200 nm band could respond to degraded endosperm (Pearson *et al.,* 2001). This technique is limited just like fluorescence as it suffers from overlapping from other compounds associated with AFB1. As a result of this it gives very high classification errors. Therefore absorbance cannot be used on its own to detect aflatoxins. In this work, absorption spectroscopy was used to identify the characteristic absorption band of AFB1 and also to identify whether the lasers available for use in our Raman setup (532 nm and 785 nm) can excite it resonantly or not.

2.2.4 Infrared spectroscopy

Infrared Spectroscopy, just like Raman Spectroscopy, gives a detailed information on molecular bonds and vibrations of substances (Wellner *et al.,* 2011). This property has been explored by Pearson and co-workers in detection of aflatoxin in single corn kernels (Pearson *et al.,* 2001).

However both infrared and near infrared cannot detect aflatoxins to concentration limits set for human food and infant milk (about 0.05 ppb) (Frelka and Harris, 2014). This is because infrared has a low diffraction resolution caused by higher excitation wavelength that renders it limited in studying micron-sized particles. Moreover, infrared spectroscopy is sensitive to water molecules vibrations and as a result, it is limited in detecting solutes in aqueous samples (Medders and Paesani, 2015).

2.2.5 Raman spectroscopy

On the other hand in Raman spectroscopy the samples are excited at shorter wavelengths. The shorter wavelength excitation gives it better resolution than infrared spectroscopy and it can attain up to a micron resolution power (Ryder *et al.*, 2000). At the same time, the weak Raman signal from water renders it insensitive to HOH vibrations (Galvin and Zerulla, 2011). This makes Raman spectroscopy not experience interference from water molecules while analysing wet biological samples or samples in aqueous form. It is for these reasons that we explore the use of Raman Spectroscopy in detection and quantification of AFB1 in single maize kernels. Maize is especially chosen because it is consumed in different parts of the world and in particular it is a staple food in this country (Kenya). While AFB1 is specifically chosen due its toxicity levels as compared to other aflatoxins as mentioned in the introductory part of this thesis.

Even though the use of Raman Spectroscopy in the research of aflatoxin has been limited over the years, several researchers have recently indicated its potential in analysis of aflatoxins and related compounds in cereals. Dheeraj and co-workers for example used silver substrates and Raman spectroscopy to detect mycotoxins in citrinin (Dheeraj *et al.*, 2013). Ivanova and Spiteller on the other hand used Raman and Mass spectrometers to determine aflatoxin (Ivanova and

Spiteller, 2014). Lee and co-workers recently reported on the use of Raman spectroscopy in qualitative and quantitative analysis of aflatoxins and fumonosins in ground maize and were able to determine concentrations of both fumonosins and aflatoxins in processed and unprocessed contaminated maize products (Lee *et al.*, 2014; Lee *et al.*, 2013). Some other researchers have shown that Raman Spectroscopy can give more sensitive results if samples are deposited on surface enhanced substrates (specially prepared silver-coated) (Wu *et al.*, 2012). Despite the fact that Surface Enhanced Raman Spectroscopy (SERS) is highly recommended due to its sensitivity, the procedure of first preparing and depositing samples on roughened silver, copper, aluminium or any other alkali metal coated substrates makes it a less attractive cheap alternative and also not possible for rapid screening purposes in the field or sorting of contaminated kernels on a conveyer belt in milling factories. Since the sole purpose of this work was to provide lay farmers, manufactures, exporters and importers with a rapid, reliable and field deployable method of aflatoxin detection without long hours of preliminary training on its use, bulk Raman spectroscopy was used.

In as much as the use of Raman spectroscopy in studying aflatoxins seems ideal it should be noted that this technique has its own limitations. Raman spectroscopy is a weak scattering process (one out of a million scattered processes is Raman) (Dieing *et al.*, 2011). Furthermore, maize samples contain other components like starch, protein, fat and fibre in varying percentages. Starch in particular is a major component of maize and has many Raman active vibrational modes (see Figure 2.1). The starch peaks at 719, 770, 1125, 1261, 1343 and 1659 nm found by Wellner and colloquies (Wellner *et al*., 2011) could overlap with AFB1 peaks at 686, 752, 1147, 1279 and 1355 nm found by SERS (Wu *et al*., 2012). To overcome these challenges we employed machine learning (ML) models to enable the Raman spectroscopy to identify

patterns in Raman data sets that will aid in classification and quantification of AFB1 in maize samples. However, Raman spectra have to be pre-processed before constructing multivariate models for quantification.

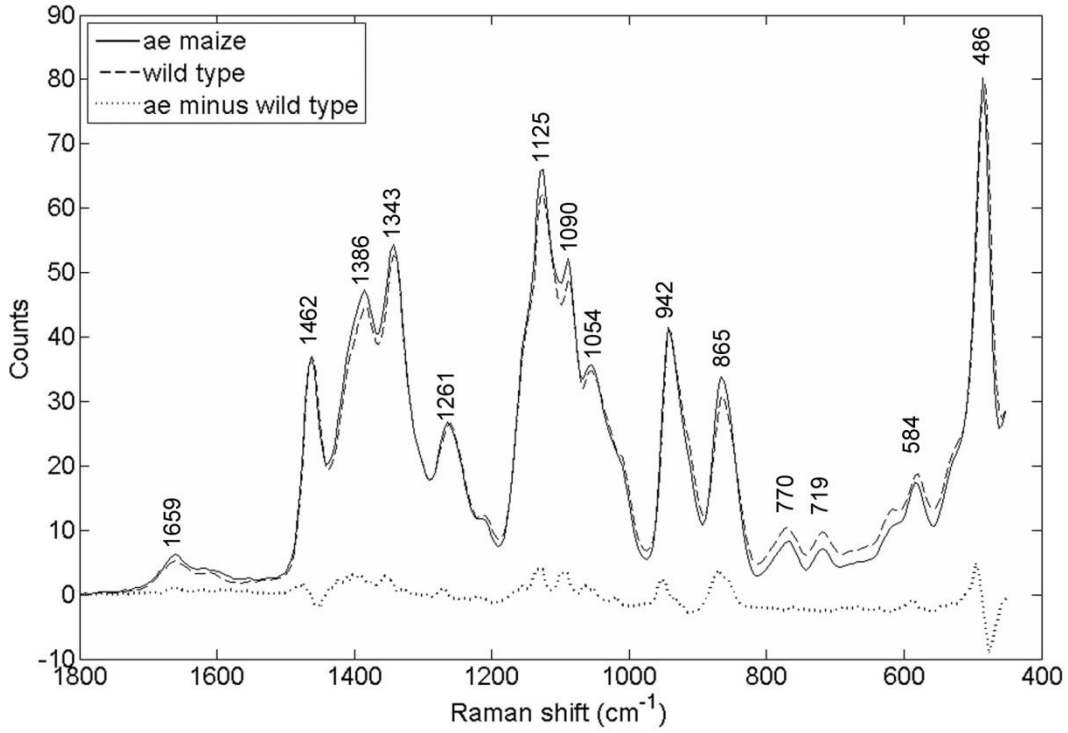

Figure 2.1: Raman spectra of ae maize kernel and wild specie maize kernel adopted from (Wellner et al., 2011). The excitation of samples was done by a 532 nm Nd-YAG laser and the spectra were obtained from 50 µm spot size. The dotted spectrum at the bottom represents the difference between the two spectra.

2.3 Data pre-processing of Raman Spectra

The vibrational information from Raman spectroscopy make the technique as shown in the previous section popular for characterization of materials (Torii *et al.*, 1997). However, the spectra from Raman spectroscopy often overlaps spectrally with fluorescence signals from organic compounds present in samples being studied which at times are stronger than the weak

Raman scattered radiation creating huge baselines that make the research difficult (McCreery, 2005).

Numerous data pre-processing methods have been used over time to make both resolution and analysis of Raman spectra possible ranging from instrumental to mathematical methods (Burke, 2001). The traditional use of anti-stoke Raman spectroscopy (Mosier-Boss *et al.,* 1995) and low energy 785 nm excitation adopted in this work cannot remove florescence rather it reduces the sensitivity of the Raman instrument since Raman scattering has a positive relationship with the fourth power of excitation frequency (Dieing *et al.*, 2011; Wu *et al.*, 2006). Mathematical methods like the use of derivatives, polynomial fits, moving averages, and wavelet transforms which are often used either over fits or changes the shape of the spectra depending on which method was adopted. Though manual fitting is subjective to the experimenter and tedious if the samples are many, it was adopted in this work since it allows the user to create the baseline fit manually. This eliminates the possibilities of over fitting and changing of shapes of Raman spectra caused by other methods.

Smoothing as a universal process of data pre-treatment has been used by several researchers in this field to pre-process Raman data before applying multivariate techniques. Lee and co-workers used smoothing with Savitzky-Golay filter to study different concentrations of aflatoxins (Lee *et al.*, 2013). Even though the use of filters is not advisable in data pre-processing since filters can cause loss of information, Savitzky-Golay (Digital Smoothing Polynomial) filter is exceptionally good as it maintains the curve shapes of Raman spectra while smoothing the data which prevents loss of spectral information unlike what happens in other filters.

Furthermore, Savitzky-Golay is not a strong filter like Moving Average filter that will filter off important spectral information (Wu *et al.*, 2015).

Apart from fluorescence arising from samples, Raman spectra also experience distortions from cosmic rays. These rays can be filtered out using instrumental and mathematical methods. Dieng and co-workers proposed the use of cameras with faster (as fast as 0.76 milliseconds) readout like full vertical binning modes (CCD cameras with 1600 x 200 pixels) that readout specific regions (Dieing *et al.*, 2011). However, the camera on our Raman system could not allow such spectra acquisition as it is connected via USB cable. This implies that data streams are controlled by the processor which also controls the microscope and thus limited in rapid readout. As a result of this, cosmic rays could only be eliminated after the spectra has been recorded using mathematical methods such as filters (Saviztky-Golay) which compares each pixel with its adjacent pixel and if the two pixel are dissimilar the pixel in question is identified as a cosmic ray (Quintero *et al.*, 2006). While this method is problematic in handling sharp and thin based peaks, it was found appropriate in filtering AFB1 Raman spectra peaks whose line widths (FWHM) exceed 3 cm^{-1} and have broad base resembling Lorentztian curves (Dieing *et al.*, 2011). Moreover, the software (OriginPro 9.1 32Bit) used in this work allowed previews and adjustments to correct parameters by the user.

2.4 Raman spectroscopy and chemometrics

Chemometrics incorporate the science of getting information from chemical systems by data-driven means. Thus chemometric techniques are used to solve both descriptive and predictive phenomena in experimental sciences where the datasets are often very bulky and complex. They extract information by use of mathematical, statistical and symbolic ways of encompassing

simultaneous observation and analysis of many variables (Jurado-López and Luque de Castroothers, 2003). This is achieved through minimizing the amount of noise in the datasets. The information obtained is then used in modelling and making predictions of the unknown samples. These multivariate techniques are also known for capturing information of correlated and covariant trends in datasets which would be difficult to find by use of classical analytical spectroscopy (Myakalwar *et al.,* 2011). Several researchers in this field have used different machine learning methods in detection and quantification of aflatoxins. Wu and co-workers used surface enhanced Raman spectroscopy to analyse different types of aflatoxins and employed PCA on the obtained Raman data to classify them and different patterns were displayed on the score plot (Wu et al., 2012). PC 1 was able to differentiate between aflatoxin B and aflatoxin G by placing them in different quadrants of the score plot. PC 2 then grouped samples of AFB1 together separating them from AFB2 samples. Similar results were also observed using aflatoxin G (Wu *et al.*, 2012). Lee and co-workers using regression models (PCR, PLSR and MLR) also used PCA for pattern variation in maize flour samples before employing other discriminant methods (Lee *et al.,* 2014). In all these works PCA has performed well in pattern recognition and clustering of different concentrations of aflatoxins. It is for these reasons that we employ PCA in this work.

Apart from pattern recognition, other multivariate techniques have also been used by several researchers for calibration and spectral modelling of aflatoxins. Lee and co-workers for instance employed PCR, PLSR and MLR to Quantify aflatoxin in ground maize (Lee *et al.*, 2014). It was found that PLSR was the best model among the three regressions while MLR was the worst regression as it carried the highest errors among the three models. For this work, we also chose

MLR and PLSR in order to compare with what was reported by lee and co-workers (Lee *et al.*, 2014).

CHAPTER 3: THEORETICAL BACKGROUND

In this chapter absorption and emission spectroscopic techniques are discussed. The classical and quantum principles of Raman spectroscopy are also presented followed by a brief description of molecular vibrations and how assignment of Raman peaks is done. The concepts of multivariate chemometrics techniques MLR, PCA and PLSR are also discussed.

3.1 Absorption and emission spectroscopic techniques

The absorption or emission of EM wave by atoms and molecules is shown by spectroscopic techniques that give information about the molecules or atoms. There are several spectroscopic techniques; absorption, emission and fluorescence spectroscopy. In absorption spectroscopy the radiation absorbed by the sample is measured as a function of wavelength. When an atom or molecule is shown with light of correct wavelength (with photon energy between ground and excited state) molecules or atoms absorbs energy in form of photons and get excited to higher electronic energies (see Figure 3.1). The measurement of the intensity of light absorbed at the resonant frequency as light passes through atoms or molecules is what we call absorption spectroscopy. From Equation (3.1) (Boltzman distribution function) most of atoms or molecules will be at the ground at room temperature (Csele 2004).

$$\frac{N_n}{N_m} = \frac{g_n}{g_m} \exp\left[\frac{-(E_n - E_m)}{kT}\right] \tag{3.1}$$

where n and m are excited and ground vibrational levels respectively, N_m stands for the number of molecules in the ground vibrational energy level, N_n represents the number of molecules in the excited vibrational energy level, E_n - E_m is the change in energy between the vibrational energy levels, g is the degeneracy of the levels n and m, T is temperature and k is Boltzmann's constant

Equation (3.1) shows that the molecules at ground vibrational state will absorb more light than the molecules at the excited vibrational states since at the ground state the density of molecules is high. Therefore if light absorbed is measured in several concentrations of a substance at a constant temperature then the information can be used for quantitative analysis in the unknown samples of the same substance since increase in the number of molecules increases the amount of light absorbed.

Just like absorption emission of a substance takes place when the substance is excited with an energy source that consists of a collection of the allowable emission wavelengths due to the quantum nature of the emitted wavelengths. Many substances though do not emit light after absorption because absorbed energy can be dissipated without emitting photons. Secondly when molecules of a substance are excited molecules absorb light to various excited states. Thus we expect that we expect that emission will take place from the different excited states the molecules were excited to as shown in Figure 3.1. However this does not happen, rather when molecules interact with EM wave they get excited to higher state but most of them settle at lowest excited state S1 according to Equation (3.1). Thus emission is initiated from the ground state of the excited state (S1). From Figure 3.1 it can be seen that the emission is similar to absorption but opposite in direction. Thus if the spectra of both absorption and emission were to be plotted they will show the same spectrum. However experimentally this does not happen because the highest excited molecule does not always occupy the lowest excited state. Some highly excited molecules can go directly to the ground state in which there will be no emission of radiation while others will occupy other vibrational states and emit radiation. These are normally shown in the spectrum as small maxima (Demtröder, 2011).

Fluorescence spectroscopy incorporates absorption and emission spectroscopy. As absorption a laser light or a light emitting diode can be used to excite molecules to higher vibrational modes of the excited state as shown in Figure 3.1. However in fluorescence instead of measuring the light absorbed as it is done in absorption, here we measure emission caused by decay of atoms or molecules excited by the incident light. The emitted molecules can also occupy different vibrational states and thus result to small maxima in the characteristic spectra. Furthermore, just like in absorption the light emitted increases with increase in concentration of atoms or molecules. Hence this technique can also be used for quantitative analysis (Csele, 2004).

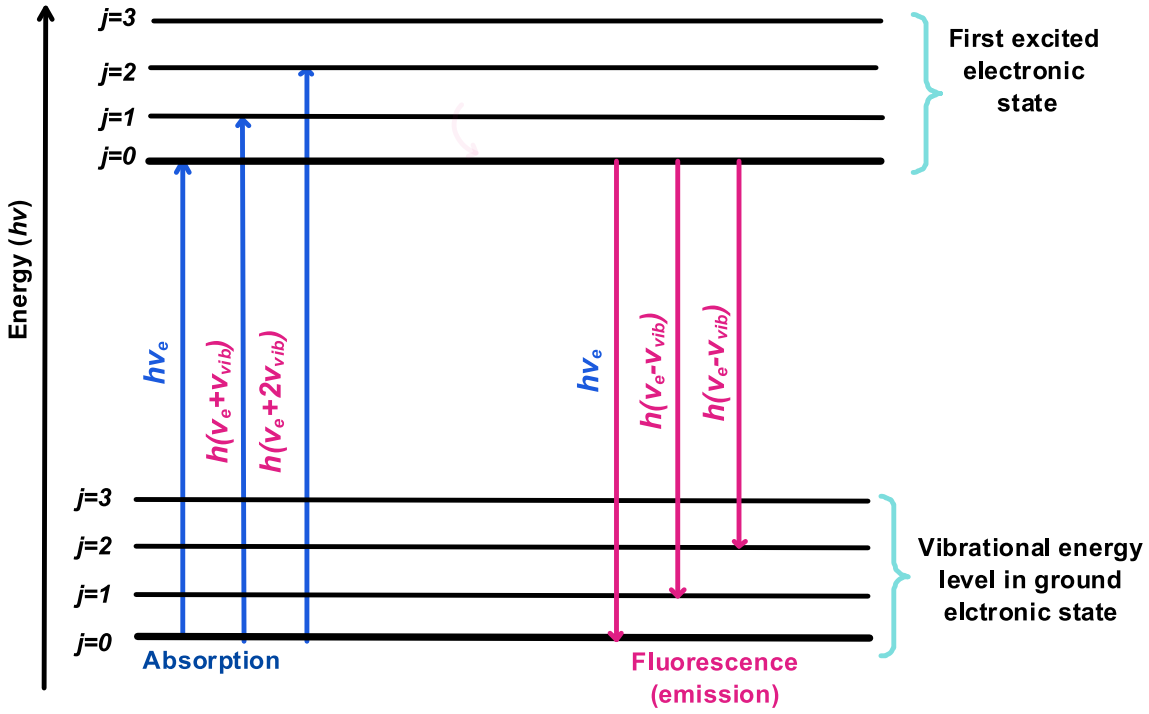

Figure 3.1: A Jablosky diagram showing absorption, emission and fluorescence processes between the ground electronic state and the first electronic excited state (Csele, 2004)

3.2 Classical framework of Raman scattering

A beam of light scatters either elastically or inelastically or both processes take place simultaneously when an electromagnetic (EM) wave encounters an obstacle as shown in Figure 3.2 (Smith and Dent, 2005). This is the essence of Raman spectroscopy. An EM wave interacts with a sample and causes perturbation in the electron orbits of its molecules. This electron cloud perturbation results in induced dipole moment which oscillates at a frequency (υ_0) equal to that of the incident beam's electric field (Demtröder, 2011). The most intense and probable scattering process is the elastic scattering (often referred to as Rayleigh scattering) where the emitted beam's frequency is the same as incident frequency. At the same time some light is scattered inelastically (i.e. emitted at different frequencies from those of the incident beam). This latter process is called Raman scattering. Figure 3.2 shows a schematic of the interaction between incident beam (beam drawn in thick green line) and the sample with Rayleigh scattering as the strongest process (multiple rays drawn in thin green lines) since most photons scatter elastically and do not involve frequency change while Raman scattering is displayed as the weakest process (few rays drawn in thin red lines).

As mentioned earlier, the incident EM wave induces a dipole moment (*p*) when the light and sample interact (Sato-Berrú *et al.*, 2004). This induced dipole moment is given by Equation 3.2

$$P(E) = \alpha \overline{E} \qquad (3.2)$$

where *P(E)* is the said electric dipole moment, α is electric polarizability tensor and $\overline{E}$ is the electric field which can be expressed as shown in Equation 3.3.

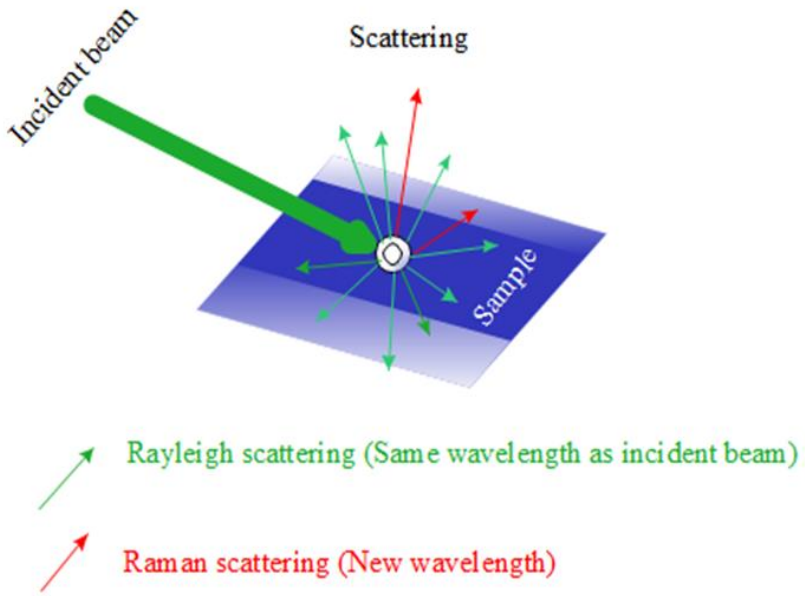

Figure 3.2: A schematic showing Rayleigh and Raman scattering. Raman scattering is a very weak process as compared to Rayleigh process (Smith and Dent, 2005)

$$\overline{E} = \bar{E}_0 \cos \omega t = \bar{E}_0 \cos(2\pi \upsilon_0 t) \tag{3.3}$$

with υ_0 as the incident frequency in hertz *(Hz)*, ω is the angular frequency and E_0 is the initial electric field. Substituting Equation (3.3) into (3.2) we obtain Equation (3.4).

$$p(E) = \alpha E_0 \cos(2\pi \upsilon_0 t) \tag{3.4}$$

However, to perturb the electron cloud of a molecular structure we need to know where different atoms are situated. Molecular bonds cause atoms to be confined to specific quantized vibrational energy levels with unique modes just like electronic energies and can be expressed as in Equation (3.5).

$$E_{vib} = \left(j + \frac{1}{2} \right) h\upsilon_{vib} \tag{3.5}$$

where E_{vib} is vibrational energy of a particular mode, j is the vibrational quantum number and is an integer (0, 1, 2…), h is the Planck's constant and υ_{vib} is the frequency of individual vibrational modes. If energy E_{vib} from a particular vibrational mode can cause a displacement (dQ) to an atom at equilibrium state, then the displacement (dQ) is given by Equation (3.6).

$$dQ = Q_0 \cos(2\pi\nu_{vib} t) \tag{3.6}$$

where Q_0 represents the highest displacement the atom can attain from the equilibrium position. Therefore the polarizability (α) can be expressed by a Taylor series expansion of Equation (3.7).

$$\alpha = \alpha_0 + \frac{\partial \alpha}{\partial Q} dQ \tag{3.7}$$

Obviously α_0 is the polarizability when the molecular bond is at equilibrium. Substituting Equation (3.6) into (3.7) we obtain Equation (3.8).

$$\alpha = \alpha_0 + \frac{\partial \alpha}{\partial Q} Q_0 \cos(2\pi\upsilon_{vib} t) \tag{3.8}$$

Thus the Electric dipole in Equation (3.4 is given by Equation (3.9) which can be expanded further to Equation (3.10).

$$P(E) = (\alpha_0 + \frac{\partial \alpha}{\partial Q} Q_0 \cos(2\pi\upsilon_{vib} t)) E_0 \cos(2\pi\upsilon_0 t) \tag{3.9}$$

$$P(E) = \alpha_0 E_0 \cos(2\pi\upsilon_0 t) + \frac{\partial \alpha}{\partial Q} Q_0 E_0 \cos(2\pi\upsilon_0 t) \cos(2\pi\upsilon_{vib} t) \tag{3.10}$$

Using the trigonometric identity in Equation (3.11), Equation (3.10) expands to Equation (3.12).

$$\cos a \cos b = \frac{1}{2}\left[\cos(a-b)+\cos(a+b)\right] \tag{3.11}$$

$$P(E) = \alpha_0 E_0 \cos(2\pi\upsilon_0 t) + \left[\frac{\partial\alpha}{\partial Q}\frac{Q_0 E_0}{2}\right]\left\{\cos\left[2\pi(\upsilon_0 - \upsilon_{vib})t\right] + \cos\left[2\pi(\upsilon_0 + \upsilon_{vib})t\right]\right\} \tag{3.12}$$

From Equation (3.12) it is clear that the induced dipole moment is affected by two terms; the first term with frequency (υ_0) is responsible for elastic (Rayleigh) scattering while the second term causes inelastic (Raman) scattering. Under Raman scattering there are two distinct frequencies; down-shifted (υ_0-υ_{vib}) and up-shifted (υ_0+υ_{vib}) frequencies (Smith and Dent, 2005). The down shifted frequencies results into Stoke's Raman scattering while the up-shifted frequency causes anti-Stoke's Raman scattering. In short, for Raman scattering to take place there must be vibrational displacement of atoms corresponding to individual vibrational modes that cause change in the polarizability ($\frac{\partial\alpha}{\partial Q} \neq 0$ in Equation (3.12)).

3.3 Quantum framework of Raman scattering

Raman scattering depends on the quantized vibrational energy states of different molecular vibrational modes as shown in the Jablonski diagram of Figure 3.3. The discrete vibrational states respectively correspond to the vibrational quantum numbers as explained in Equation (3.5) (Dieing *et al.*, 2011).

At room temperatures molecules occupy different vibrational states according to Boltzmann's distribution function with the ground vibsrational state (j=0) being highly populated. The incident EM wave with energies below the first excited electronic state promotes molecules to a

virtual energy state above the electronic ground state (Smith and Dent, 2005). Normally the molecule occupies its ground electronic state but in the presence of the incident beam, some quantum of energy (equal to the vibrational mode) is transferred to the molecule, as shown in

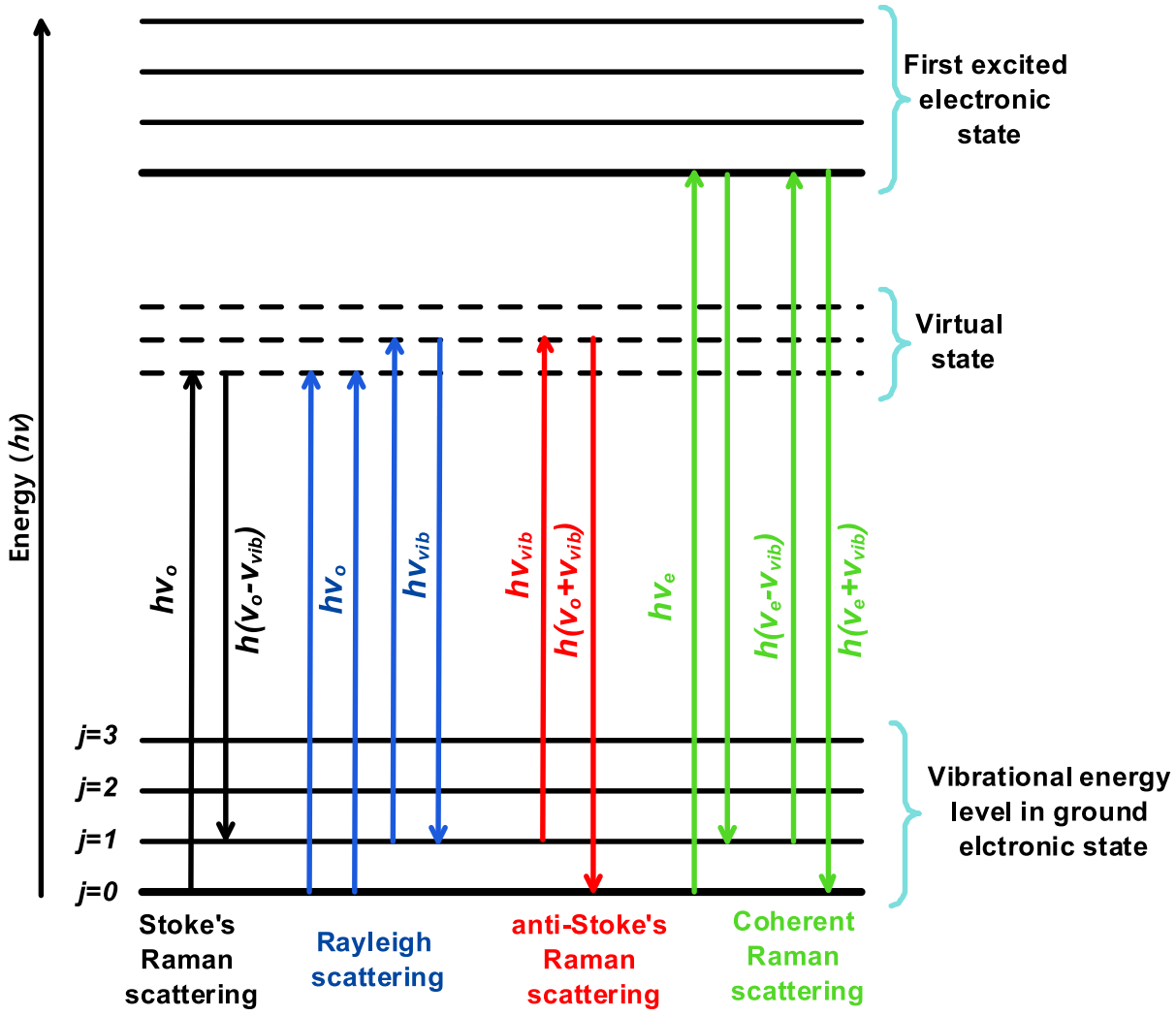

Figure 3.3: A Jablonski diagram showing Raman and Rayleigh scattering processes (Demtröder, 2011). The usual Raman scattering does not excite the molecules to first excited electronic levels but if the rare phenomenon does occur we term it as 'coherent Raman scattering

Figure 3.3 causing the emitted beam to be Raman scattered (inelastically scattered). If the molecular system is at equilibrium at the ground vibrational state then the scattering originating from this point is the Stokes Raman shown in Figure 3.3. For Anti-Stokes Raman scattering, the molecule initially occupies the excited vibrational state (more likely j=1). When this molecule interacts with the incident photon, the vibrational energy state relaxes to a lower level (j = 0). As a result a change in vibrational quantum energy ($\Delta E = h\upsilon_{vib}$) will be experienced by the system and will be added to the incident photon causing the scattered photon to have more energy than the incident photon (Demtröder, 2011).

3.4 Intensity of Raman scattered light

Intensity of Raman scattering is given by Equation (3.13) which shows the factors that affect Raman scattering process (Torii *et al.*, 1997).

$$I = K(v)A(v)v^4 I_0 J(v)C \tag{3.13}$$

where I is Raman scattered intensity, K is spectrometer response, A is the absorption of the medium, v is frequency of the exciting laser, I_o is the excitation intensity, J is the molar scattering coefficient and C is the concentration of a given sample.

Raman spectrum is a representation of intensity as a function of wave shift (the difference between the excitation frequency and the Raman scattered radiation frequency). In the classical framework of Raman scattering Raman power and intensity depend on the polarizability of the molecules, the concentration of these molecules in the sample and the excitation source (Sato-Berrú *et al.*, 2004). Thus the Raman scattering intensity is proportional to the forth power of the exciting laser radiation frequency (energy) (Dieing *et al.*, 2011). Therefore increase in excitation frequency decreases the signal to noise ratio.

Moreover, the measured Raman spot size depends on wavelength of the exciting laser which in turn determines the spatial resolution of the spectrometer. Thus the laser spot diameter (LSD) is dependent on the excitation wavelength and the objective of the microscope in use and can be expressed in Equation (3.14).

$$LSD = \frac{1.22\lambda}{NA} \tag{3.14}$$

where *LSD* is laser spot diameter, λ is the excitation wavelength and NA represents the numerical aperture.

Equation (3.14) indicates that the LSD has a positive relationship with the wavelength of the Raman laser. This implies the higher the wavelength the larger the spot size. This explains why lasers with low wavelength have higher resolution than lasers with high wavelengths (Smith and Dent, 2005).

3.5 Molecular vibrations

High intensity of Raman scattering is experienced by vibrations which cause alteration in the polarizability of the electron cloud around the molecules. Symmetric vibrations are usually responsible for the greatest changes and give the intense scattering (Demtröder, 2011). Sampling also affects the Raman scattering intensity band width and the band position just like electron cloud polarization. The energy of the system experiences six degrees of freedom provided energy is conserved. Three of which are responsible for the translation of the molecules while the other three describe the rotational modes of the molecules except for linear molecules that have only two rotational modes. This is because linear molecules have 3N - 5 vibrational modes instead of 3N - 6 vibrations as usual (N is the number of molecules in an atom) (Smith and Dent 2005).

3.6 Assignment and interpretation of Raman peaks

Different vibrations occupy different positions on the spectral line. To assign and interpret various vibrations distributed on the spectral line one must know the type of bonds involved and different positions each bond occupies on the spectral peaks. There is a possibility of giving energy ranges that characterize the frequencies of frequent groups that are strong in Raman. The wave shift of a particular peak give a confirmation that the correct vibration has been selected (Smith and Dent, 2005) (see Table 3.1).

Table 3.1: Raman vibrational modes and their strength adopted from (Dieing et al., 2011)

Functional Group/ Vibration	Raman shift (cm^{-1})	Strength
υ(C-O-C)	800 -970	Medium
υ(C-O-C) asym	1060 – 1150	Weak
υ(CC) alicyclic, aliphatic chain vibrations	600 – 1300	Medium
υ(CC) aromatic ring chain vibrations	1580	Strong
δ(CH3)	1380	Medium
δ(CH2)	1400 – 1470	Medium
υ(C=C)	1500 – 1900	Strong
υ(C=O)	1680 – 1820	Medium
υ(C≅C)	2100 – 2250	Strong
υ(C−H)	2800 – 3000	Strong
υ(=(C-H))	3000 – 3100	Strong
υ(≅(C-H))	3300	Weak

3.7 Multivariate techniques

Multivariate analysis entails statistical analysis of data that has many variables such as Raman spectral data. These techniques extract the most important information by taking in consideration of all the variations in the data sets, removing redundancy and correlating information in the same data set. In this study AFB1 is detected and quantified using multivariate analysis. The use of chemometrics is necessary since maize constitutes some vibrational modes in the same range as AFB1 which cause a lot of interference in the spectral data acquired and make conventional data analysis limited in giving molecular information and spectral correlation (Lee *et al.*, 2014). Thus the use of multivariate analysis to find the correlation between Raman intensity of AFB1 and its concentration is a necessity in this study. It is for this reason that PCA is used for pattern recognition while PLSR and MLR are used for calibration and modelling.

When Equation 3.13 is critically analysed it is found that holding other factors constant, the scattered Raman intensity should be proportional to the number of molecules (AFB1) present in the sample (Dieing *et al.*, 2011). However this relationship is hardly obeyed due to several factors. Self-reabsorption for example in highly concentrated samples is unavoidable. In this case molecules at the lower vibrational levels easily reabsorb the radiation emitted by molecules at higher vibrational levels which results into non-linear relationship between Raman intensity and concentration. This makes the characteristic line intensity to deviate from the ideal straight line as the number of molecules increases (Smith and Dent, 2005). Interference from other components of the samples is also expected. In the case of maize, starch (the main component) has vibrational bands in the same range as AFB1 (Wellner *et al.*, 2011).

However, other influential factors such as fluctuations in laser power and lens to sample distances caused by movements around the Raman setup can be minimized by scanning through

different parts of the sample and averaging the measured signals. This can further be improved by use of data pre-processing techniques discussed earlier in this thesis. These factors affect the positive correlation that exists between Raman intensity and concentration of AFB1 (Wang *et al.*, 2011). Thus the ideal way of extracting information from characteristic line of different concentrations is to get full spectrum range of each concentrations and use multivariate techniques to cater for these deviations. Below is a brief description of the three selected techniques used in this work.

3.7.1 Principal component analysis (PCA)

Principal component analysis (PCA) is one of the common methods of identifying dominant clusters in data sets by use of eigenvalue-eigenvector technique of matrix algebra. The developing of PCA model involves the decomposition of a correlation or covariant matrix into eigenvalue and corresponding eigenvectors, which are orthogonal to each other among other properties (Shaver, 2001). The eigenvectors are found as orthogonal vectors along an n^{th} coordinate system that explains the maximum variance in the original matrix (Raman dataset). Analysis of eigenvectors aids in the identification of spectral features and the understanding of the PCA clusters. In order to remove noise and reproduce spectra, mean centring (subtracting the mean of the spectrum) is advisable as it takes care of the mean changes in all the factors (Ryder *et al.*, 2000). The removal of noise, redundancy and multi-collinearity in data sets is done by use of principal component analysis by sorting out the most influential factors (principle components/factors) from the data set followed by less influential factors. As a result unwanted information is discarded without losing important spectral information (Ryder *et al.*, 2000). However, some weak signals maybe considered by PCA as noise and lost, thus less influential factors should be carefully analysed before they are discarded.

Mathematically, if a matrix can be expressed as a function x, then the sum of the product of all subsets (vectors/ principal components) and their weighting factor reproduces the matrix as shown in Equation (3.15) (Shaver, 2001).

$$x = t_1 p_1 + t_2 p_2 + ... + t_n p_n + e \quad (3.15)$$

where *x* represents any spectrum, *t* score (weighting factor), *p* is vector (subset of components) and *e* is the residual signal that was not modelled. From Equation (3.15) it is clear that factors (principle components) are the basis behind groupings (clusters) in score plots since for some spectra to be clustered in one group they must have the same factors that are similar (Shaver, 2001).

Generally in this work, PCA was used as an initial investigative multivariate approach to find out the differences and similarities in the Raman datasets in preparation for quantitative analysis. Moreover, PCA can also be used for developing calibration and predictive models if its regression is invoked. However, in this work only the exploratory properties of PCA are employed (Shaver, 2001).

3.7.2 Regressions

A regression is a statistical modelling technique that fits a relationship describing joint variability between two or more variables. The fitted model will be used for prediction purposes. Before carrying out any regression, it is important to form an X and Y matrix which will be used in forming the model ($Y= f(X)$). X represents the predictors (independent variables) and Y represents responses (dependent variables). The model establishes a link between X and Y variables by forming a set of samples from both X and Y.

There are two types of regressions: univariate regression and multivariate regression. Univariate regression uses only one predictor while multivariate regression uses many predictive variables at the same time. In this research measurement of known concentrations were taken, regressions (PLSR and MLR) were then used to predict unknown concentrations.

The results of the regression modelling are generally measures of the model's goodness usually summarized by the so-called analysis of variance table (ANOVA). In this study, the measures of performance used are the R-squared value (R^2), the root mean square error of calibration (RMSEC), correlation coefficients (p), the slope, Standard Error of Calibration (SEC), Standard Error of Prediction (SEP) and Root Mean Square Error of Prediction (RMSEP). Models with R^2 value close to unity are preferred to models with low R^2 values. Whereas RMSEC measures how well the models fit the calibration data, RMSEP measures how well the models fit the prediction data. The accuracy of the model can also be measured by calculating its SEP. Ideally RMSEC and RMSEP should have low values.

Partial Least Squares Regression (PLSR)

PLS is a regression that relates two sets of data (independent variables (X) and dependent variable (Y)) by establishing a linear model. It does this by extracting important information that relates the dependent and independent variables. It is this information that is crucial for prediction of targets. In this work Partial Least Squares regression (PLSR) will find a relationship between variations in different concentrations of AFB1 (dependent variables) and variations in Raman spectra of these concentrations (independent variable) as explained in Equation (3.16) (Westland, 2007).

$$Y = BX \tag{3.16}$$

where Y represents the concentrations of different samples, B stands for the matrix of regression coefficient and X is the intensity of the spectra

Equation (3.16) can only hold if the spectra is bulky and if there exists consistency in the spectra (Wold *et al.*, 1984). Once the relationship is established PLS just like PCA uses dependent variables (concentration) to extract the most important information (breaks in to principal components) with the first PLS component carrying the most relevant information. Thus in PLSR dependent variable aids in finding PLS components from independent variables.

Multiple Linear Regression (MLR)

MLR is a mathematical method that uses many variables to make predictions on the response variables (Sidik and Center, 1972). It does this by finding a best linear fit statistically with the relationship in Equation (3.17).

$$y_i = \beta_0 + \beta_1 x_{i1} + \beta_2 x_{i2} + ...\beta_p x_{ip} + e_i \tag{3.17}$$

where β_o is the intercept, $\beta_{1\text{-}p}$ are coefficients and *i* varies from *1* to *n*. Equation (3.16) holds on condition that all variances are equal (standard deviations are the same). Since equation (3.16) is a linear combination, the linear fit usually explains how the mean varies with explanatory variables and the fitted values are the coefficients of the linear fit. As stated earlier in MLR, *y* values oscillate around their mean thus the residual *e* represent the deviations of *y* variables from their mean. Therefore just like PLSR the best fit is found by minimizing the values of the intercept and slope (we try to make vertical deviation of all data points to be zero) (Kelly and McNeil, 1975).

CHAPTER 4: MATERIALS AND METHODS

This chapter presents the equipment, materials and methods used in carrying out the experiments. It further explores how data was initially handled.

4.1 Equipment and materials

4.1.1 Introduction

In order to make different concentrations of AFB1 solutions, standard AFB1 in powder form (5 mg) was bought from Libios SARL (Pontcharra Sur Turdine, France) and the ELISA kit was obtained from Helica Biosystems Inc to run confirmatory tests. Methanol and acetonitrile solvents of analytical grade, sulphuric acid, sodium hypochlorite and other essentials such as gloves, mouth masks and lab coats were sourced locally. Pure methanol was the main solvent in this work and was used to dissolve the standard AFB1 powder. The locally supplied acetonitrile, sulphuric acid, sodium hypochlorite and distilled water were used for cleaning the glasswares as described in section 4.2

The maize kernels used in the study were obtained from Kimaeti Kenya Seed in Bungoma County, Nairobi open markets and the International Maize and Wheat Improvement Centre (CIMMYT), University of Nairobi. Samples from Kimaeti Kenya Seed were used for developing the models to predict AFB1 levels in samples obtained from Nairobi open markets. AFB1 levels in maize kernels supplied by CIMMYT were determined by ELISA method and the results served as reference data sets in validation of the AFB1 predicted concentrations from MLR and PLSR models.

4.1.2 Confocal Raman spectrometer

The confocal laser Raman spectrometer (STR Raman Spectrum System, Seki Technotron Corp) used in this study was equipped with a 300 mm imaging triple grating monochromator spectrograph and two lasers emitting at 532 nm and 785 nm. The 300-mm imaging spectrometer had 1800, 1200 and 600-lines/mm grating optimized as discussed in section 4.1.2. The spectrometer was also equipped with a back-illuminated CCD camera that aided in capturing the spectra within a specified period.

For any measurement to take place the green laser at 532 nm or the red laser at 785 nm beam is delivered to the Raman optics via an optical fiber which gives the beam a total internal reflection. Once at the Raman optics, the beam is passed through the ND filter where it is 1-100% filtered to the shutter. The shutter then delivers the beam to either 532 or 785 nm band pass filter depending with the laser in use. In our set up this was done manually by the laboratory technologist. The band pass filter delivers the beam to the beam splitter which splits the beam in two equal parts; fifty percent of the beam is reflected while the remaining fifty per cent passes through the beam splitter to the sample where Raman and Rayleigh scattering takes place (see Figure 4.1).

The scattered beam is then passed through the objective to the 532/785 nm low pass filter which blocks the Rayleigh scattered beam and only allows the Raman beam to pass through. From the low pass filter the beam is passed through a black optical fiber of the spectrogram to the CCD camera then to the computer. The spectrometer is equipped with a microscope that uses a lever to control the motorized stage. The spectrometer also has two switches that allow one to observe the sample using light from above or below the sample depending on the nature of the sample (opaque or transparent).

Once the NIR laser beam has excited the sample, the weak Raman scattering is measured using the imaging spectrometer and CCD camera. Sample focusing was done using the motorized stage, the computer equipped with STR software and the camera attached to the microscope. The spanner in the software aided in choosing the detector settings and the time limit for opening and closing the camera shatter. The motor driven stage also helped in scanning through the sample and collecting data at the randomly identified spots.

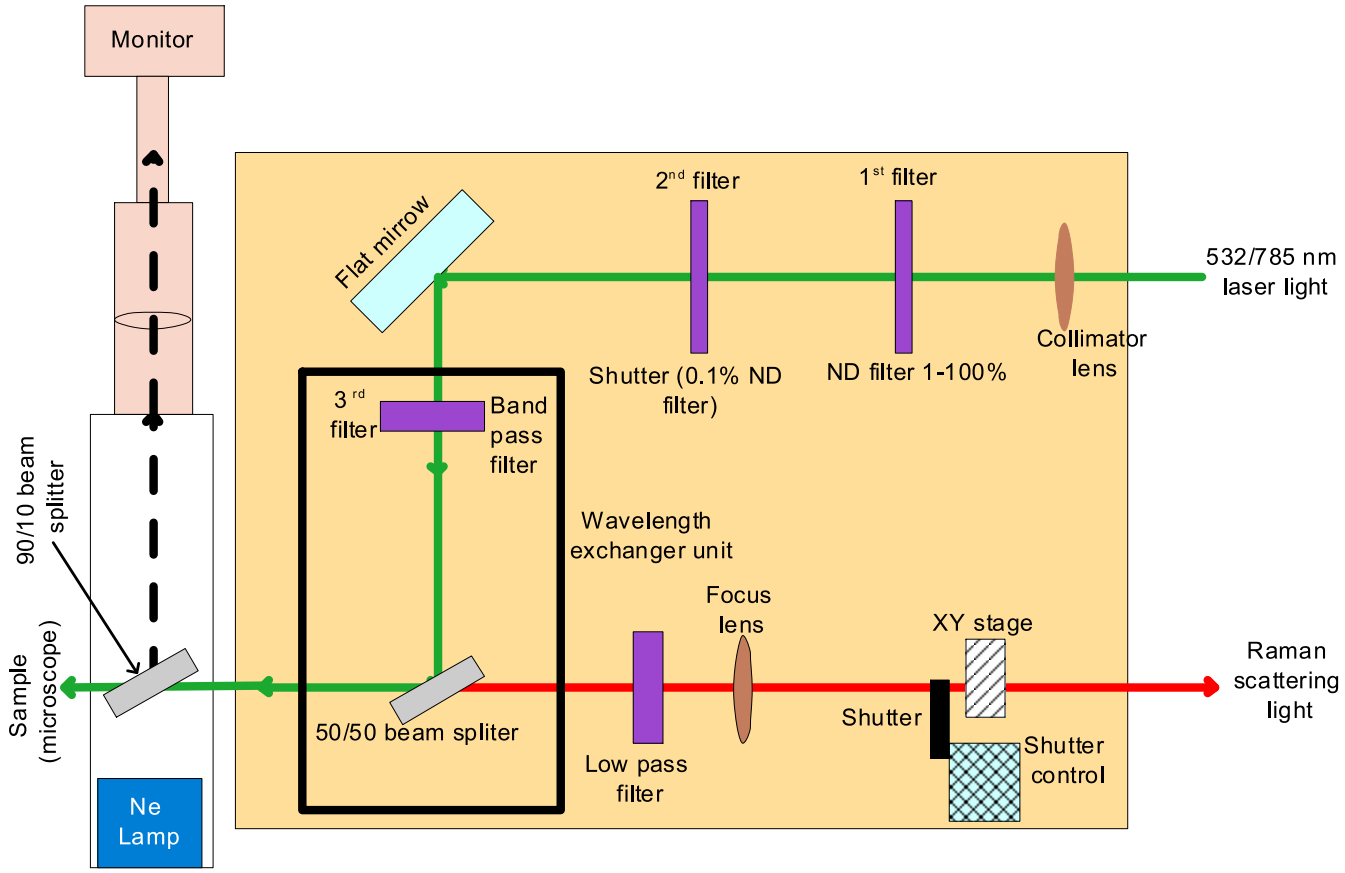

Figure 4.1: The layout of Confocal Raman spectrometer adopted from (CORNES, 2012). The system is equipped with two lasers (532 nm and 785 nm lasers) and a spectrograph fitted with a 256 x 1024 pixel CCD camera

4.1.3 Optimisation of the Raman instrument

The Raman spectrometer was equipped with a shift of 1800, 1200 and 600 lines mm^{-1} spectral window. Measurements with the three windows were taken and 600 mm^{-1} showed best spectra. Thus the Raman shift spectral window was optimized at the 600 lines mm^{-1} grating window with the shift range of 400 – 1800 cm^{-1} since this is the region where most vibrational bands for AFB1 are found. The excitation laser intensity was controlled using Neutral Density Filters (NDF) with different attenuation coefficients (see Table 4.1) and the spectrograph was fitted with a 256 x 1024 pixel CCD camera. The excitation field power was measured using Orion Laser Power Meter from Ophir Photonics and the field powers displayed in Table 4.1. The 50% NDN transmission intensity and the powers transmitted at this level were used in exciting samples with both 532 and 785 nm laser (see Table 4.1).

Table 4.1: The measured excitation optical field powers used in Raman spectroscopy in exciting all samples with excitation wavelengths at 532 nm and 785 nm laser

NDF Transmission Intensity (%)	Power after the objective		Power after first filter	
	785 nm laser	532 nm laser	785 nm laser	532 nm laser
5	0.4 µW	24.0 mW	8.0 mW	0.695 W
10	0.3 µW	24.1 mW	5.0 mW	0.709 W
25	0.6 µW	28.0 mW	11.0 mW	0.733 W
50	1.0 µW	32.0 mW	23.0 mW	0.759 W
100	3.0 µW	41.0 mW	48.0 mW	0.765 W

The Raman laser spot diameter (LSD) was approximately 40 µm and 50 µm for 532 nm and 785 nm lasers respectively. The LSD found agrees with literature since wavelength is directly proportional to the LSD as discussed in section 3.4. This implies that the 532 nm laser has higher

resolution than 785 nm laser. And in order to obtain all the expected AFB1 peaks the Raman spectra recorded was centred at 1,100 cm^{-1}. Several spectra were taken from 10 different parts of the samples and averaged in order to get a single spectrum. For each measurement three minutes of exposure time were used for 10 scans in order to reduce fluorescence and noise in the spectra acquired.

For purposes of determining which laser among the two was best suited for detection and quantification of AFB1, the signal to noise ratio (SNR) was also determined using Equation (4.1) and averaged for various samples excited by the two lasers (Carranza *et al.*, 2003).

$$SNR = \frac{I_p}{I_n} \tag{4.1}$$

where I_p and I_n represents intensity of the main peak (1593 cm^{-1}) of AFB1 and the average intensity of the 12 adjacent noise peaks respectively. Each spectrum's SNR of AFB1 levels greater than 10^5 was calculated according to Equation 4.1. Later the SNR of each matrix; AFB1 on glass slide, cuvette, and maize were averaged and classified according to the excitation wavelength.

In order to determine the least AFB1 concentration that could be detected and quantified by the Raman instrument, the Limit of Detection (LOD) and the Limit of Quantification (LOQ) were calculated using Equation (4.2) (Lee *et al.*, 2014).

$$LOD = \frac{3s}{r}$$
$$LOQ = \frac{10s}{r} \tag{4.2}$$

Where *s* is the standard deviation of Raman intensity and *r* is the slope of the intensity vs the Raman shift. The standard deviation and the slop were obtained from the entire Raman spectra and averaged.

4.1.4 The ultraviolet-visible-near infrared (UV-VIS-NIR) spectrophotometer

In order to find out the purity of the prepared solutions, the absorbance of standard AFB1 solutions was measured using UV-VIS-NIR spectrophotometer (Solidspec-3700 DUV, Shimadzu Corporation). The beam of light from the UV-VIS-NIR source is split into two; reference and sample beams using the half mirror (see Figure 4.2). The reference beam intensity is set at 0% absorbance and 100% transmittance. The ratio of the two beam intensities were measured using the two detectors (photodiodes), with the aid of a computer connected to the system (Figure 4.2). The computer was installed with UVprobe 2.221 software for better data collection. The UVprobe thus helped in optimizing wavelength range between 200-600 nm, a region in which AFB1 and methanol absorbs.

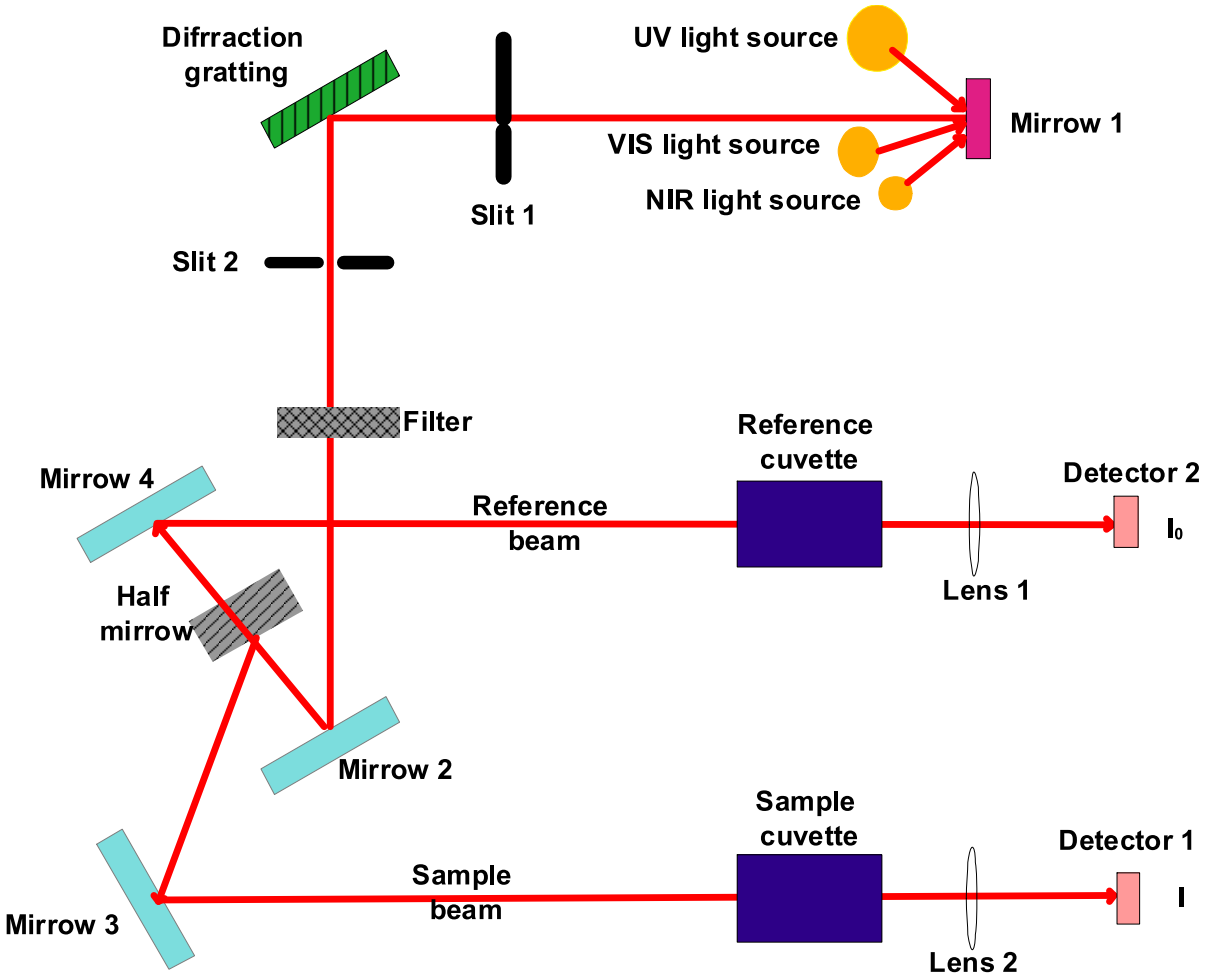

Figure 4.2: Schematic diagram for the setup of the UV-VIS-NIR spectrophotometer used to measure absorbance of standard AFB1 in methanol. The data was acquired using UVprobe 2.21 software installed in the computer which was connected to the optical system

4.1.5 Fluorescence spectroscopy

For purposes of confirming the purity of the standard AFB1 fluorescence spectroscopy was measured using the USB Ocean Optics (USB 2000) spectrometer. The LED light was made to illumine the sample at 2 mm distance and the emitted light was emitted at the same distanceThe LED light with centre wavelength of 375 nm was used to excite AFB1 in methanol in a cuvette using an optical fibre and a USB cable (Figures 4.3).The fluorescence procedure was carried out in the dark room to avoid interference from other sources of UV light. The obtained fluorescence

spectra were optimized between 400 - 600 nm since it is in this region that the fluorescence characteristics of AFB1 in methanol are seen. A computer installed with the Spectra Suite software was connected to the Ocean Optics spectrometer to aid in data acquisition (Figure 4.3).

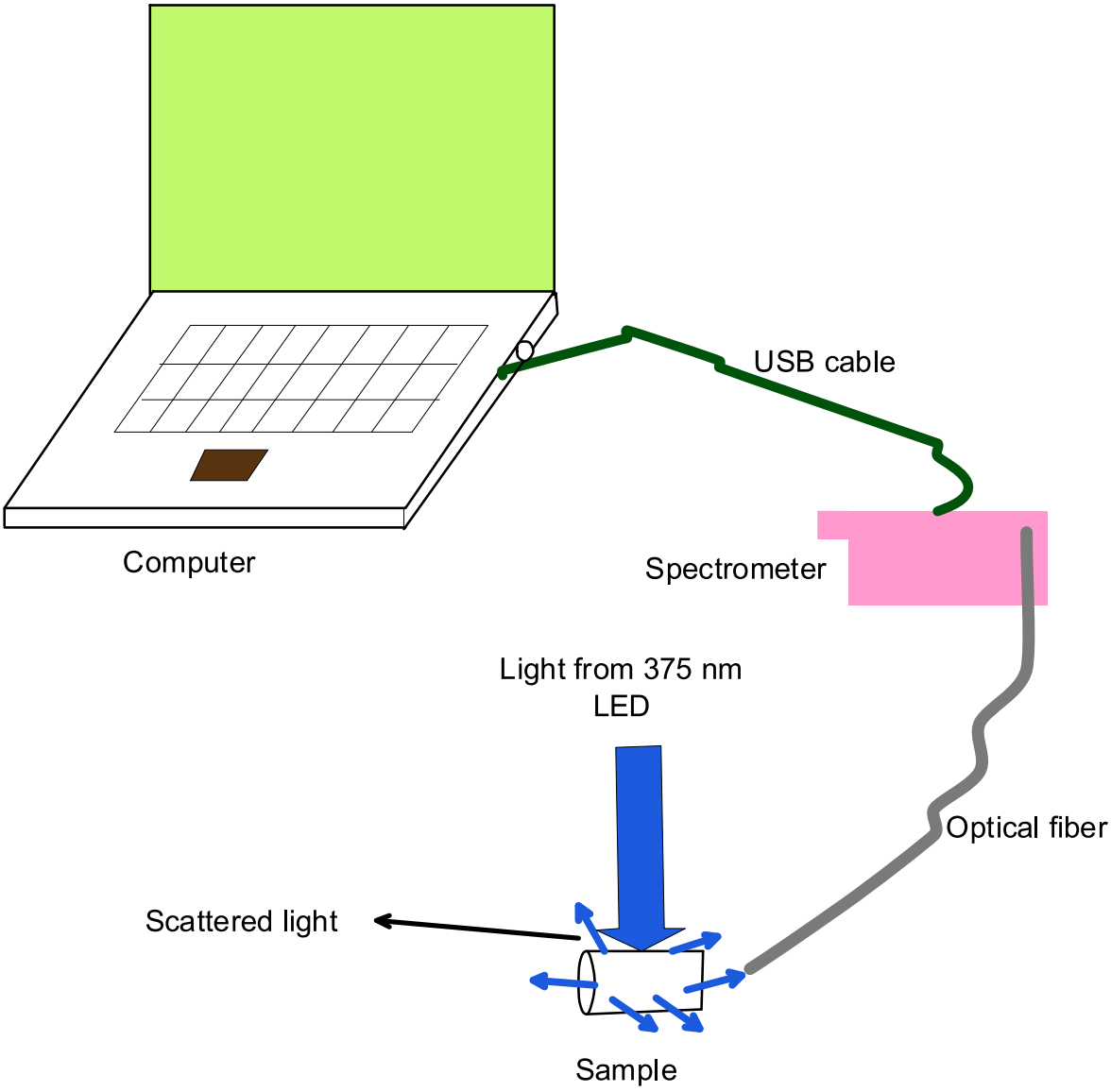

Figure 4.3: Schematic diagram of the setup used to measure fluorescence spectra of standard AFB1 in methanol. The spectra were captured to the computer with the help of Spectra Suite software. All fluorescence measurements were taken in a dark room to minimize noise

4.2 Safety precautions and cleaning of glassware

The solution preparations and experimental procedures were all performed at room temperature (~24^{o}C). Moreover AFB1 solutions were made in the fume chamber and stored in a demarcated part of the laboratory to prevent exposure of AFB1 to people and other equipment. Other safety precautions taken while handling AFB1 are explained in Appendix I.

Before using any glassware; beakers, glass slides and cuvettes were first put in dilute sulphuric acid (105 ml H_2SO_4 in one litre of water) for two hours, then rinsed five times with distilled water to remove traces of the acid (checked with litmus paper). This was done to prevent decomposition of aflatoxin as use of acid stained glassware may accelerate this process. After use, all glassware exposed to aflatoxin were rinsed with methanol and then soaked in a solution of methanol and 1% NaOCl for 2hrs. After this the glassware was soaked again with 5% acetone solution for 30 minutes before being rinsed five times in distilled water.

4.3 Developing multivariate models

The pre-processed data was later transferred to Unscrambler software for chemometrics analysis (PCA, MLR and PLSR). Prior to the qualitative and quantitative sample analysis maize samples with AFB1 levels below 1 ppb were labelled C1, C2 for 15 - 950 ppb, C3 for 150 - 950 ppb and C4 for 1500 - 9500 ppb as shown in Appendix II. Thus calibration and validation analysis involved use of Raman spectral data from samples with aflatoxin B1 concentration values ranging from 0.15 ppb – 4950 ppb which covers majority of aflatoxin levels found in Kenyan maize. And the Raman spectra range of 400 cm^{-1} and 1800 cm^{-1} was used as these covers most of the Raman active vibrational modes. The scan of large sampled concentrations would provide

better results in low concentrated samples (Lee *et al.*, 2014). PCA was then used to reduce dimensionality of the data sets and to find patterns in the Raman spectra.

In order to develop multivariate models, Raman spectra extracted from one hundred and twenty intentionally contaminated maize samples were split randomly into two groups of calibration (80) and validation (40) models. The PLSR and MLR models were then developed and used to predict unknown concentrations in maize obtained from Nairobi open markets. To validate Raman spectroscopy as a method of detecting and quantifying AFB1, the predicted concentrations obtained from different models were compared with the reference values obtained from ELISA.

PLSR was used to decompose the data sets by finding principal components (factors) that explained the variance in the data and compared between AFB1 concentration in the data and the Raman spectral information like intensity and the width of the peaks. The calibration models of PLSR were developed by full cross validation that involved considering one variable at a time untill all spectra were considered. MLR model was also developed using a step wise regression. The accuracy of the calibration models were determined by the R-Squared value and root mean square error of calibration (RMSEC). The models were afterward validated with a validation scheme that was chosen based on the accuracy of the developed models.

4.4 Sample preparation

4.4.1 Solutions of different concentrations

To protect the researcher and other laboratory users from intoxication since AFB1 powder is electrostatic in nature, the weight of 5 mg of AFB1 powder was assumed to be correct as indicated by the supplier. The supplier's bottle and its content of AFB1 powder was therefore

measured and noted in Table 4.2. Then using a needle and syringe methanol was carefully added to the brim of the bottle and its contents shaken for 5 minutes to allow AFB1 dissolve in methanol to a clear colourless solution (A) and its final weight noted in 4.2. Other solutions in solutions (B, C, D, E and F) were made from solution (A) and their concentrations were evaluated using equation (4.3).

$$concentration = \frac{M_{AFB1}}{M_{Sol}} \times 10^9 \; ppb \tag{4.3}$$

where M_{AFB1} is mass of AFB1 powder and M_{sol} is mass of AFB1 solution

A total of 126 different solutions with varying AFB1 concentrations ranging from 0.1 ppb to $1.1x10^6$ ppb were prepared. Table 4.2 shows six solutions with the levels of AFB1 (concentrations of the solutions prepared) and the procedure of determining their weights as shown in Table 4.2. Samples made from solutions whose concentrations were greater than 10^5 ppb were used to obtain Raman characteristic spectra. Due to the weak nature of Raman scattering, we needed highly concentrated solutions to obtain the weak AFB1 Raman peaks that would not have been physically visualized in lowly concentrated solutions such as the 1751 cm^{-1} peak. Samples with AFB1 levels ranging from 1.0 x 10^{-1} ppb to 9.95 x 10^4 ppb were used for developing classification and quantification models (see Appendix II) because this region covers the AFB1 levels found in Kenya. These samples were further categorized in terms of AFB1 level ranges C1 (0.15 - 0.95 ppb), C2 (15 - 95 ppb), C3 (150 - 950 ppb) and C4 (1500 - 9500 ppb) as shown in Appendix II. The C1 range would cover the contamination in human infant food, C2 adult human food, C3 domestic animal feeds and C4 in fungi infected maize mostly used for second generation alcohol ‘chang’aa’.

Table 4.2: Different concentrations (Conc.) in ppb of AFB1 in methanol (A_p) and determination of the masses of quantities measured

B_e (g)	B_e+M (g)	M (g)	A_{sol}+B_e+M (g)	A_{sol} (g)	A_p (g)	Conc. Symbol	Conc.(ppb)
5.166	9.757	4.591	14.353	4.596	5.0×10^{-3}	A	1.1×10^{6}
6.946	8.270	1.324	9.414	1.144	1.2×10^{-3}	B	5.0×10^{5}
6.193	9.776	3.583	10.434	0.658	7.2×10^{-4}	C	1.7×10^{5}
8.117	9.744	1.627	9.967	0.223	1.2×10^{-4}	D	6.9×10^{4}
8.068	9.740	1.672	9.816	0.076	8.3×10^{-5}	E	4.7×10^{4}
8.150	9.833	1.680	10.106	0.273	4.6×10^{-5}	F	2.4×10^{4}

Where A_p+B_e+M is the sum of mass of aflatoxin powder, methanol and empty bottle, B_e+M is mass of methanol plus mass of empty bottle, B_e is mass of empty and A_{sol} mass of AFB1 solution A_{sol}.

For purposes of obtaining characteristic AFB1 Raman spectra, solution (A) (concentration 6.1 x 10^6 ppb) was placed in the cuvette and 10 Raman spectra acquired from it at both 785 nm and 532 nm excitation. Later the same solution was pipetted onto a clean microscope glass slide and left for 15 minutes to allow methanol to evaporate. This resulted in a thin layer of AFB1 getting adsorbed onto the glass slide as shown in Figure 4.4.

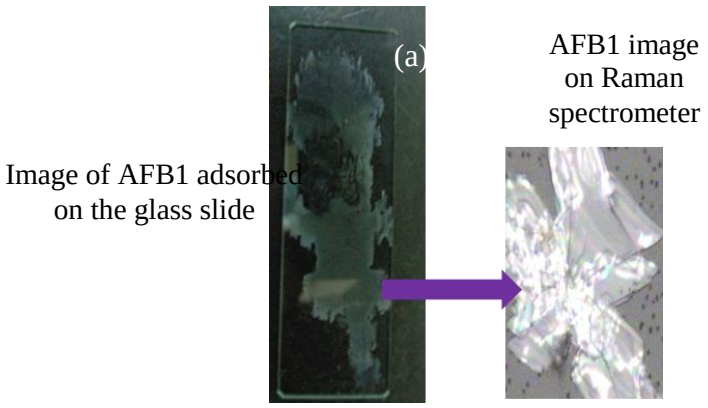

Figure 4.4: The image of AFB1 adsorbed on a glass slide (a) and under Raman spectrometer at 50 µm spot size (b) when excited at 785 nm

4.4.2 Maize samples

The maize samples used to develop classification and quantification models were obtained from Kimaeti Kenya Seed, Bungoma County. The kernels were uniformly mixed then 120 samples of 20 g each made from it randomly for analysis. These samples were then randomly labelled with same codes given to the AFB1 solutions in Appendix II. Five grams of each sample was then sent to CIMMYT for detection of AFB1 levels by ELISA. It was found that the maize samples had an average value of 4.31 ppb of AFB1. This AFB1 level was considered negative as in Kenya human food is allowed to have up to 10 ppb. Due to unavoidable circumstances we could not access maize with 0 ppb. As a result of this we had no option than to use Kenya seed maize to develop our models. Ten kernels were randomly picked from each sample and soaked in the solutions bearing same labels for 24 hours after which the maize was removed from the AFB1 solution and left to dry for one hour. Raman spectroscopy was then done on each of them. For every kernel ten suspected spots were chosen for Raman analysis. The ten spectra obtained were averaged to give one spectrum. Thus for each sample we had ten Raman spectra. The intentionally contaminated maize kernels were later ground using a blender to get flour samples. The Raman spectra of flour samples were taken by scanning through 10 different spots of 5g of each sample. The 10 spectra acquired in each sample were then averaged to get one spectrum for every sample.

Maize collected from Nairobi open markets were used for predictions. The maize was divided into two samples of suspected and unsuspected samples. This was based on the visual appearance of the maize. The moldy (fungi visually observed) maize samples were labelled as suspected samples while non-moldy (fungi not visually observed) maize were labelled as unsuspected samples. The unsuspected maize samples were also randomly divided into 50

samples (M1, M2, M3… M50) of 20 g each. Ten kernels from each sample were thereafter randomly picked and Raman spectra collected from each sample as described above. The suspected maize samples were grouped into 20 samples (N1, N2, N3… N20) of ten kernels each and Raman spectra collected from them in a similar way.

4.4.3 Sample preparation for ELISA

Maize samples supplied by CIMMYT, University of Nairobi were labelled as P6, P9, P12, P14, P27, P38, P41, P43, P62, P130 and P116 (see Table 4.3). The samples were grown at Machakos County – Kenya in various plots identified by the various numerical numbers hence the designation P in Table 4.3. In order to extract aflatoxin from the ground samples an extraction solution was prepared from methanol and distilled water in the ratio 7:3. To 5g of each representative sample, 25 ml of the extraction solution was added. The suspension was vortexed in a sealed cuvette for 2 minutes and left to settle for 15 minutes after which the filtrate was filtered off using a Whatman 1# filter paper (Hyunh *et al.*, 2012).

The ELISA procedure proposed by Helica Biosystem inc was adopted as a method for quantifying the AFB1 in the samples. The samples and the standard to be quantified were each represented on the dilution well and on a microwell holder. Then 200 µl of the conjugate was dispensed into each dilution well followed by 100 µL of each sample. The conjugate and the sample were then mixed by priming the pipette up and down three times. 100 µl of the contents in the dilution well were later transferred to the corresponding antibody coated microtiter well and incubated for 15 minutes. The contents of the microwell were afterwards decanted off and the microwell washed 5 times using distilled water to remove the residual. The microwells were then tapped (face down once) onto an absorbent towel to ensure that all the residuals from the mixture were all eliminated. 100 µl of substrate was then added to each microwell and incubated

for 5 minutes at room temperature. To stop the reaction in the microwells 120 µl of stop solution was added in each microwell in the same sequence as substrate solution. Finally light was made to pass through a 450 nm polarizer that was placed on the contents of the microwell. The optical density of each microwell was then measured using a microtiter plate reader and the results noted in Table 4.3. These optical densities of the standard samples plus their concentrations and optical densities of the samples were then fed into elisaanalisis.com online software which calculated the concentrations of the samples as shown in Table 4.3. The dilution factor was multiplied by concentration in ppb to obtain the AFB1 levels in each sample (Hyunh *et al.*, 2012).

Table 4.3: Results of AFB1 levels in maize samples obtained from CIMMYT. To find the AFB1 in each sample dilution factor was multiplied by conc. in ppb

PLOT NO:	Well optical density	Mean optical density	Conc. in ppb	Confidence interval	dilution factor	Conc. of AFB1
P38	0.458,0.427	0.443	4.202	1.743 - 3.339	x200	840.459
P43	0.295,0.295	0.295	2.994	2.467 - 4.031	x200	598.800
P41	0.212,0.212	0.212	2.327	2.897 - 4.852	x200	465.400
P130	0.285,0.285	0.285	2.029	1.274 - 5.426	x200	405.800
P27	0.475,0.475	0.475	1.255	0.999 - 3.512	x100	125.500
P116	0.519,0.519	0.519	2.043	0.945 - 3.193	x20	40.860
P9	0.266,0.266	0.266	3.208	1.305 - 5.683	x30	96.250
P14	0.418,0.418	0.418	3.874	1.074 - 3.983	x20	77.470
P12	0.364,0.364	0.364	3.501	1.151 - 4.503	x200	700.200
P62	0.162,0.162	0.162	2.683	1.490 - 7.412	x30	80.500
P6	0.098,0.098	0.098	3.501	1.615 - 8.839	x200	700.200
Standard	2.376,2.376	2.376	0	N/A		
Standard	1.735,1.735	1.735	0.2	N/A		
Standard	1.348,1.348	1.348	0.4	N/A		
Standard	0.939,0.939	0.939	1	N/A		
Standard	0.534,0.534	0.534	2	N/A		
Standard	0.203,0.203	0.203	4	N/A		

4.5 Data pre-treatment

The confocal Raman spectrometer system was embedded with mechanism of background noise removal. Further noise removal was done by constantly calibrating the Raman spectrometer using the standards (silicon) before taking any measurement (Dieing *et al.*, 2011). Once the data was acquired it was first transferred to OriginPro 9.1 32Bit software for pre-processing, graphing and thereafter to Unscrumbler software (version 9.2, CAMO) for analysis.

In order to remove fluorescence background from the spectra baseline offsetting was done on the raw data using Origin software. This was done manually by adjusting 25 to 35 points of a constant line in all the spectra (Wu *et al.*, 2015). These points were neither too much for manual adjustment nor too little to fit the whole spectra. Baseline offsetting was followed by manual denoising under a wavelet of DB5 and periodic extension mode accustomed at a third level with ten percent threshold for each point.

Once denoised the data was smoothened using Savitzky Golay method of 8 window points. The savitzky Golay was applied to remove cosmic ray peaks. The first polynomial smoothing was made better with no boundary conditions attached on it. The denoising and smoothing were specifically carried out to remove cosmic signals (Dieing *et al.*, 2011). In order not to have negative peaks the minimum value in each spectrum was subtracted and the result used for chemometrics.

The aforementioned parameters for baseline offsetting, denoising and smoothing were selected based on how the preview fitted the data. The parameters employed in this work thus were found to remove most of the noise in the spectra without posing overfitting challenges.

CHAPTER 5: RESULTS AND DISCUSSIONS

In this chapter, the results of optical characterization and Raman spectroscopy of AFB1 and aflatoxin-contaminated maize kernels and flour samples are presented and discussed. The steady state characteristics of AFB1, Raman profiles and results from application of chemometric tools PCA, MLR and PLSR on the Raman spectral data of AFB1 obtained from the maize kernels and flour are also presented and discussed.

5.1 Steady state absorption and fluorescence spectroscopy

The absorbance and fluorescence of standard AFB1 in methanol were measured as described in sections 4.1.4 and 4.1.5 respectively. Figure 5.1 (a) shows the steady state absorption spectra of different concentrations of AFB1 in methanol at room temperature obtained with a UV- VIS-NIR spectrophotometer. AFB1 showed a broad spectrum centred at 340 nm. The absorption peak around 280 nm belongs to methanol. In addition the small maxima at around 340 nm, 354 nm and 375 nm can be ascribed to vibrational transitions in the first excited singlet state which agree with literature as discussed in section 3.1. Similar results were found by Netto-Ferreila and companion when they showed that AFB1 in acetonitrile absorbed at around 355 nm (Netto-Ferreira *et al.*, 2011).

The fluorescence spectra of different concentrations of AFB1, is shown in Figure 5.1 (b) and reveal small maxima around 448 nm, 480 nm and 500 nm. These peaks are attributed to the vibrational bands in the ground state. Both absorption and emission spectra displayed intensity dependence on AFB1 concentration as expected due to increase in AFB1 absorbing and emitting molecules in the solutions as discussed in the theoretical background (section 3.1). In studies done by Yao and companions also showed that AFB1 fluorescence at around 360 nm (Yao *et al.*,

2010). Netto-Ferreira and colloquies on the other hand showed that the emissive properties of AFB1 are solvent dependent with AFB1 dissolved in acetonitrile, Benzene and lipids fluorescing at 418, 393 and 418 nm respectively (Netto-Ferreira *et al.*, 2011).

In short the absorbance and fluorescence characteristics indicated that the purity of AFB1 solution was unquestionable since they agreed with literature. Thus the quantification models made from these solutions were reliable as the purity of the AFB1 solutions used to develop chemometric models was not questionable.

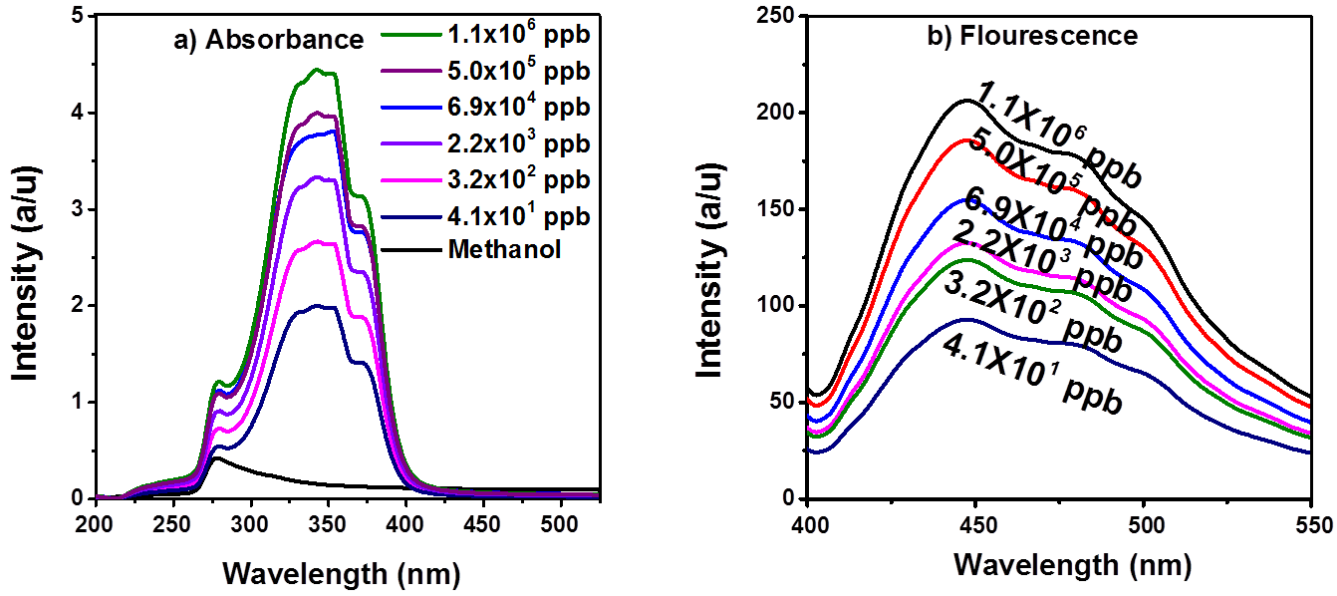

Figure 5.1: Absorbance (a) and Fluorescence (b) spectra of AFB1 in methanol. The absorbance spectra of different concentrations of AFB1 in methanol were obtained from UV-VIS-NIR DUV spectrophotometer (Solidspec-3700 DUV, Shimadzu Corporation) while the fluorescence spectra were obtained at 375 nm excitation with a light emitting diode (LED)

5.2 Optimization of Raman data

To evaluate the suitability of the two lasers in detection of AFB1, the SNR of the two excitation wavelengths were determined as described in section 4.1.3 and results noted in Table 5.1. The SNR of samples excited by 785 nm were generally higher than those excited by 532 nm laser. For instance, among all the samples, solutions adsorbed on glass slides had the highest SNR. The 785 nm excitation on the glass slide showed SNR of 14.02 which was higher than the SNR of 6.28 when the same sample was excited at 532 nm. Samples in cuvette followed the same trend and among the three matrices (glass slide, cuvette and maize) this recorded the lowest SNR. This therefore shows that cuvettes holding fluids to be studied with Raman spectrometer should be made from Raman inactive materials. Table 5.1 also showed that maize kernel had higher SNR (12.53) than flour samples (11.29). This is the reason why quantitative models developed from kernels were characterized with higher accuracy than those developed from flour samples.

The fact that 785 nm has bigger laser spot diameter (LSD) caused it to have higher SNR than 532 nm which agrees with literature as discussed in section 3.4. The 532 nm has higher resolution because of its smaller LSD which makes it zoom into the matrix of either glass or maize thus bringing out more noise (maize or glass signal) instead of AFB1 signal. As result of this the AFB1 signal was marred with a lot of noise and fluorescence background at 532 nm excitation. The fluorescence back ground causes the spectrum to hang instead of lying on the x-axis thus making analysis difficult. These fluorescence signals were also stronger in 532 nm than in 785 nm resulting to significant noise as shown in Figure 5.2. The effect of this noise and fluorescence on 532 nm excitation is even higher in low concentration (C1 and C2 ranges) when the matrix almost masks the whole of AFB1 signal completely. Furthermore, the higher excitation power

from 532 nm laser contributed a lot in the glass slide and cuvette interference see Figures 5.2 and 5.3.

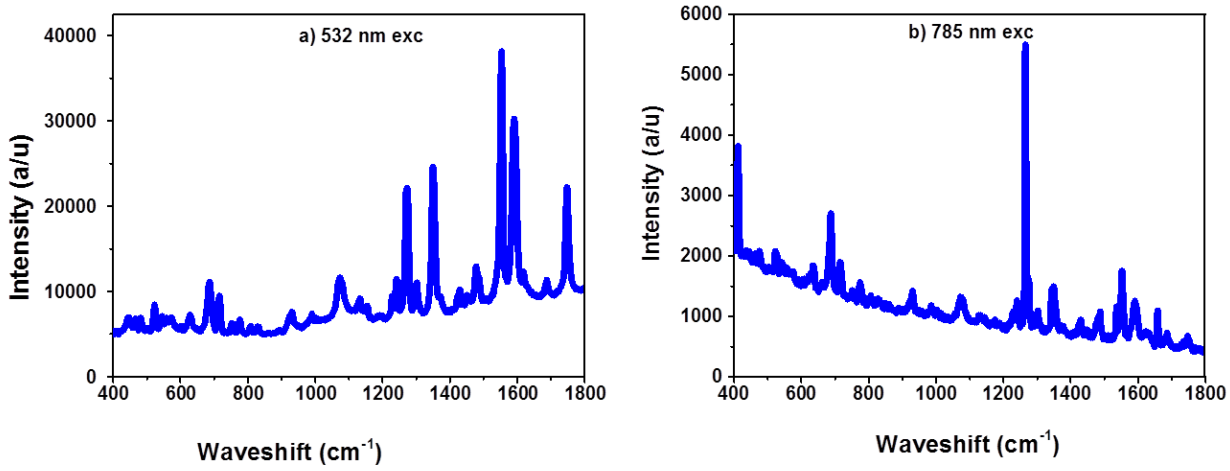

Figure 5.2: Raw Raman spectra of AFB1 adsorbed on glass slide. The spectra were obtained from excitation with 532 nm laser (a) and 785 nm laser (b) and the two excitations resulted in a significant background attributed to fluorescence

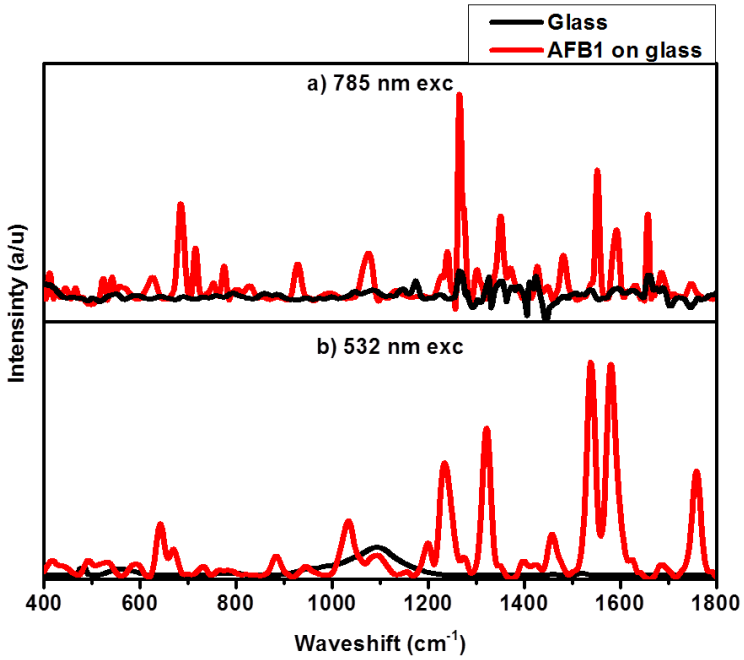

Figure 5.3: Comparing the interference of glass slide on Raman spectra of AFB1 at 785 nm (a) and 532 nm (b) excitation. The spectra from 785 nm excitation showed more glass interference than the spectra excited at 532 nm

Moreover, the interference of glass slide and cuvettes signals introduced foreign peaks to the spectra analyzed. A number of Raman data pre-processing techniques were employed in order to fluorescence offset background and noise as described in section 4.5 of this thesis. The Raman spectral profiles of Figure 5.2 are displayed in Figure 5.3 after pre-processing procedures. The effect of glass slide on AFB1 Raman spectrum is displayed in Figure 5.3. The signals (both Raman and fluorescence) emanating from the glass slide matrix were subtracted in order to obtain the AFB1 characteristic spectra. Samples excited at 785 nm experienced more glass interference as opposed to 532 nm laser which was expected as was discussed in the literature. This was due to the high photon power generated by 532 nm laser which resulted in intense Raman signal that suppressed the noise signal.

The interference from glass signals were even more prominent in the results obtained after exciting AFB1 solution in a cuvette as seen in Figure 5.4. These noise signals from cuvette material were observed to greatly mask the signal from AFB1. The glass peaks are the most prominent at 1267 nm and 450 nm and tend to overlap AFB1 peaks found in this region. This is because the material of the cuvette (glass) is Raman active and the AFB1 solution was inside it. So the laser beam first interacted with the glass before it reached the solution. As result of this the glass signal was stronger in samples placed in the cuvette. On the glass slide however, laser beam first interacted with the AFB1 adsorbed on the slide before interacting with the glass. Therefore AFB1 signal were more intense on the glass slide. It was observed that even after subtracting the signal from cuvette only 7 peaks (out of 22 found from glass slide) of AFB1 Raman are observed in Figure 5.4. It was for this reason that AFB1 was adsorbed onto a glass slide and the resulting layer (see Figure 4.4 section 4.4.1) excited at 532 nm and 785 nm separately.

The presence of Raman signal peaks attributable to AFB1 in samples inside cuvette showed the great potential of Raman spectroscopy in operating remotely. The findings also show that liquid and gaseous samples can be probed while inside transparent containers such as cuvettes (made from Raman inactive materials) for extraction of Raman spectra as earlier implied by other researchers in the work quoted here (Sharma *et al.*, 2002; Bowen *et al.*, 1989). However, analysis of fluids in cuvettes can only be possible with higher excitation wavelengths (785 nm and above) because at 532 nm excitation and other lower wavelengths will only show cuvette signal.

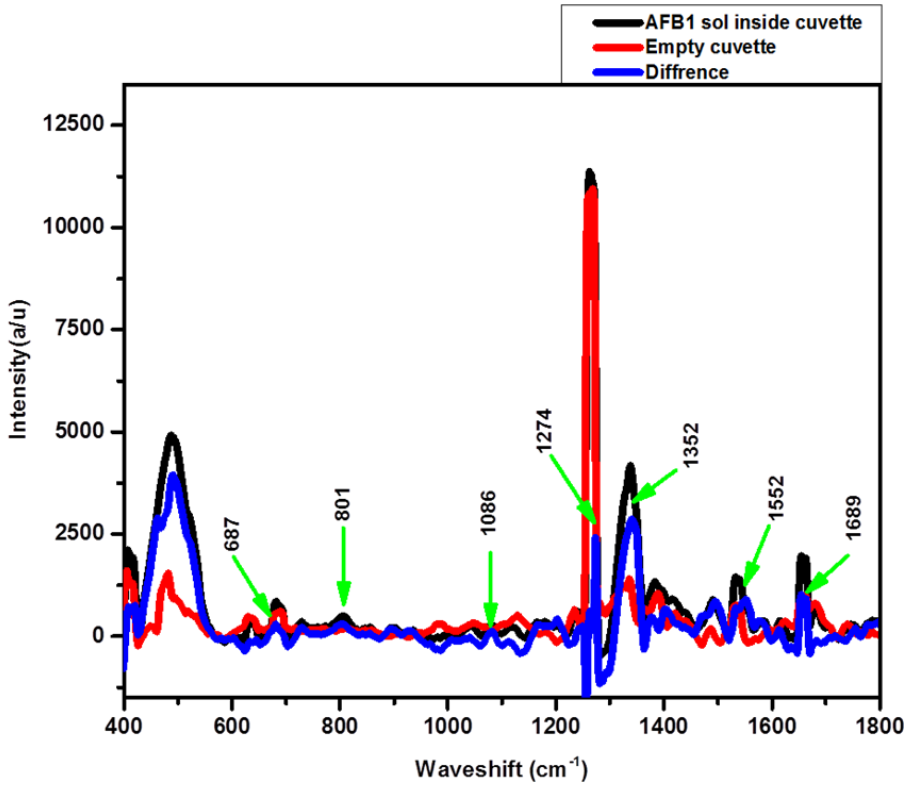

Figure 5.4: Raman spectra of AFB1 solution in cuvette, empty cuvette and the difference of the two spectra excited at 785 nm. The spectra were obtained at center 1,100 cm^{-1} with 50 µm spot diameter

In order to further confirm the suitability of the two lasers in the analysis of AFB1, the LOD and LOQ were calculated and noted in Table 5.1 as described in section 4.1.3 of this document. The two limits revealed the least concentration of AFB1 the Raman spectrometer could detect and quantify at the two excitations on various samples. Just like in the SNR 785 nm laser showed better results of LOD and LOQ. AFB1 adsorbed on the glass slide and excited at 785 nm showed the lowest LOD (1.59)/ LOQ (3.14) (see Table 5.1) and that is why all Raman spectra of AFB1 adsorbed on glass slide showed most of the peaks needed for analysis. This also explains why the characteristic spectra of AFB1 in this work were extracted from data whose solutions were adsorbed on the glass slide. Maize kernels gave better LOD (3.16) and LOQ (10.53) than flour of 4.26 and 12.85 respectively. Samples excited at 532 nm showed the same trend but with higher LOD (32.24; 40.30) and LOQ (104.30; 129.36) in maize and flour respectively. The LOD and LOQ in Table 5.1 show that our Raman spectrometer at 785 excitation can be used to detect and quantify AFB1 in human adult food and domestic animal feeds whose limit of consumption is at 10 ppb and 300 ppb respectively. However, the 785 nm laser is limited in monitoring AFB1 levels in human infant food whose consumption limit is at 0.5 ppb. With 532 nm we will only be able to monitor AFB1 levels in animal feeds. Table 5.1 also reveals that monitoring AFB1 levels in liquid foods adsorbed on surfaces would give accurate results than monitoring solid foods.

Finally the LOD and LOD in kernel matrix and flour matrix show the need of testing for aflatoxin levels in maize in the fields and silos before milling and other processing procedures are carried out.

Table 5.1: A table showing the SNR of various samples at 785 nm and 532 nm excitation and the LOD and LOQ in ppb that the two lasers achieved

Sample	**SNR**		**LOD**		**LOQ**	
Excitation wavelength	**785**	**532**	**785**	**532**	**785**	**532**
STD AFB1 on glass slide	14.021	6.284	1.590	14.965	3.136	32.555
STD AFB1 in cuvette	4.526	2.512	280.147	3000.147	693.820	687.156
Maize	12.350	4.123	3.159	32.248	10.530	104.367
Flour	11.285	3.458	4.255	40.298	12.850	129.361

5.3 Characteristic Raman spectrum of AFB1 standard

The characteristic Raman spectra in Figures 5.5 (a) and (b) with assigned peaks were obtained after AFB1 solution (6.1 x 10^6 ppb) was adsorbed on a glass slide as described earlier in section 4.4.1 after exciting it at 532 nm and 785 nm respectively. It is evident that the Raman intensity of the spectra obtained after 532 nm excitation was higher than those from 785 nm excitation. A sample excited at 532 nm and 785 nm under the same spectroscopic parameters showed 32 mW and 50 µW power for 532 and 785 nm excitation. This is expected since Raman intensity is known to be proportional to the fourth power of excitation frequency as discussed by (Dieing *et al.*, 2011) in section 3.4. The prominent peak at 1552 cm^{-1} was attributed to v(C-C) and ring deformation while 1593 cm^{-1} peak was attributed to v(C-C) and v(C-C-C) and are less intense in 785 nm excitation compared to 532 nm excitation. The high intensity of the spectrum from 532 nm excitation was also caused by the small LSD of 40 µm unlike in 785 nm which showed 50 µm.

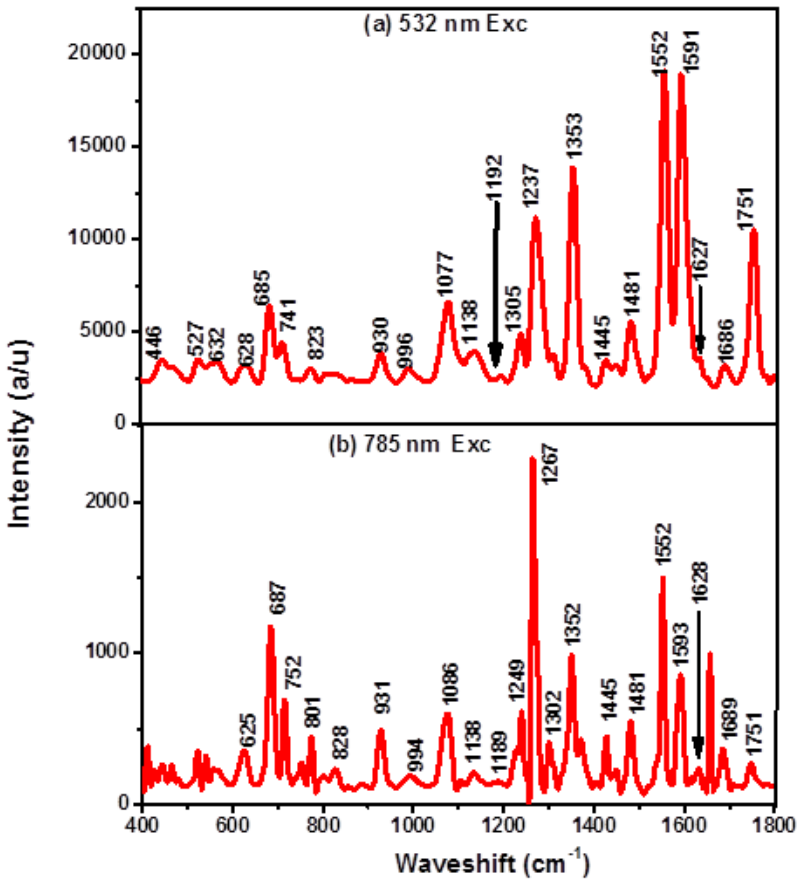

Figure 5.5: The characteristic Raman spectra of standard AFB1 after background subtraction. Both spectra were obtained at centre 1100 cm^{-1} with spot diameter of 40 µm and power of 32 mW (532 nm laser) and 50 µm spot diameter for 785 nm laser and 1 µW power

Table 5.2 gives a summary of Raman signal peak positions obtained from AFB1 adsorbed on glass in our work and the corresponding positions plus assignments from SERS (Wu *et al.*, 2012) and AFB1 powder (Móricz *et al.*, 2008) done elsewhere. The positions were found to be fairly close indicating the good prospects of glass substrates as an alternative to the specially prepared metal-based SERS substrates (Wu *et al.*, 2012).

Table 5.2: Assignment of AFB1 Raman peaks with excitation at 785 nm and 532 nm. The 785 nm laser measurements of AFB1 were taken first followed by the 532 nm laser measurement. The experimental peaks found in this work are compared with results reported by Wu and co-workers using SERS (Wu et al., 2012) and Móricz and colleagues from AFB1 powder (Móricz et al., 2008)

Laser		Reference peak		Peak assignment
785 nm	532 nm	SERS (Wu *et al.*, 2012)	AFB1 powder (Móricz *et al.*, 2008)	
-	446	-	-	Skeletal modes
-	527	-	-	Skeletal modes
560	570	-	-	Skeletal modes
628	628	624	-	Ring deformation
685	685	686	-	C–H in-plane bending
714	712	752	-	C–H out-of-plane bending
756	776		-	Ring modes
776	816	813	-	Ring deformation
829	827	830	832	Ring deformation
930	930	934	-	Ring breath, υ(C–O)
997	988	993	-	β(C–O), υ(C–C)
1079	1077	1086	1072	υ(C–C–C) ring deformation)
1134	1136	1147	1134	β(C–H)(ring), β(C–H)(–CH_3)
1188	1188	1186		γ(C-H_2) (ring)
1238	1237	1249	1242	β(C-H_2) (ring)
1267	1271	1274	1270	β(C–H) ring deformation
1302	1301	1303	1305	A(C–H_2)(ring)(C–H)
1350	1353	1355	1350	δCH3
1427	1445	1440	1431	β(C-H)(CH_3), β(C-H)(ring)
1481	1479	1491	1485	υ(C_7=C_8), ring deformation
1552	1553	1550	1549	υ(C-C) and ring deformation
1592	1591	1592	1591	υ(C-C) and υ(C-C-C)
1630	1630	1620	1616	υC_{17}(H)=C_{18}(H)
1689	1686	1693		υ(C=O) (cyclopentene ring)
1752	1750	1756	1747	υ(C=O) (pyran ring)

5.4 Raman spectroscopy of AFB1 contaminated and uncontaminated maize

Both intentionally AFB1 contaminated and uncontaminated maize kernels and flour were excited with the two lasers and Raman signals detected and measured. Figure 5.6 shows Raman spectra obtained from contaminated kernels and flour after 532 nm and 785 nm excitation. The spectral profiles of the two samples (kernels and flour) were identical with maize kernels having higher intensity than flour at 1552 cm^{-1} and 1593 cm^{-1} peaks in both excitations which could be explained by the high SNR noticed in maize kernel samples discussed in section 5.2. However, at 785 nm excitation the powerful glass peak at 1267 cm^{-1} (that persisted in AFB1 spectrum even after pre-processing) deviated from this since because it does not belong to AFB1. The 1353 cm^{-1} and 1751 cm^{-1} peaks under 532 nm excitation also showed deviations which can be attributed to experimental errors during data acquisition.

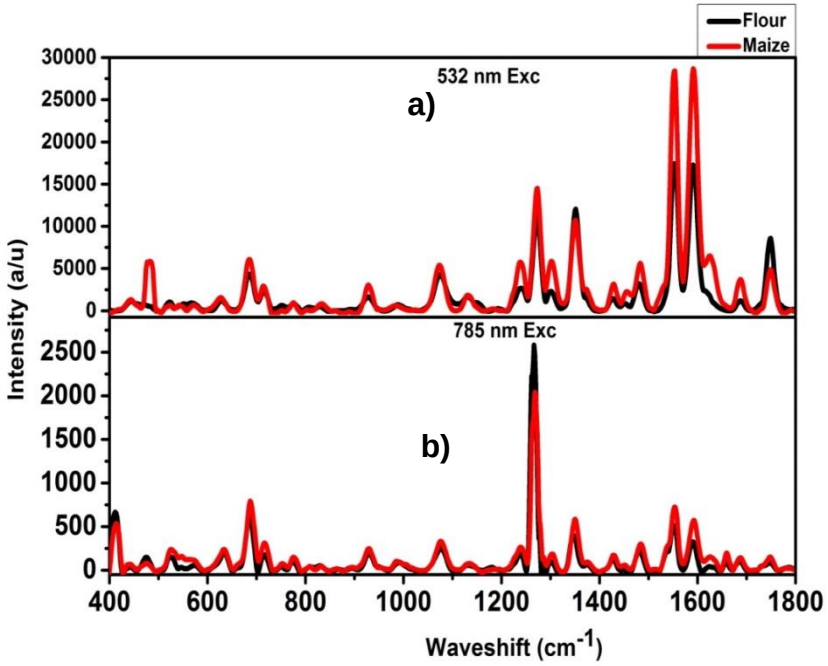

Figure 5.6: Raman spectra of spiked maize and flour excited at 532 nm and 785 nm and centred at 1,100 cm^{-1}. Both maize kernels and flour samples were spiked with $6.1X10^{6}$ ppb

Figure 5.7 displays Raman spectra obtained from maize kernels spiked with different AFB1 concentrations after excitation with a 785 nm laser. Increase in intensity of Raman peaks with concentration was observed (see inset of Figure 5.7) thus showing the great potential of the technique as an AFB1 detection and quantification method. This result also agrees with Equation (3.13) which predicts increase in intensity of Raman spectral profiles with concentration of the active molecule as discussed by (Dieing *et al.*, 2011; Torii *et al.*, 1997). A similar positive relationship between aflatoxin concentration and Raman intensity was also reported by Lee and co-workers on maize flour (Lee *et al.*, 2014).

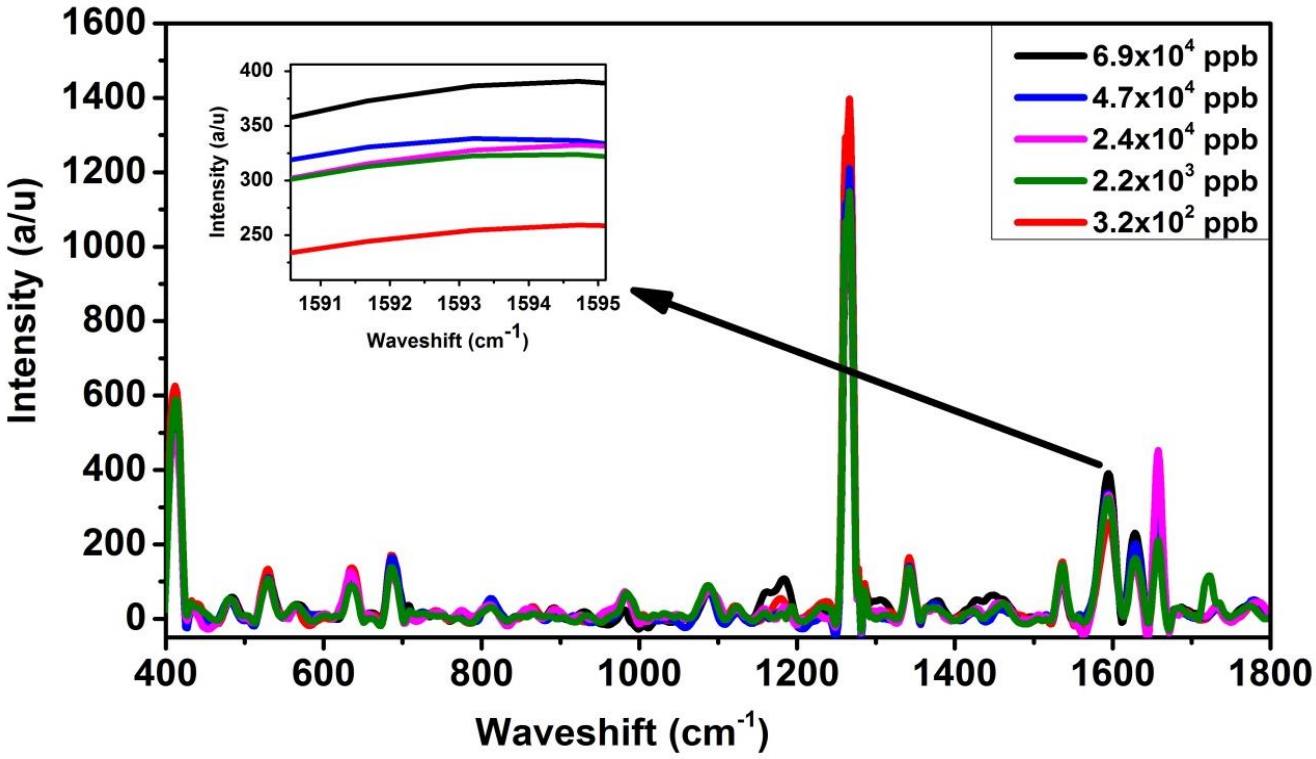

Figure 5.7: Raman spectra of different concentrations of AFB1 in spiked maize kernels excited at 785 nm. The inset shows increase in Raman peak at 1593 cm^{-1} with AFB1 concentration

When many samples are to be screened for presence of aflatoxins, a rapid and sensitive inspection technique is needed. In order to explore the potential of Raman detection technique for this purpose, AFB1 contaminated and uncontaminated maize kernels were both excited with 532 nm and 785 nm laser separately, the spectra were recorded and compared as displayed in Figure 5.8. In both excitations, a significant difference was noticed between Raman profiles from kernels laced with AFB1 and those not laced. Raman peaks attributable to the presence of AFB1 such as 1552 cm^{-1}, 1481 cm^{-1} 1353 cm^{-1} and 1751 cm^{-1} among others were clearly prominent in the contaminated kernels. The results show that Raman spectroscopy can be adapted for a fast screening of maize kernels for example in conveyer belts or inspection in a storage places such as silos. Figure 5.8 also show that the Kenya seed maize used in developing models were not AFB1 free as earlier shown in section 4.4.2. However the levels were low (4.31 ppb) and cannot be quantified by our Raman spectrometer (at 785 and 532 nm excitation) that has maize quantification limit of 10.53; 12.85 ppb and 40.30; 129.36 ppb for maize kernels and flour respectively (see section 5.2).

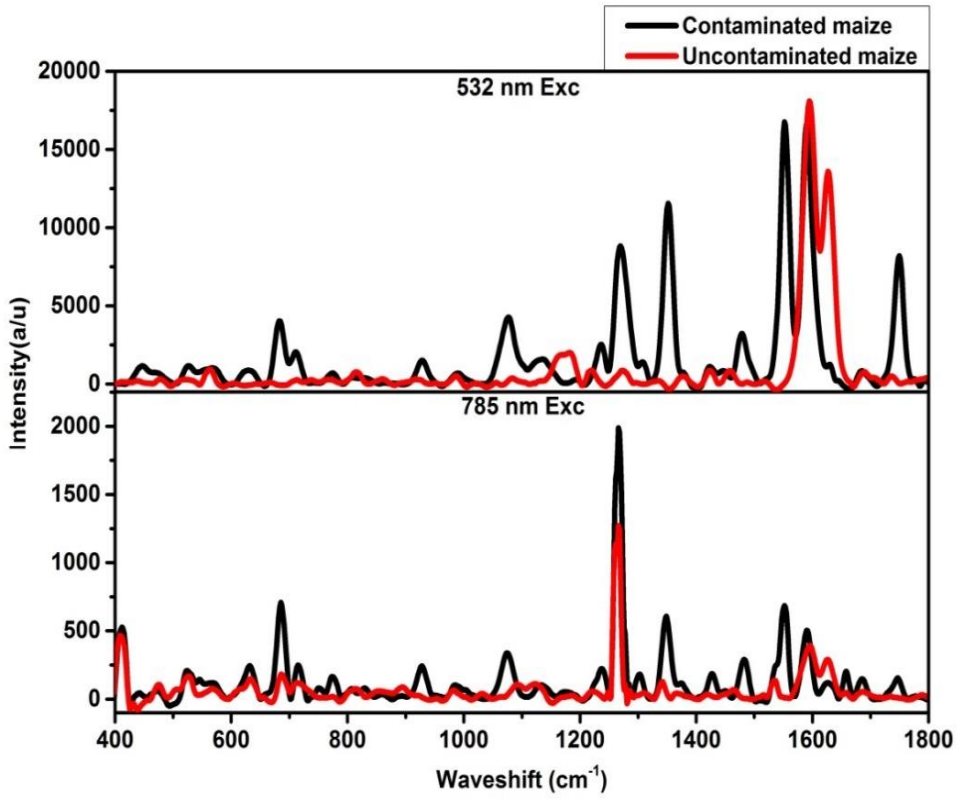

Figure 5.8: Raman spectra of intentionally contaminated and uncontaminated maize kernel excited at 532 and 785 nm. The Contaminated samples displayed spectral profiles with peaks such as 1552 cm^{-1}, 1481 cm^{-1} and 1353 cm^{-1}

5.5 Principal Component Analysis (PCA)

The pre-processed spectral Raman data collected from samples of various concentrations of AFB1 were analysed using PCA. PCA was applied as described earlier in section 3.4.1. The technique uses mathematical projections to express data with many variables (of which some may be correlated) using few variables called principal components (PCs). These new variables (PCs) which are perpendicular to each other are a linear combination of the original variables (Raman signal intensity at each wave shift value). Each PC consists of scores and a loadings counterpart where scores describe associations between samples while loadings describe how

variables relate. Data with identical information will be clustered together in a principal component (PC) score plot.

In the current study, PCA was used to characterize the intentionally contaminated AFB1 maize samples whose concentrations were grouped as described in section 4.4.2. The patterns created by different groups of concentrations were recognized by PCA as shown in the score plots in Figure 5.9. The first two principal components (PCs), PC 1; PC 2 explained the variance in the clusters with 785 nm and 532 nm having the variance of 59 %; 28 % and 62 %; 22 % (71 %; 6 % and 79 %; 7 %) for kernels and flour respectively. This implied that majority of the data points were represented by PC 1. The increased explained variance in PC 1 for samples excited at 532 nm can be attributed to low SNR encountered while acquiring Raman spectra.

For samples excited at 785 nm, (Figures 5.9 (a) and (b)) PCA score plot shows the transition from one concentration range of AFB1 to another. The Raman spectra at this excitation have been clustered into extremely high (C4), high (C3), low (C2) and very low (C1) concentrations based on the strength of υ(C-C) ring deformation, υ(C-C) and υ(C-C-C) molecular bonds as revealed by the loading profile in Figures 5.10 (a) and (b). PC 2 further, classified samples based on AFB1 concentrations with C1 and C2 having lower PC 2 scores as compared to C3 and C4 in both kernels and flour as shown in Figures 5.9 (a) and (b) respectively. The positive loadings observed in Figure 5.10 explains the positive correlation that exists between concentration and Raman intensity just as predicted by Equation 3.12 (Torii *et al.*, 1997).

At 785 nm excitations the spectrometer has highest SNR and low LOD (see section 5.2) and that is why PCA is able to recognize the patterns of both kernel and flour matrix. The concentration ranges are also recognized due to the same reasons. It was difficult to discuss the PCA results

obtained from samples excited at 532 nm as seen in Figure 5.9 (c) and (d). This was thought to be due to the high noise emanating from maize components like starch and fluorescence signals that limit the model from classifying the Raman spectra based on AFB1 concentrations. This noise and fluorescence background were characteristic of 532 nm spectra due to its high excitation power and smaller LSD that caused this laser to have low SNR and high LOD.

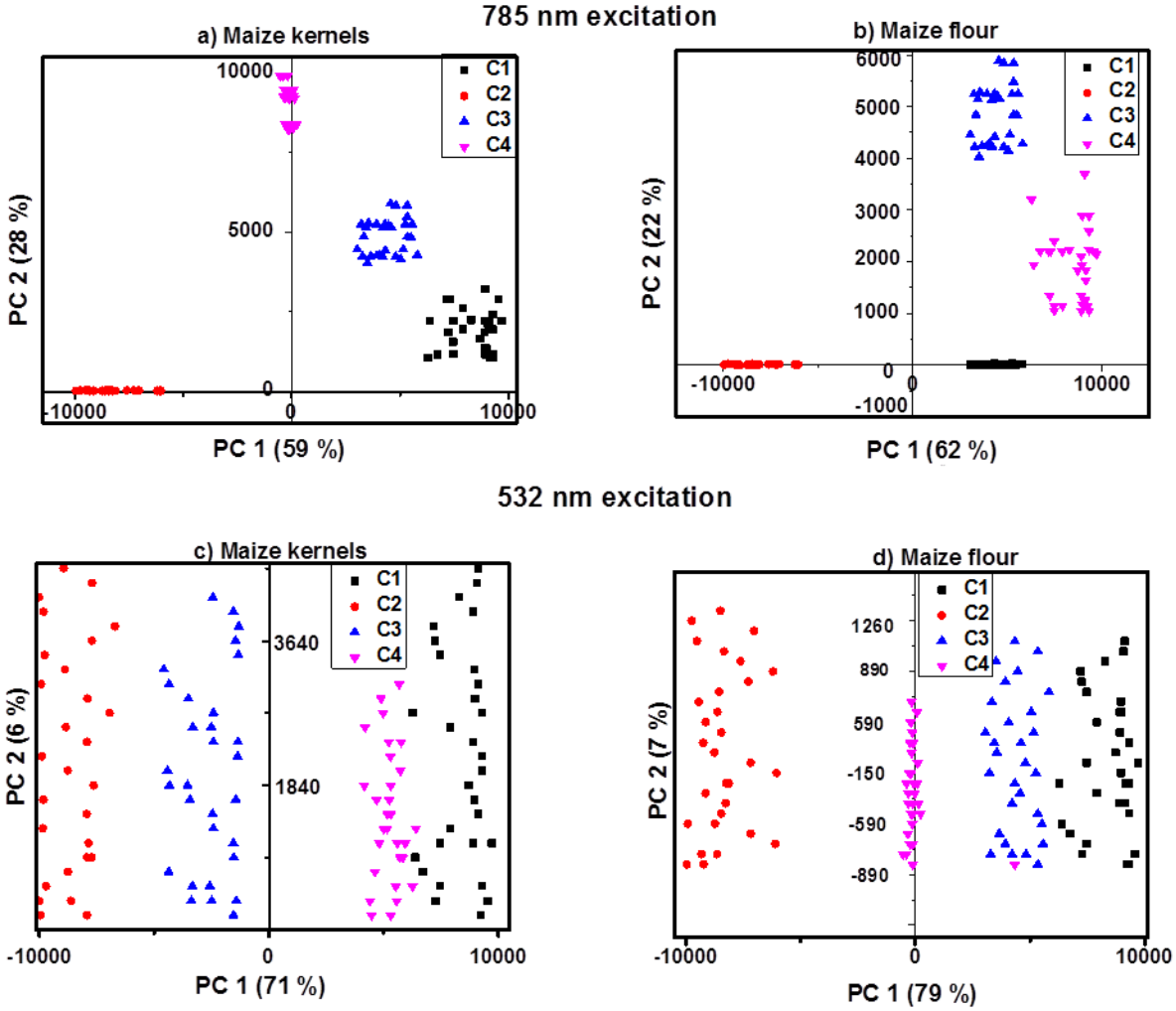

Figure 5.9: PCA score plots of Raman spectra of samples excited at 785 ((a) and (b)) and 532 nm (c) and (d)

All the Raman peaks obtained at 532 nm excitation were found to influence the random clustering in the score plots of Figures 5.9 (c) and (d). This explained why PCA could not classify data obtained with this excitation based on AFB1 concentrations as displayed in PCA profile Figures 5.10 (c) and (d). This was also contributed by low SNR and high LOD as shown in Table 5.1.

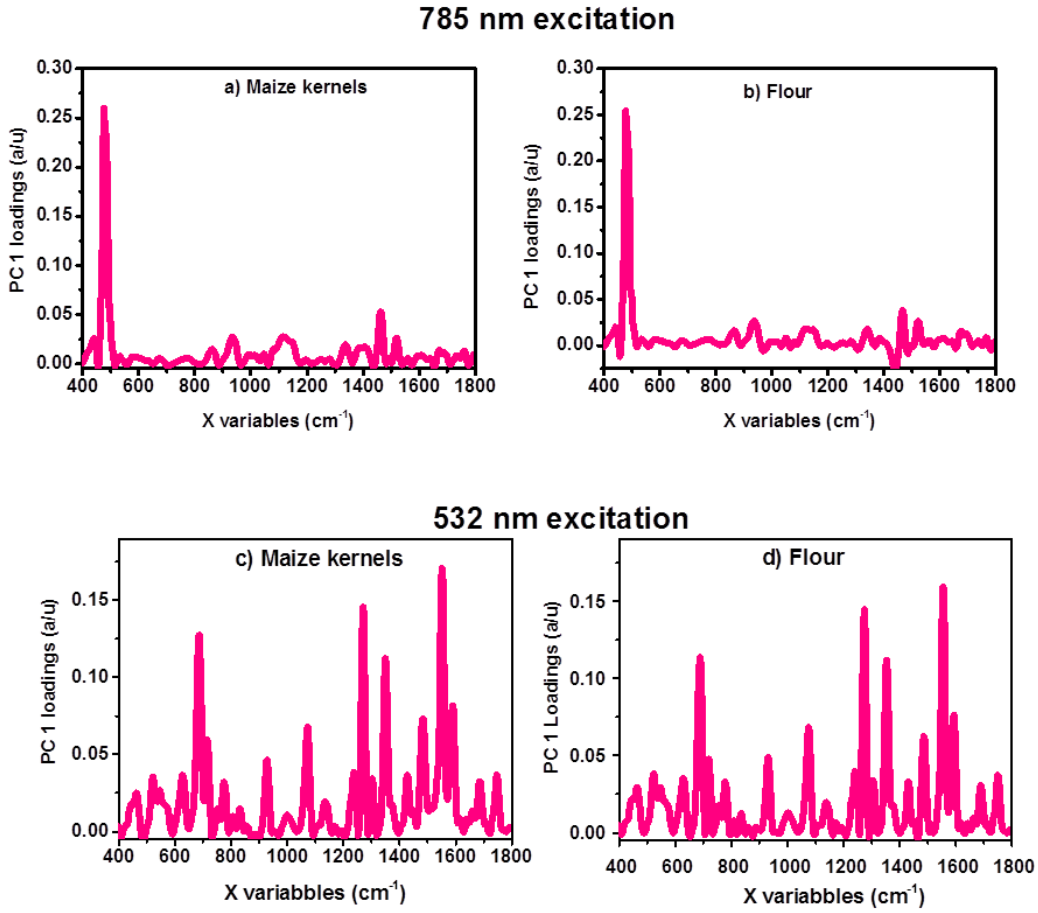

Figure 5.10: PCA loading profiles responsible for score plots for maize kernels and flour samples excited at 785 nm ((a); (b)) and 532 nm ((c); (d)) respectively

In order to find out if PCA could identify samples excited at different wavelengths PCA was done on a few selected samples excited by the two lasers. Figure 5.11 shows the score plot of PCA and the samples represented in the plot had concentrations ranging from 0.15 ppb to 9500

ppb. The explained variance for the two principal are 82 % and 11 % respectively. Samples excited at 785 nm displayed negative scores on both PC 1 and PC 2 (3rd quadrant) while those excited at 532 nm displayed largely positive PC 2 scores. The two data were therefore statistically different as expected due to the different amounts of Raman intensity *(Dieing et al., 2011).*

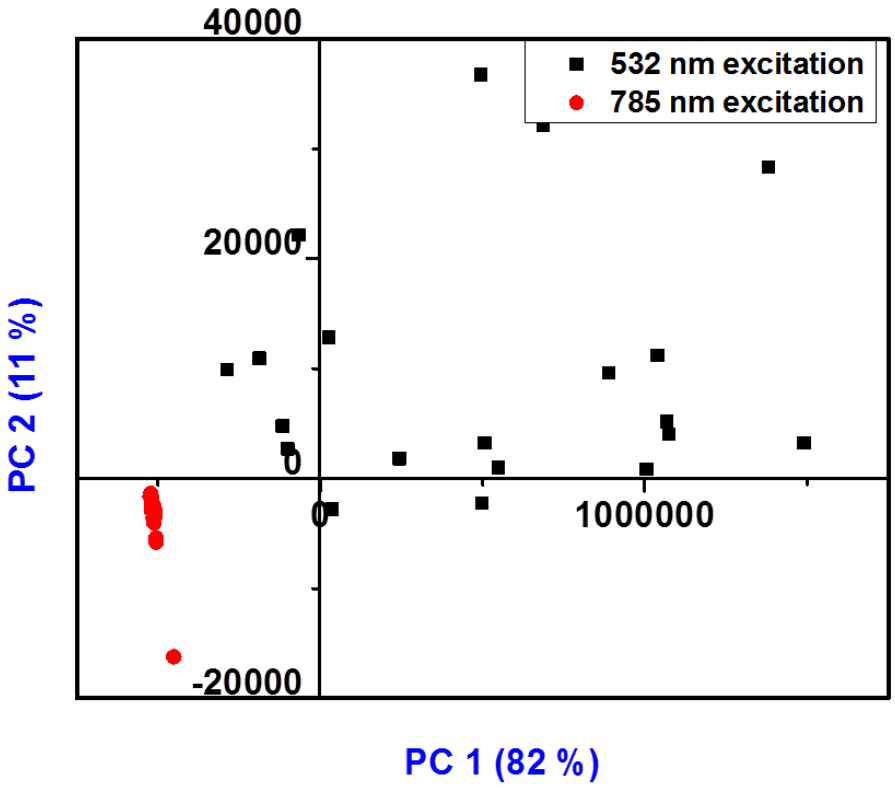

Figure 5.11: PCA score plot of samples excited at both 532 nm and 785 nm. Samples excited at 785 nm laser are clustered at the negative part of PC 1 and PC 2

5.5 Regressions of different samples

Among the maize kernels obtained from Nairobi open markets were those that were suspected to be contaminated already and those that were not. The sorting of these samples was based on visual appearance of the maize. Kernels with coloration were labelled suspected samples and

samples with no colour (white maize) were labelled unsuspected samples as described in section 4.4.2. The task was now to determine the amount AFB1 in the samples.

Furthermore, AFB1 quantification results obtained from Raman spectroscopy had to be compared with the conventional ELISA method whose data served as reference results in this work. For quantification, two chemometric techniques, namely MLR and PLSR were employed. The two methods were shown recently to perform well by Lee and company when applied on maize flour (Lee et al, 2014).

5.5.1 Partial Least Squares Regression (PLSR)

PLSR is a powerful regression algorithm that uses few factors to represent Raman spectral data to predict aflatoxin concentration in the maize samples under study. PLSR calibration models were developed from Raman spectral data that were acquired from maize samples obtained from the Kimaeti Kenya seed with the concentration ranges as described in Table 4.3. The ability of PLSR to predict unknown concentration was determined by full cross validation method of one spectra at a time (Wold *et al.*, 1984). The spectral range of 400 cm^{-1} to 1800 cm^{-1} from 120 samples was used to develop the models that were later used to predict AFB1 concentrations in unknown samples obtained from Nairobi open markets.

Figure 5.12 shows a representative plot of the PLSR calibration and validation models (the other PLSR predicted vs measured plots are shown in Appendix II). The PLSR calibration models resulted in linear regression equations with slopes of 0.94 - 1.03 for kernels and 0.93 - 1.01 for flour and with an average correlation coefficient of determination (R^2) of 0.97 for kernels excited at 785 nm and 0.77 for 532 nm excitation (see Table 5.3). The R^2 obtained from flour were on average 0.93 and 0.74 for 785 nm and 532 nm excitations respectively as shown in Table 5.3.

The high values of Pearson's correlation (0.99 and 0.97 for maize kernels and flour samples respectively) for samples excited at 785 nm indicate that the Raman spectra were well correlated. This resulted in high R^2 values (> 0.93) in samples excited by 785 nm, an indication that these models performed better than models developed from samples excited at 532 nm which had low R^2 value (0.76) and Pearson's correlations (0.83).

Meanwhile the average values of RMSEC (5.74; 7.83), RMSEP (8.29; 8.96), SEC (7.70; 8.29) and SEP (11.00; 9.30) for maize and flour samples excited at 785 nm suggest that these models were accurate and in agreement with the work of Lee and co-workers (Lee *et al.*, 2014). Similar increase in errors is seen in kernels and flour samples excited at 532 nm which have RMSEC values of 12.41 and 40.21 respectively. The high errors in models developed from samples excited at 532 nm were replicated in average values of RMSEP (14.27; 36.88), SEC (14.01; 38.36) and SEP (15.53; 76.43) for maize kernels and flour respectively (see Table 5.3). This still emphasize that PLSR models from 532 nm excitation data were less accurate than 785 nm laser.

In general, based on R^2 and RMSEC, PLSR performed better in predicting AFB1 concentration from Raman spectral data obtained at 785 nm excitation than the models developed from samples excited at 532 nm due to the high SNR exhibited by 785 nm laser as earlier shown in section 5.2. In studies done elsewhere on maize flour, a similar observation on the robustness of PLSR to predict AFB1 concentration was observed (Lee *et al.*, 2014).

The high accuracy in calibration and validation models of samples excited at 785 nm are attributed to the high LSD and low excitation power which caused the laser to have high SNR and low LOD. The R^2 (~1) indicate that the values predicted with this model are accurate and can be adopted in monitoring AFB1 in human food and animal feeds. The high correlation of >

0.9 showed that the data analysed here has minimal experimental errors and that no much information was lost during data pre-processing. Hence the predictions that would be done using these models are valid

However, the high errors characterizing 532 nm laser confirm that this laser is not good in monitoring AFB1 levels and can have serious negative implications if used solely to quantify AFB1 levels in maize. The high calibration errors were due to low SNR that made this laser to have high LOD. The errors particularly affected the C1 and C2 concentration ranges which could not be detected by this laser.

Further research in this field (AFB1 in maize) using Raman spectroscopy should thus involve higher excitation levels of 785 nm and above. However care should be taken while choosing higher excitations as increase in wavelength reduces the power of excitation and result to a low intensity spectrum. The resolution of the spectrometer also reduces with increase in excitation wavelength caused by increase in LSD. The problem with large LSD is the samples will not be well-focused due low resolution.

5.5.2 Multiple Linear Regression (MLR)

MLR is a mathematical technique that makes predictions of one variable based on many variables. Unlike PLSR which uses few components to represent a large data, multiple linear regression (MLR) uses a number of variables in the calibration equation as described earlier in section 3.7.2. It models by finding the coefficients of the linear fit of Equation (3.16). The predictions in MLR models can only take place if the variables are linearly independent since Equation 3.16 involves matrix inversion (Sidik and Center, 1972). This is the reason why some variables were rejected while developing this models. As a result it was only the independent

variables (predictors) that were used in developing the model (Kelly and McNeil, 1975). The requirement of having more samples than predictors for the matrix conversion was achieved using the Unscrumbler Camo software that uses singular value decomposition. MLR does not recognise missing values and as result rejects all variables with missing values.

MLR performs a similar function as PLSR and here both were used for comparison sake. As can be seen in Figure 5.13 (a representation of MLR models, others are found in Appendix III), MLR also gives a linear regression equation. As in the previous regression model (i.e. PLSR), its performance is judged by the value of R^2 and RMSEC. The regression model had average R^2 values of 0.93 and 0.86 for kernels and flour respectively excited at 785 nm. However, at 532 nm excitation we had 0.61 and 0.41 for kernels and flour respectively as displayed in Table 5.4.

From the R^2 squared values it is confirmed 785 nm laser is superior to 532 nm in detection of AFB1 as shown in PLSR. Other errors shown in Table 5.4 also replicate the same conclusion above. Generally in both excitations, MLR performed poorer than PLSR. A similar observation on the performance of both MLR and PLSR models were also reported by Lee and company recently (Lee *et al.*, 2014).

The MLR models were characterized by higher errors than MLR because this model is non-linear and involves matrix inversions thus posing the problem collinearity as discussed in section 3.7.2. The errors were even worse with 532 nm excitation. Thus in choosing chemometric techniques for quantifying AFB1 in maize linear models like PLSR should be used so that the predictions are accurate and reliable.

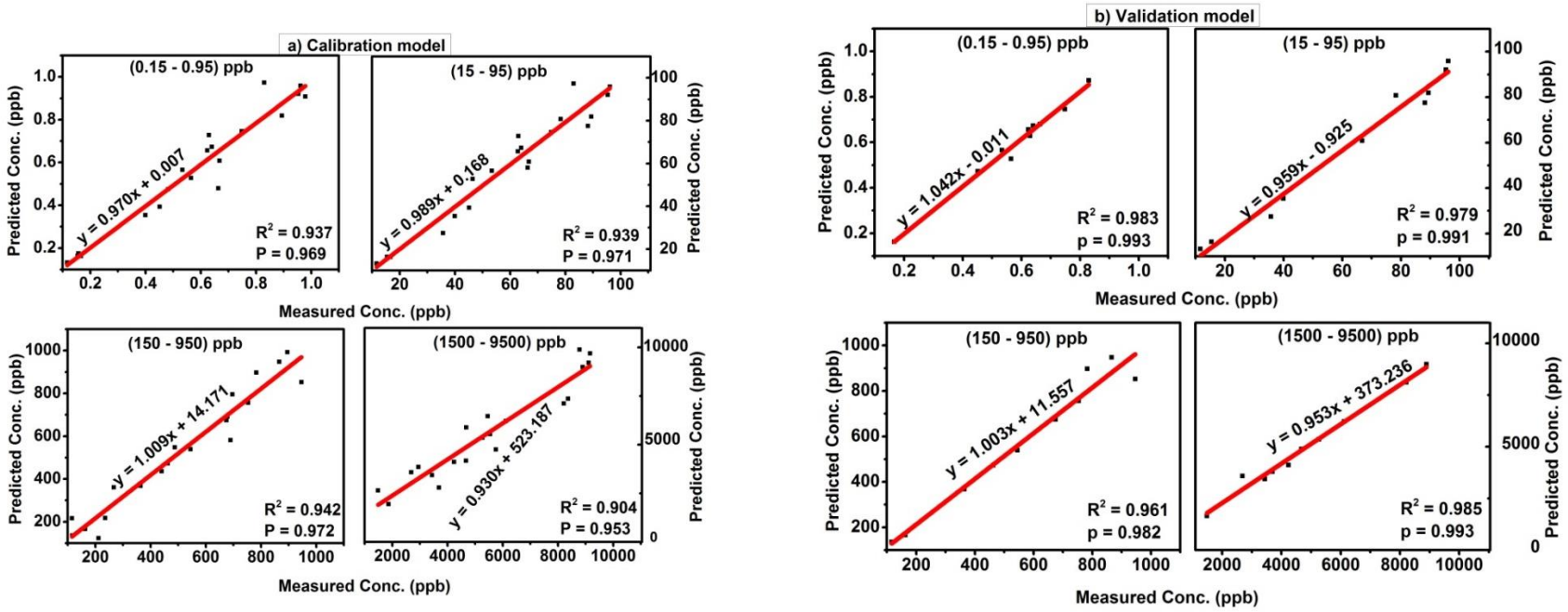

Figure 5.12: The predicted vs measured plot of PLSR for maize kernels excited at 785 nm, (a) the calibration models and (b) validation models

Table 5.3: Extracted PLSR results for maize kernels and flour samples excited at 532 nm and 785 nm

Excitationn	Conc.	RMSEC	RMSEP	SEC	SEP	Correlation		R^2		Slope	
						Calib.	Valid.	Calib.	Valid.	Calib.	Valid.
					Kernels						
785 nm	C1	0.018	0.012	0.008	0.091	0.989	0.98	0.978	0.957	1.031	0.964
	C2	0.096	0.555	0.689	0.119	0.990	0.956	0.978	0.902	0.959	0.829
	C3	3.135	7.123	4.147	13.789	0.980	0.998	0.958	0.995	0.935	1.049
	C4	19.698	25.466	25.963	29.999	0.998	0.992	0.975	0.982	1.011	0.917
	Ave.	5.737	8.289	7.702	11.000	0.989	0.982	0.972	0.959	0.984	0.940
532 nm	C1	0.032	0.066	0.039	0.071	0.45	0.781	0.331	0.462	0.549	0.577
	C2	0.631	0.752	0.788	0.793	0.965	0.999	0.927	0.999	0.867	1.001
	C3	9.835	10.258	11.598	15.147	0.991	0.975	0.982	0.976	0.981	0.862
	C4	39.158	45.987	43.624	46.123	0.918	0.998	0.833	0.997	0.934	1.045
	Ave.	12.414	14.266	14.012	15.534	0.831	0.938	0.768	0.859	0.833	0.872
					FLOUR						
785 nm	C1	0.002	0.006	0.002	0.06	0.969	0.993	0.937	0.983	0.970	1.042
	C2	0.116	0.125	0.118	0.129	0.971	0.991	0.939	0.979	0.989	0.959
	C3	9.835	10.258	9.598	10.147	0.972	0.982	0.942	0.961	1.009	1.003
	C4	21.369	25.466	23.456	26.845	0.953	0.993	0.904	0.985	0.930	0.953
	Ave.	7.831	8.964	8.294	9.295	0.966	0.990	0.931	0.977	0.975	0.989
532 nm	C1	0.120	0.109	0.116	0.458	0.772	0.489	0.574	0.144	0.711	0.463
	C2	0.960	0.882	0.802	2.147	0.752	0.915	0.510	0.817	0.546	1.605
	C3	45.258	40.812	41.852	82.147	0.988	0.980	0.976	0.956	1.012	1.000
	C4	114.524	105.711	110.654	220.961	0.950	0.952	0.917	0.894	0.958	0.942
	Ave.	40.214	36.8785	38.356	76.428	0.866	0.834	0.744	0.703	0.807	1.003

Where Conc., Ave., Calib. and Valid. represent concentration, average, calibration and validation values respectively. The wavelengths used to excite the samples are shown in the first column.

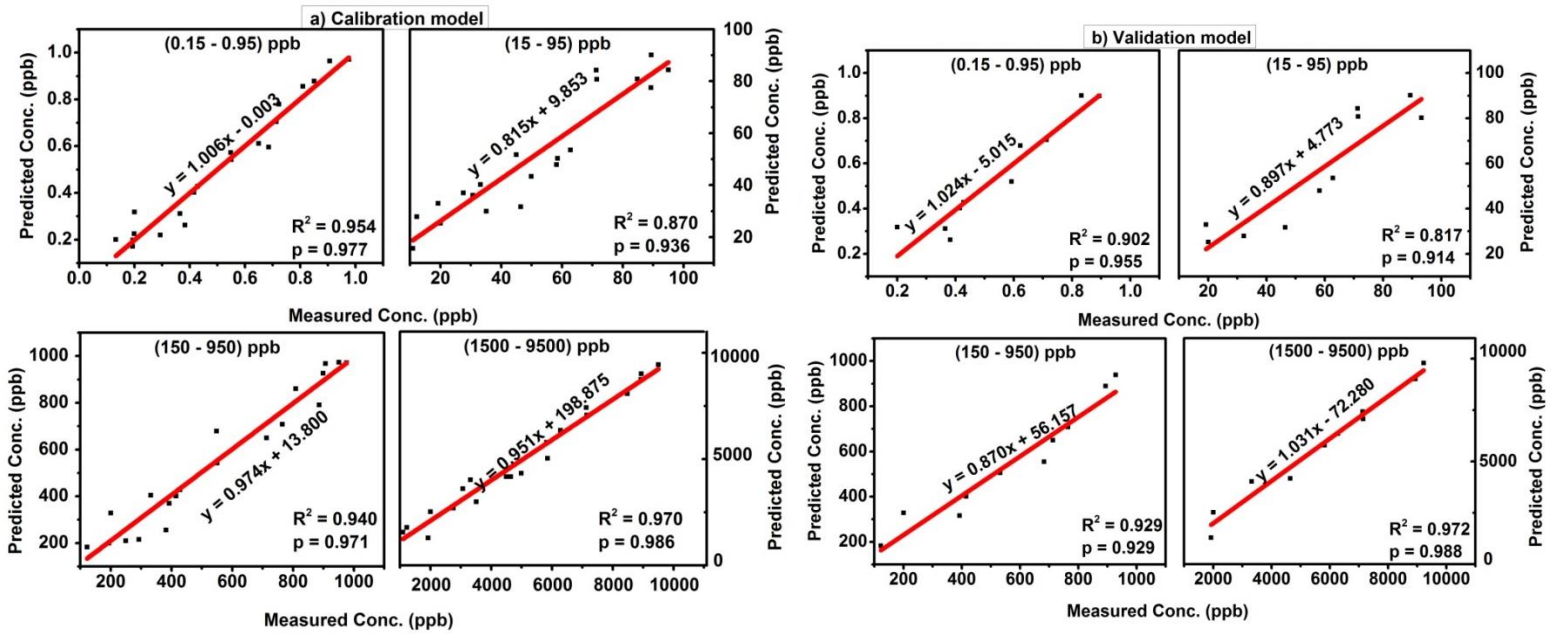

Figure 5.13: The predicted vs measured plot of MLR for maize kernels excited at 785 nm, (a) the calibration models and (b) validation models

Table 5.4: The MLR results for maize kernels and flour samples excited at 785 nm and 532 nm. MLR models revealed more errors than PLSR with samples excited at 532 nm having the highest values

Excitation	Conc.	RMSEC	RMSEP	SEC	SEP	Correlation		R^2		Slope	
						Calib.	**Valid.**	**Calib.**	**Valid.**	**Calib.**	**Valid.**
Kernel samples											
785 nm	C1	0.111	0.210	0.119	0.221	0.969	0.993	0.937	0.983	0.97	1.042
	C2	0.126	0.897	0.574	0.995	0.971	0.991	0.939	0.979	0.989	0.959
	C3	5.115	9.369	7.259	10.725	0.972	0.982	0.942	0.961	1.009	1.003
	C4	23.289	30.789	28.657	34.598	0.953	0.993	0.904	0.985	0.93	0.953
	Average	7.160	10.316	7.702	11.634	0.967	0.990	0.931	0.977	0.975	0.989
532 nm	C1	1.132	1.366	1.214	1.522	0.45	0.781	0.331	0.4621	0.549	0.577
	C2	1.191	2.052	1.968	2.096	0.965	0.999	0.927	0.999	0.867	1.001
	C3	19.835	21.001	20.321	22.512	0.991	0.975	0.982	0.976	0.981	0.862
	C4	95.108	98.258	96.331	99.998	0.918	0.998	0.833	0.997	0.934	1.045
	Average	29.317	30.669	29.959	31.532	0.831	0.938	0.768	0.8586	0.833	0.871
Flour samples											
785 nm	C1	0.201	0.986	0.789	0.823	0.989	0.980	0.978	0.957	1.031	0.964
	C2	0.419	1.212	0.933	1.936	0.99	0.956	0.978	0.902	0.959	0.829
	C3	6.353	7.222	7.123	8.012	0.98	0.998	0.958	0.995	0.935	1.049
	C4	22.060	28.442	27.146	30.179	0.998	0.992	0.975	0.982	1.011	0.917
	Average	7.258	9.466	9.000	10.237	0.989	0.982	0.972	0.959	0.984	0.940
532 nm	C1	2.591	3.698	3.334	5.994	0.772	0.489	0.574	0.144	0.711	0.463
	C2	5.981	6.146	6.019	7.290	0.752	0.915	0.51	0.817	0.546	1.605
	C3	25.211	29.169	27.412	31.224	0.988	0.98	0.976	0.956	1.012	1
	C4	125.159	147.937	140.684	159.355	0.95	0.952	0.917	0.894	0.958	0.942
	Average	39.736	46.738	44.362	50.966	0.866	0.834	0.744	0.705	0.807	1.003

5.5.3 Predictions of unknown samples

Raman spectra obtained from maize samples collected from Nairobi open markets were preprocessed as described earlier in section 4.3. The PLSR and MLR models developed in sections 5.5.2 and 5.5.3 were then used to predict AFB1 concentrations in the samples. Models developed from data generated by 785 nm excitation were selected for predictions as they gave the least errors of prediction and highest R^2 values. The results of this predictions were averaged and classified according to the labels of the samples (suspected and unsuspected) as indicated in Tables 5.5.

Samples predicted by PLSR models gave better predictions with low deviations (mean standard deviation of 3.48 in unsuspected and 27.02 for suspected maize flour samples). However, MLR models were characterized by high mean standard deviations of 22.33 and 71.85 for the unsuspected and suspected samples respectively, which could be linked to the low R^2 values obtained while developing these models due to the non-linearity nature of this model.

Tables 5.5 show that suspected maize had higher levels of AFB1 than unsuspected samples in both PLSR and MLR just as expected. PLSR model predicted that the unsuspected maize consumed in Nairobi had AFB1 levels ranging from 12 ppb to 869 ppb while suspected samples had AFB1 levels as high as 1.87×10^4 ppb. Similar results were found in North Eastern province of Kenya in the year 2007 (Daniel *et al.*, 2011) using ELISA method. MLR models were characterized by extreme standard deviations that were averaged to 25 and 48 for suspected and unsuspected samples respectively which make predictions of this model unreliable.

The levels of AFB1 in unsuspected maize were higher than the allowable AFB1 levels consumed in Kenya with PLSR. Thus it is not always accurate to conclude that white looking maize is good

for consumption. The suspected maize was confirmed to be unsuitable for consumption. Thus for the fungi to be physically observed in maize it means that maize has extremely high AFB1 levels (> 1000 ppb) and should be sorted out of food meant for human consumption. Suspected maize also should not be used as animal feed as the levels in them are higher than the allowable levels (300 ppb) in animal feeds.

The MLR models are characterized with very high deviations and that is why they misclassified suspected maize as unsuspected maize and vice versa. These errors also contributed in sample M24, M31, M35 and M44 having same standard deviations even though they had different levels of AFB1. The predictions also confirm that PLSR model is superior to MLR model.

Table 5.5: Average predictions and deviations of suspected and unsuspected maize flour excited at 785 nm

Model	**Suspected samples**		**Unsuspected samples**	
	Predicted levels (ppb)	Mean standard deviation	Predicted levels (ppb)	Mean standard deviation
PLSR	$1.19 \times 10^3 – 1.88 \times 10^4$	27.02	12.05 – 818.00	3.48
MLR	$560.59 – 1.84 \times 10^4$	71.85	94.04 – 971.35	22.02

5.5.4 Validation of Partial Least Squares regression (PLSR) and Multiple Linear Regression (MLR) models using ELISA

The ground maize samples from CIMMYT were first analysed by Raman spectra as earlier described in section 4.4.2 and AFB1 concentrations were predicted by PLSR and MLR models developed in section 5.5.1 and 5.5.2. These levels of AFB1 found by Raman spectroscopy are compared to those obtained from ELISA in Table 5.6. Sample P6 was not reflected in Table 5.6 because its spectra was averaged with that of P12 as the two samples were found to have the same level of AFB1. Using these results PLSR and MLR models developed in this work were validated.

AFB1 levels in most of the samples excited at 785 nm were correlated with the reference (ELISA) measurements with only sample P27 having a deviation greater than 15 ppb. This could have been brought about with experimental errors since Raman is a weak scattering and any movement near the system may cause the peaks on the spectrum to shift. The shift from reference values increased with MLR up to a difference of 60 ppb in P27 sample (see Table 5.6)

The mean deviations in samples excited at 785 nm with PLSR was -5.40 which makes this model valid in detection and quantification of AFB1. However the MLR models had higher errors (> 10 ppb) which are even higher than the allowable limits in human food. The errors are even worse in samples excited at 532 nm (in hundredths) in both PLSR and MLR. Therefore this excitation should not be used to detect AFB1 in food and feeds. Samples excited at 532 nm deviated most from the reference values in both regressions (PLSR and MLR) especially in P27, P116, P9 and P62

Table 5.6: Compares the results of AFB1 levels obtained by ELISA and Regression models (PLSR and MLR)

Flour samples	Conc. (ppb) of AFB1 using ELISA	PLSR (ppb)		MLR (ppb)	
		785 nm	532 nm	785 nm	532nm
P38	840.459	850.600	945.567	885.222	1042.245
P43	598.800	565.040	660.381	644.812	359.876
P41	465.400	455.258	550.179	525.114	651.984
P130	405.800	408.640	506.658	445.778	609.781
P27	125.500	183.400	678.369	65.590	372.359
P116	40.860	42.688	100.158	85.596	241.001
P9	96.250	95.147	112.369	36.487	296.555
P14	77.470	79.976	105.987	117.445	277.547
P12/P6	700.200	715.162	790.125	691.004	505.230006
P62	80.500	89.510	110.815	40.335	298.522

Pearson's correlation coefficients of 0.99 and 0.74 for PLSR and 0.99 and 0.59 for MLR models of flour samples excited by 785 nm and 532 nm respectively were obtained as given in Figure 5.14. This implied that the AFB1 levels in unknown samples were satisfactorily predicted with an average R^2 value of 0.99 for 785 nm excitation. The 532 nm excitation models gave low R^2 values (0.74 and 0.59 for PLSR and MLR models) which could be linked to low SNR obtained from spectra of samples excited at this wavelength. The ratio of the standard deviation of the reference (ELISA) values to the standard error of cross-validation values followed the same trend as presented in Table 5.7.

Generally the data obtained in this work was well correlated both in model development and in validating them (Table 5.7). The high R^2 values are indications that the models were accurate. In studies done elsewhere on maize flour, Raman spectroscopy predicted AFB1 concentration

values that were highly correlated with reference HPLC values (Lee et al, 2014) thus confirming the potential application of this technique for aflatoxins screening and quantification.

Table 5.7: Statistical summary of PLSR and MLR models in predicting the unknown concentration of AFB1 in Nairobi open market maize

Chemometric technique and excitation	s	R^2	p
PLSR with 785 nm	4.199	0.993	0.997
PLSR with 532 nm	2.927	0.735	0.974
MLR with 785 nm	3.259	0.993	0.987
MLR with 532 nm	2.025	0.591	0.798

Where s and p represent the ratio of standard deviation of reference values and the standard error of cross validation and Pearson's correlation coefficient respectively

From the ratio of standard deviation of reference values and the standard error of cross validation it can be concluded that PLSR model can quantify AFB1 in maize better than MLR model. The high R^2 (0.99) and Pearson's correlation coefficient (0.99) obtained at 785 nm excitation confirms that Raman spectrometer is indeed a robust, rapid and non-invasive method of aflatoxin B1 detection and quantification.

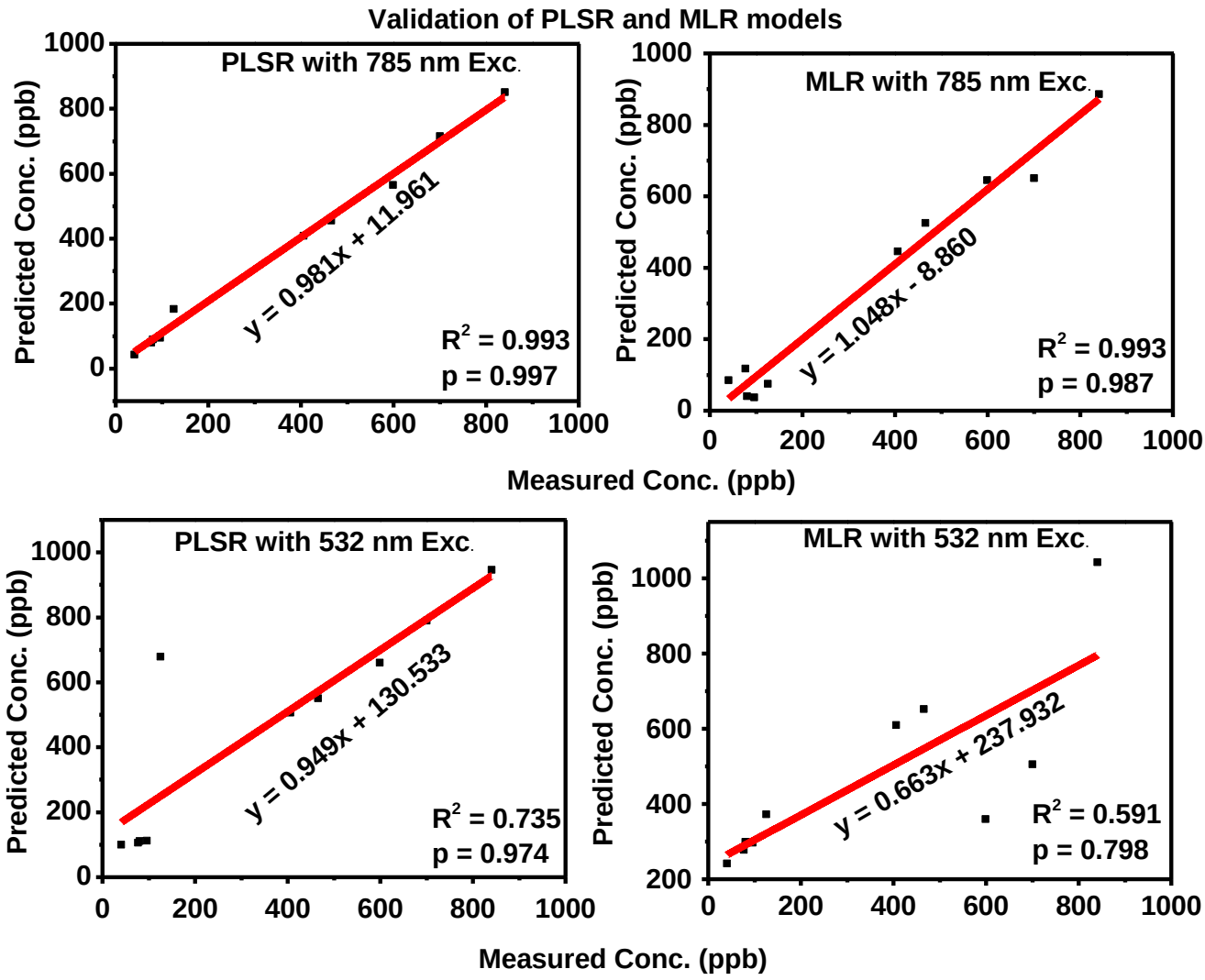

Figure 5.14: The predicted (measurements from PLSR and MLR models) vs measured (ELISA measurements) plot of samples excited at 785 nm and 532 nm

CHAPTER 6: CONCLUSION AND RECOMMENDATIONS

6.1 Conclusion

This study was undertaken to explore Raman spectroscopy as an alternative AFB1 detection technique which is fast, non-invasive, reliable and with a potential for field deployment. There are few reports on the application of this technique in detection and quantification of this highly toxic and carcinogenic chemical in maize kernels and flour. Here Raman data obtained from intentionally contaminated and uncontaminated samples were analysed using chemometric models; PCA, MLR and PLSR. Steady state absorption and fluorescence spectroscopy on AFB1 in methanol was also carried out in order to obtain its characteristic ground state and excited state absorption and emission spectra respectively.

AFB1 being toxic has limited researchers studying its steady state characteristics and this has made this information rare in literature. Here we report of fluorescence and absorbance steady state properties of AFB1. The absorption and fluorescence were centred at 340 nm and 440 nm respectively. Both absorbance and fluorescence intensities increased with increase in concentration and had three small maxima attributed to first three vibrational states in the ground state and first excited states respectively. Methanol absorption was also found at 280 nm when excited in the UV-VIS-NIR regions.

It has been shown that most of Raman peaks found either by long procedures of SERS can easily be found by adsorbing AFB1 on a glass slide. The twenty two Raman active peaks were registered on the Raman signature with the most prominent peak being 1552 cm^{-1} and 1593 cm^{-1} for 785 nm and 532 nm lasers respectively which agree with literature. Raman spectra of AFB1 found with 532 nm excitation have ten times more intensity than 785 nm excitation with SNR of

4 and 12 respectively. This was contributed by the high excitation power at 532 nm. At the same time standard AFB1 adsorbed on a glass slide gave a better Raman profile than AFB1 dissolved in methanol inside cuvette giving an alternative to SERS done by other researchers. The SNR of AFB1 adsorbed on glass slide and in cuvette was found as 14 and 4.5 respectively for 785 nm excitation. However, SNR of AFB1 adsorbed on glass slide at 532 nm excitation was 6 and for AFB1 solution in cuvette were 2.5.

Moreover, it has been shown that chemometric aided Raman spectrometer model is a superior alternative to the traditional quantitative methods used in detection of AFB1 such as ELISA and HPLC. PCA was used for data exploration and it was found that 1552 cm^{-1} and 1593 cm^{-1} peaks (assigned to υ(C-C) ring deformation and υ(C-C)/ υ(C-C-C)) were responsible for detection of AFB1. The use of Chemometrics also confirmed that 785 nm excitation of AFB1 is better than 532 nm excitation. Raman spectrometer with the help of PLSR was able to quantify AFB1 levels in Nairobi in white maize (unsuspected samples) meant for human consumption within 12 ppb to 869 ppb range. It was also confirmed in this work that suspected maize (fungi infected) is neither good for human nor animal consumption. Suspected maize samples recorded AFB1 concentrations with PLSR in the order of 10^4 ppb values. These levels are far higher than the accepted limits of feeds and human food. Indeed Raman spectrometer can provide a rapid cheap and reliable method of detecting AFB1.

In conclusion, Raman spectroscopy equipped with 785 nm laser with PLSR models can be used to monitor AFB1 levels in human food and animal feeds. Models developed from samples excited at 532 nm and PLSR can only be used in monitoring AFB1 levels in animal feeds. MLR models should be avoided in AFB1 monitoring systems since they are nonlinear and pose

collinearity problems in quantifying AFB1 levels in maize. This is because AFB1 levels depend on a linear relationship between intensity and number of molecules of AFB1.

6.2 Recommendations

Use of pellets and simulates could be considered in the future to improve on the spectra acquired and consequently improve the detection and quantification limits. This will aid in detection and quantification of AFB1 in lower concentrations found in infant cornmeal. Other aflatoxins (B2, G1, G2 and total) could also be studied in maize kernels since they are also carcinogenic. This could be done in selected regions of Kenya. Such studies could be important in monitoring aflatoxin intake among Kenyans. We also recommend the use 785 nm excitation or higher excitation wavelengths in the analysis of AFB1.

REFERENCES

Abdi, H. and Williams, L. J. (2010). Principal component analysis. *Wiley Interdiscip. Rev. Comput. Stat.* **2**, 433–459.

Afoakwa, E. O. and Sefa-Dedeh, S. (2001). Chemical composition and quality changes occurring in Dioscorea dumetorum pax tubers after harvest. *Food Chem.* **75**, 85–91.

Alcaide-Molina, M., Ruiz-Jiménez, J., Mata-Granados, J. M., and Castro, M. L. de (2009). High through-put aflatoxin determination in plant material by automated solid-phase extraction on-line coupled to laser-induced fluorescence screening and determination by liquid chromatography–triple quadrupole mass spectrometry. *J. Chromatogr. A* **1216**, 1115–1125.

Ali, N., Hashim, N. H., Saad, B., Safan, K., Nakajima, M., and Yoshizawa, T. (2005). Evaluation of a method to determine the natural occurrence of aflatoxins in commercial traditional herbal medicines from Malaysia and Indonesia. *Food Chem. Toxicol. Int. J. Publ. Br. Ind. Biol. Res. Assoc.* **43**, 1763–1772.

Bacaloni, A., Cavaliere, C., Cucci, F., Foglia, P., Samperi, R., and Laganà, A. (2008). Determination of aflatoxins in hazelnuts by various sample preparation methods and liquid chromatography–tandem mass spectrometry. *J. Chromatogr. A* **1179**, 182–189.

Basappa, V. S. (1970). Aflatoxin and kojic acid production by resting cells of Aspergillus flavus Link. *J. Gen. Microbiol.* **61**, 81–6.

Bhat, R. V., Shetty, P. H., Amruth, R. P., and Sudershan, R. V. (1997). A foodborne disease outbreak due to the consumption of moldy sorghum and maize containing fumonisin mycotoxins. *J. Toxicol. Clin. Toxicol.* **35**, 249–255.

Bowen, J. M., Sullivan, P. J., Blanche, M. S., Essington, M., and Noe, L. J. (1989). 'Optical-fiber raman spectroscopy used for remote in-situ environmental analysis.' Google Patents.

Burke, E. A. (2001). Raman microspectrometry of fluid inclusions. *Lithos* **55**, 139–158.

Carranza, J. E., Iida, K., and Hahn, D. W. (2003). Conditional data processing for single-shot spectral analysis by use of laser-induced breakdown spectroscopy. *Appl. Opt.* **42**, 6022–6028.

Cary, J. W., Klich, M. A., and Beltz, S. B. (2005). Characterization of aflatoxin-producing fungi outside of Aspergillus section Flavi. *Mycologia* **97**, 425–432.

Centers for Disease Control and Prevention (CDC) (2004). Outbreak of aflatoxin poisoning-eastern and central provinces, Kenya, January-July 2004. *MMWR Morb. Mortal. Wkly. Rep.* **53**, 790–793.

Csele, M. (2004). 'Fundamentals of light Sources and Lasers'.J. A. John Wiley and sons, Inc., New Jersey Canada.

Cornes, T. (2012). 'STR Spectrum System Manual.' Software Version, Chome Tokyo

Daniel, J. H., Lewis, L. W., Redwood, Y. A., Kieszak, S., Breiman, R. F., Flanders, W. D., Bell, C., Mwihia, J., Ogana, G., Likimani, S., Straetemans, M., and McGeehin, M. A. (2011).

Comprehensive Assessment of Maize Aflatoxin Levels in Eastern Kenya, 2005–2007. *Environ. Health Perspect.* **119**, 1794–1799.

Demtröder, W. (2011). 'Atoms, Molecules and Photons: An Introduction to Atomic-, Molecular- and Quantum Physics', 2nd ed. 2010 editionth ed. Springer, Heidelberg; London.

Dheeraj, K. S., Erdene-Ochir, G., Eun-min, C., Kwang-Hwi, C., Jaebum, C., and Sehun, K. (2013). Detection of the mycotoxin citrinin using silver substrates and Raman spectroscopy. *J. Hazard. Mater.* **265C**, 89–95.

Dieing, T., Hollricher, O., and Toporski, J. (2011). 'Confocal Raman Microscopy.' Springer Berlin Heidelberg, Berlin, Heidelberg.

Dirr, H. W. (1987). Solvent effects on the spectroscopic properties of aflatoxin B1. *Int. J. Bichemistry* **19**, 1137–1140.

Egmond, H. P. van, Schothorst, R. C., and Jonker, M. A. (2007). Regulations relating to mycotoxins in food. *Anal. Bioanal. Chem.* **389**, 147–157.

Falk, M. and Ford, T. A. (1966). Infrared Spectrum and Structure of Liquid Water. *Can. J. Chem.* **44**, 1699–1707.

Frelka, J. C. and Harris, L. J. (2014). Nuts and Nut Pastes. *In* 'The Microbiological Safety of Low Water Activity Foods and Spices' (J.B. Gurtler, M.P. Doyle, J.L. Kornacki, Eds.), pp213–244. Springer New York.

Fujita, K., Sugiyama, J., Tsuta, M., Shibata, M., Kokawa, M., Onda, H., and Sagawa, T. (2013). Detection of Aflatoxins B_1, B_2, G_1 and G_2 in Nutmeg Extract Using Fluorescence Fingerprint. *Food Sci. Technol. Res.* **19**, 539–545.

Fung, F. and Clark, R. F. (2004). Health effects of mycotoxins: a toxicological overview. *J. Toxicol. Clin. Toxicol.* **42**, 217–234.

Galvin, M. and Zerulla, D. (2011). The Extreme Low-Frequency Raman Spectrum of Liquid Water. *ChemPhysChem* **12**, 913–914.

Ghanem, I., Orfi, M., and Shamma, M. (2008). Effect of gamma radiation on the inactivation of aflatoxin B1 in food and feed crops. *Braz. J. Microbiol.* **39**, 787–791.

Gunes, A., Kalkan, H., Durmus, E., and Butukcan, M. B. (2013). Detection of aflatoxin contaminated figs using Near-Infrared (NIR) reflectance spectroscopy. *In* '2013 International Conference on Electronics, Computer and Computation (ICECCO)', pp123–126.

Herzallah, S., Alshawabkeh, K., and Fataftah, A. A. (2008). Aflatoxin Decontamination of Artificially Contaminated Feeds by Sunlight, γ-Radiation, and Microwave Heating. *J. Appl. Poult. Res.* **17**, 515–521.

Hoeltz, M., Welke, J. E., Noll, I. B., and Dottori, H. A. (2010). Photometric procedure for quantitative analysis of Aflatoxin B1 in peanuts by thin-layer chromatography using charge coupled device detector. *Quím. Nova* **33**, 43–47.

Hruska, Z., Yao, H., Kincaid, R., Brown, R., Cleveland, T., and Bhatnagar, D. (2014). Fluorescence Excitation–Emission Features of Aflatoxin and Related Secondary Metabolites and Their Application for Rapid Detection of Mycotoxins. *Food Bioprocess Technol.* **7**, 1195–1201.

Hruska, Z., Yao, H., Kincaid, R., Brown, R., Cleveland, T., and Bhatnagar, D. (2009). Evaluating the Relationship Between Aflatoxin Concentration and Hyperspectral Fluorescence Response in Single Corn Kernels. *In* 'ISM Conference.' International Society for Mycotoxicology, Tulln, Austria.

Hyunh, T., Ly, C., Knight, P., and Wolde-Mariam, W. (2012). Quantitation of Aflatoxin B1 by ELISA in Commodities that Pose a Matrix Effect. *In* 'Presented at AOAC 126th Annual Meeting.'

Ivanova, B. and Spiteller, M. (2014). Raman Spectroscopic and Mass Spectrometric Determination of Aflatoxins. *Food Anal. Methods* **7**, 242–256.

Jurado-López, A., Luque de Castro, M. D., and others (2003). Chemometric approach to laser-induced breakdown analysis of gold alloys. *Appl. Spectrosc.* **57**, 349–352.

Kalkan, H., Güneş, A., Durmuş, E., and Kuşçu, A. (2014). Non-invasive detection of aflatoxin-contaminated figs using fluorescence and multispectral imaging. *Food Addit. Contam. Part Chem. Anal. Control Expo. Risk Assess.* **31**, 1414–1421.

Kaya-Celiker, H., Mallikarjunan, P. K., Schmale III, D., and Christie, M. E. (2014). Discrimination of moldy peanuts with reference to aflatoxin using FTIR-ATR system. *Food Control* **44**, 64–71.

Kelly, F. J. and McNeil, J. T. (1975). 'Testing Research Hypotheses Using Multiple Linear Regression.' Southern Illinois University Press.

Khayoon, W. S., Saad, B., Yan, C. B., Hashim, N. H., Ali, A. S. M., Salleh, M. I., and Salleh, B. (2010). Determination of aflatoxins in animal feeds by HPLC with multifunctional column clean-up. *Food Chem.* **118**, 882–886.

Lee, K.-M., Herrman, T. J., Nansen, C., and Yun, U. (2013). Application of Raman spectroscopy for qualitative and quantitative detection of fumonisins in ground maize samples. *Int. J. Regul. Sci.* **1**, 1–14.

Lee, K.-M., Herrman, T. J., and Yun, U. (2014). Application of Raman spectroscopy for qualitative and quantitative analysis of aflatoxins in ground maize samples. *J. Cereal Sci.* **59**, 70–78.

Lewis, L., Onsongo, M., Njapau, H., Schurz-Rogers, H., Luber, G., Kieszak, S., Nyamongo, J., Backer, L., Dahiye, A. M., Misore, A., DeCock, K., Rubin, C., and Kenya Aflatoxicosis Investigation Group (2005). Aflatoxin contamination of commercial maize products during an outbreak of acute aflatoxicosis in eastern and central Kenya. *Environ. Health Perspect.* **113**, 1763–1767.

May, O. E., Moyer, A. J., Wells, P. A., and Herrick, H. T. (1931). The Production of Kojic acid by Aspergillus Flavus. *J. Am. Chem. Soc.* **53**, 774–782.

McCreery, R. L. (2005). 'Raman spectroscopy for chemical analysis.' John Wiley & Sons.

Medders, G. R. and Paesani, F. (2015). Infrared and Raman Spectroscopy of Liquid Water through 'First-Principles' Many-Body Molecular Dynamics. *J. Chem. Theory Comput.* **11**, 1145–1154.

Mirghani, M. E. S., Man, Y. B. C., Jinap, S., Baharin, B. S., and Bakar, J. (2002). FTIR spectroscopic determination of soap in refined vegetable oils. *J. Am. Oil Chem. Soc.* **79**, 111–116.

Móricz, Á. M., Horváth, E., Ott, P. G., and Tyihák, E. (2008). Raman spectroscopic evaluation of the influence of Pseudomonas bacteria on aflatoxin B1 in the BioArena complex bioautographic system. *J. Raman Spectrosc.* **39**, 1332–1337.

Mosier-Boss, P. A., Lieberman, S. H., and Newbery, R. (1995). Fluorescence rejection in Raman spectroscopy by shifted-spectra, edge detection, and FFT filtering techniques. *Appl. Spectrosc.* **49**, 630–638.

Myakalwar, A. K., Sreedhar, S., Barman, I., Dingari, N. C., Rao, S. V., Kiran, P. P., Tewari, S. P., and Kumar, G. M. (2011). Laser-induced breakdown spectroscopy-based investigation and classification of pharmaceutical tablets using multivariate chemometric analysis. *Talanta* **87**, 53–59.

Netto-Ferreira, J. C., Heyne, B., and Scaiano, J. C. (2011). Photophysics and photochemistry of aflatoxins B1 and B2. *Photochem. Photobiol. Sci. Off. J. Eur. Photochem. Assoc. Eur. Soc. Photobiol.* **10**, 1701–1708.

Norris, J. L. and Caprioli, R. M. (2013). Analysis of Tissue Specimens by Matrix-Assisted Laser Desorption/Ionization Imaging Mass Spectrometry in Biological and Clinical Research. *Chem. Rev.* **113**, 2309–2342.

Ononye, A. E., Yao, H., Hruska, Z., and Kincaid, R. (2010). Calibration of a fluorescence hyperspectral imaging system for agricultural inspection and detection. Vol. 7676, pp76760E–76760E–11.

Pearson, T. C. and Schatzki, T. F. (1998). Machine Vision System for Automated Detection of Aflatoxin-Contaminated Pistachios. *J. Agric. Food Chem.* **46**, 2248–2252.

Pearson, T. C., Wicklow, D. T., Maghirang, E. B., Xie, F., and Dowell, F. E. (2001). DETECTING AFLATOXIN IN SINGLE CORN KERNELS BY TRANSMITTANCE AND REFLECTANCE SPECTROSCOPY. *Trans. ASAE* **44**.

Pestka, J. J. and Chu, F. S. (1984). Aflatoxin B1 dihydrodiol antibody: production and specificity. *Appl. Environ. Microbiol.* **47**, 472–477.

Pitt, J. I. and Hocking, A. D. (2009). 'Fungi and Food Spoilage', 3rd ed. 2009 editionth ed. Springer, New York.

Quintero, L. A., Hunt, S. D., and Diem, M. (2006). Denoising of raman spectroscopy signals.

Ribeiro, J., Cavaglieri, L., Vital, H., Cristofolini, A., Merkis, C., Astoreca, A., Orlando, J., Caru, M., Dalcero, A., and Rosa, C. A. R. (2011). Effect of gamma radiation on Aspergillus flavus and Aspergillus ochraceus ultrastructure and mycotoxin production. *Radiat. Phys. Chem.*, 658–663.

Robens, J. and Cardwell, K. (2003). The costs of mycotoxin management to the USA: management of aflatoxins in the United States. *Toxin Rev.* **22**, 139–152.

Rocha, M. E. B., Freire, F. C. O., Maia, F. E. F., Guedes, M. I. F., and Rondina, D. (2014). Mycotoxins and their effects on human and animal health. *Food Control* **36**, 159–165.

Ryder, A. G., O'Connor, G. M., Thomas J, G., and others (2000). Quantitative analysis of cocaine in solid mixtures using Raman spectroscopy and chemometric methods. *J. Raman Spectrosc.*

Sato-Berrú, R. Y., Medina-Valtierra, J., Medina-Gutiérrez, C., and Frausto-Reyes, C. (2004). Quantitative NIR–Raman analysis of methyl-parathion pesticide microdroplets on aluminum substrates. *Spectrochim. Acta. A. Mol. Biomol. Spectrosc.* **60**, 2231–2234.

Sharma, S. K., Angel, S. M., Ghosh, M., Hubble, H. W., and Lucey, P. G. (2002). Remote pulsed laser Raman spectroscopy system for mineral analysis on planetary surfaces to 66 meters. *Appl. Spectrosc.* **56**, 699–705.

Shaver, J. M. (2001). Chemometrics for Raman spectroscopy. *Pract. Spectrosc. Ser.* **28**, 275–306.

Sidik, S. M. and Center, L. R. (1972). 'An improved multiple linear regression and data analysis computer program package.' National Aeronautics and Space Administration.

Smith, E. and Dent, G. (2005). 'Modern Raman Spectroscopy: A Practical Approach', 1st editio. Wiley, Hoboken, NJ.

Stroka, J. and Anklam, E. (2002). New strategies for the screening and determination of aflatoxins and the detection of aflatoxin-producing moulds in food and feed. *TrAC Trends Anal. Chem.* **21**, 90–95.

Technology, C. for A. S. and (2003). 'Mycotoxins: Risks in Plant, Animal, and Human Systems.' Council for Agricultural, Ames, Iowa.

Thirumala-Devi, K., Mayo, M. A., Reddy, G., Emmanuel, K. E., Larondelle, Y., and Reddy, D. V. R. (2001). Occurrence of ochratoxin A in black pepper, coriander, ginger and turmeric in India. *Food Addit. Contam.* **18**, 830–835.

Torbert, R. (2002). Special Issue: Aflatoxin/Fumonisin Elimination and Fungal Genomics Workshops; Phoenix Arizona, October 23-26 2001. *Mycopathologia* **155**, 1–122.

Torii, H., Ishikawa, A., and Tasumi, M. (1997). Electron-vibration interaction and the Raman intensities of a quinoid molecule. *J. Mol. Struct.* **413–414**, 73–79.

Tripathi, S. and Mishra, H. N. (2009). A rapid FT-NIR method for estimation of aflatoxin B1 in red chili powder. *Food Control* **20**, 840–846.

Wang, X., Niessner, R., and Knopp, D. (2014). Magnetic Bead-Based Colorimetric Immunoassay for Aflatoxin B1 Using Gold Nanoparticles. *Sensors* **14**, 21535–21548.

Wang, Z., Feng, J., Li, L., Ni, W., and Li, Z. (2011). A multivariate model based on dominant factor for laser-induced breakdown spectroscopy measurements. *J. Anal. At. Spectrom.* **26**, 2289–2299.

Wellner, N., Georget, D. M. R., Parker, M. L., and Morris, V. J. (2011). In situ Raman microscopy of starch granule structures in wild type and ae mutant maize kernels. *Starch - Stärke* **63**, 128–138.

Westland, J. C. (2007). Confirmatory analysis with partial least squares. *Abregufen Am* **20**, 2007.

Wold, S., Ruhe, A., Wold, H., and Dunn, I., W. (1984). The Collinearity Problem in Linear Regression. The Partial Least Squares (PLS) Approach to Generalized Inverses. *SIAM J. Sci. Stat. Comput.* **5**, 735–743.

Wu, X., Gao, S., Wang, J.-S., Wang, H., Huang, Y.-W., and Zhao, Y. (2012). The surface-enhanced Raman spectra of aflatoxins: spectral analysis, density functional theory calculation, detection and differentiation. *The Analyst* **137**, 4226–4234.

Wu, Y., Gao, Q., and Zhang, Y. (2015). A robust baseline elimination method based on community information. *Digit. Signal Process.* **40**, 53–62.

Wu, Z., Zhang, C., and Stair, P. C. (2006). Influence of absorption on quantitative analysis in Raman spectroscopy. *Catal. Today* **113**, 40–47.

Yao, H., Hruska, Z., Brown, R. L., and Cleveland, T. E. (2006). Hyperspectral bright greenish-yellow fluorescence (BGYF) imaging of aflatoxin contaminated corn kernels. Vol. 6381, pp63810B–63810B–8.

Yao, H., Hruska, Z., Kincaid, R., Brown, R., Cleveland, T., and Bhatnagar, D. (2010). Correlation and classification of single kernel fluorescence hyperspectral data with

aflatoxin concentration in corn kernels inoculated with Aspergillus flavus spores. *Food Addit. Amp Contam. Part Chem. Anal. Control Expo. Amp Risk Assess.* **27**, 701–9.

Zöllner, P. and Mayer-Helm, B. (2006). Trace mycotoxin analysis in complex biological and food matrices by liquid chromatography–atmospheric pressure ionisation mass spectrometry. *J. Chromatogr. A* **1136**, 123–169.

Appendix I

Safety precautions for aflatoxins

Aflatoxins are highly toxic and carcinogenic substances as mentioned earlier. Thus strict measures were taken when handling them as enlisted below.

- Disposable gloves, lab coats, aprons and mouth masks were always worn before handling aflatoxin and aflatoxin-contaminated samples as shown.

- Since aflatoxins are electrostatic in nature and can disperse easily in working areas, they were first dissolved in Methanol before carrying out any experiment on them. AFB1 solutions were made in the fume chamber.
- Aflatoxins are subject to light degradation. Therefore in order to prevent our AFB1 solution from degradation different solutions were wrapped by aluminium foil as shown below.

- The glass vessels containing aflatoxin were kept in wooden containers packed with adsorbent materia1 to protect them from UV light that would have destroyed aflatoxin

strength and the containers were clearly labelled to avoid contaminating unsuspecting individuals.

- Any accidental aflatoxin spillages were swapped with 1% sodium hypochlorite bleach (NaOCl) and left for 10 min before adding 5 % aqueous acetone.
- Laboratory areas where work with aflatoxins took place was indicated and demarcated with warning notices such as 'DANGER - AFLATOXIN - CARCINOGEN HANDLING AREA'.
- Used laboratory coats and aprons were also soaked in 5% NaOCl solution overnight before normal washing took place.
- Any contamination of working area could easily be tracked using a long-wave UV lamp due to fluorescence characteristics of aflatoxins.
- In case of aflatoxin skin contamination, the affected area were immediately washed with 5% sodium hypochlorite followed by washing the skin with soap or any skin friendly detergent and then rinsed thoroughly with water.
- Contaminated waste materials (used syringes and gloves) were kept in tightly closed containers and were not mixed with other waste materials. They were later incinerated.
- Eating, drinking and smoking in the laboratory were prohibited to avoid food contamination.

Appendix II

Levels of AFB1 in solutions meant for developing quantification models

Table 7.1: Different concentrations in ppb of solutions used to contaminate maize samples from Kimaeti Kenya seed for developing classification and quantification models

Sample	Sample group	C11	C12	C13	C14	C15	C16	C17	C18	C19	C110	C111	C112	C113	C114	C115
Conc. (ppb)	C1 (0.15-0.95)	0.15	0.2	0.25	0.3	0.35	0.4	0.45	0.5	0.55	0.6	0.65	0.7	0.75	0.8	0.85
Sample		C21	C22	C23	C24	C25	C26	C27	C28	C29	C210	C211	C212	C213	C214	C215
Conc. (ppb)	C2 (15-95)	15	20	25	30	35	40	45	50	55	60	65	70	75	80	85
Sample		C31	C32	C33	C34	C35	C36	C37	C38	C39	C310	C311	C312	C313	C314	C315
Conc. (ppb)	C3 (150-950)	150	200	250	300	350	400	450	500	550	600	650	700	750	800	850
Sample		C41	C42	C43	C44	C45	C46	C47	C48	C49	C410	C411	C412	C413	C414	C415
Conc. (ppb)	C4 (1500-9500)	1500	2000	2500	3000	3500	4000	4500	5000	5500	6000	6500	7000	7500	8000	8500
Sample	Sample group	C116	C117	C118	C119	C120	C121	C122	C123	C124	C125	C126	C127	C128	C129	C130
Conc. (ppb)	C1 (0.15-0.95)	0.9	0.95	0.15	0.2	0.3	0.4	0.5	0.6	0.7	0.8	0.9	0.15	0.25	0.35	0.45
Sample		C216	C217	C218	C219	C220	C221	C222	C223	C224	C225	C226	C227	C228	C229	C230
Conc. (ppb)	C2 (15-95)	90	95	15	20	30	40	50	60	70	80	90	15	25	35	45
Sample		C316	C317	C318	C319	C320	C321	C322	C323	C324	C325	C326	C327	C328	C329	C330
Conc. (ppb)	C3 (150-950)	900	950	150	200	300	400	500	600	700	800	900	150	250	350	450
Sample		C416	C417	C418	C419	C420	C421	C422	C423	C424	C425	C426	C427	C428	C429	C430
Conc. (ppb)	C4 (1500-9500)	9000	9500	1500	2000	3000	4000	5000	6000	7000	8000	9000	1500	2500	3500	4500

Appendix III

Partial Least Squares Regression

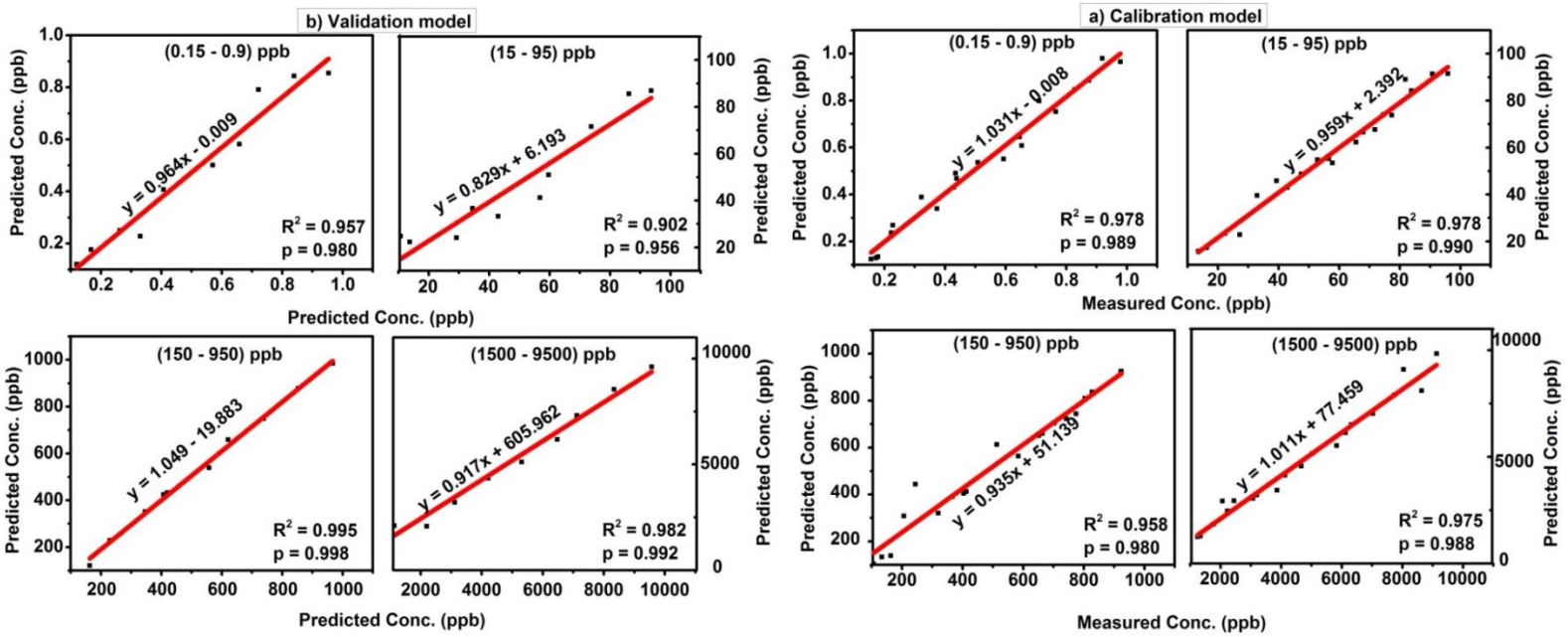

Figure 7.1: PLSR calibration and validation models for flour samples excited at 785 nm. The models are categorized according to the concentration range. In (a) the calibration samples are presented while (b) shows the validation samples. The slopes are slightly lower than their counterpart in Figure 512.. An indication that maize kernels are good for building PLSR models.

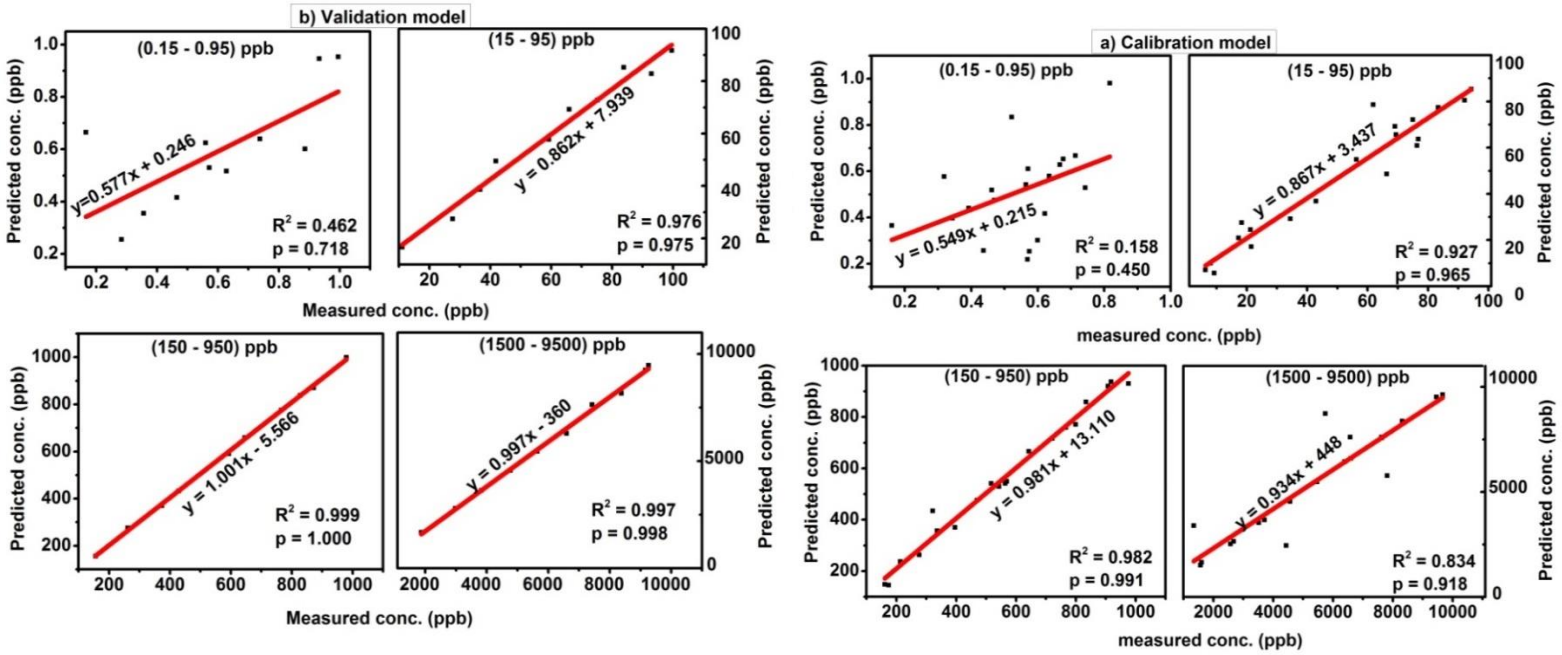

Figure 7.2: PLSR calibration and validation models for maize kernels at 532 nm excitation. PLSR gives very low slope (<6) for both calibration and validation models in the lowest concentration range (0.15 ppb – 0.95 ppb).This confirms that 532 nm laser is limited in quantification of AFB1 in lower concentrations.

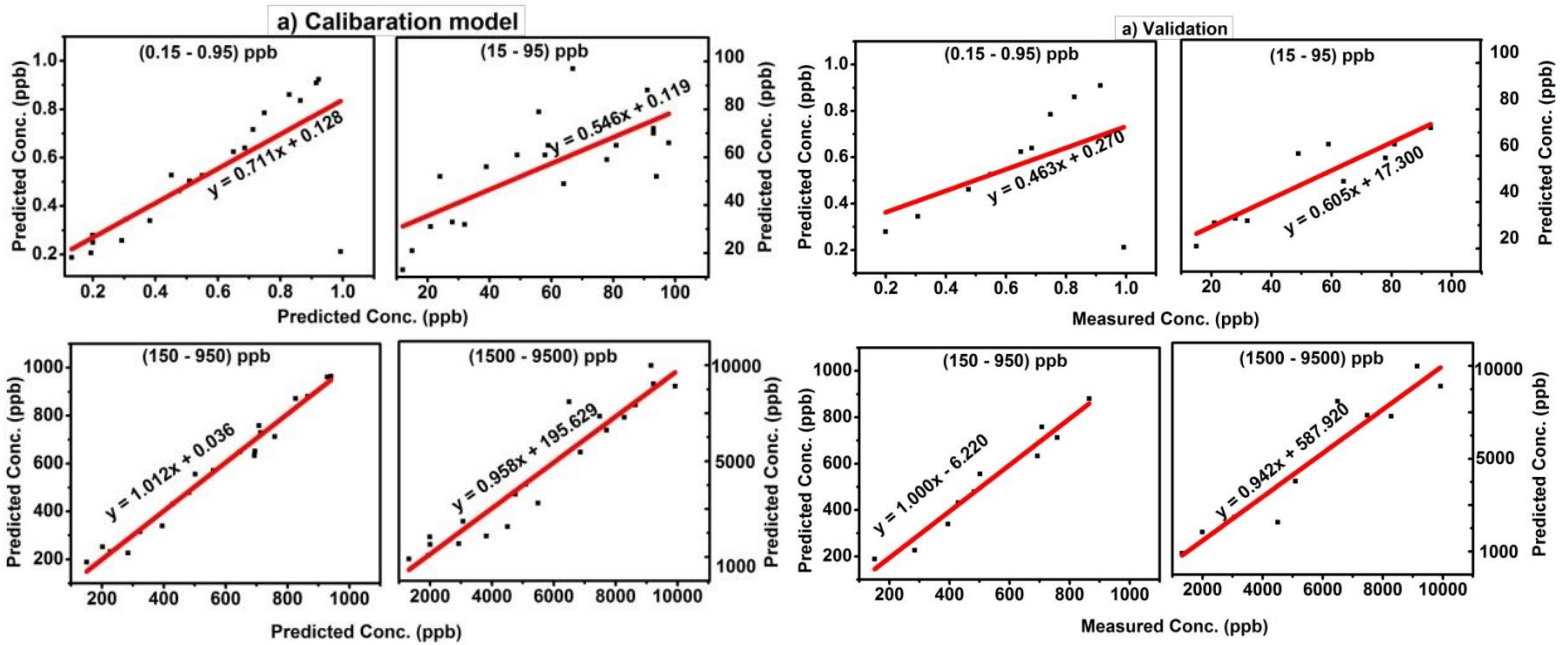

Figure 7.3: PLSR calibration and validation models for flour samples at 532 nm excitation. The models are worse than their counterpart in Figure 7.1. This is because the slope values for C1 (0.15 ppb – 0.95 ppb) and C2 (15 ppb – 95 ppb) ranges are poor (<6). This confirms that 532 nm laser is not suitable for Quantification of AFB1 in maize flour samples. In quantification AFB1 in maize using 532 nm excitation, it is advisable to use whole grains.

Appendix IV

Multiple Linear Regression models (MLR)

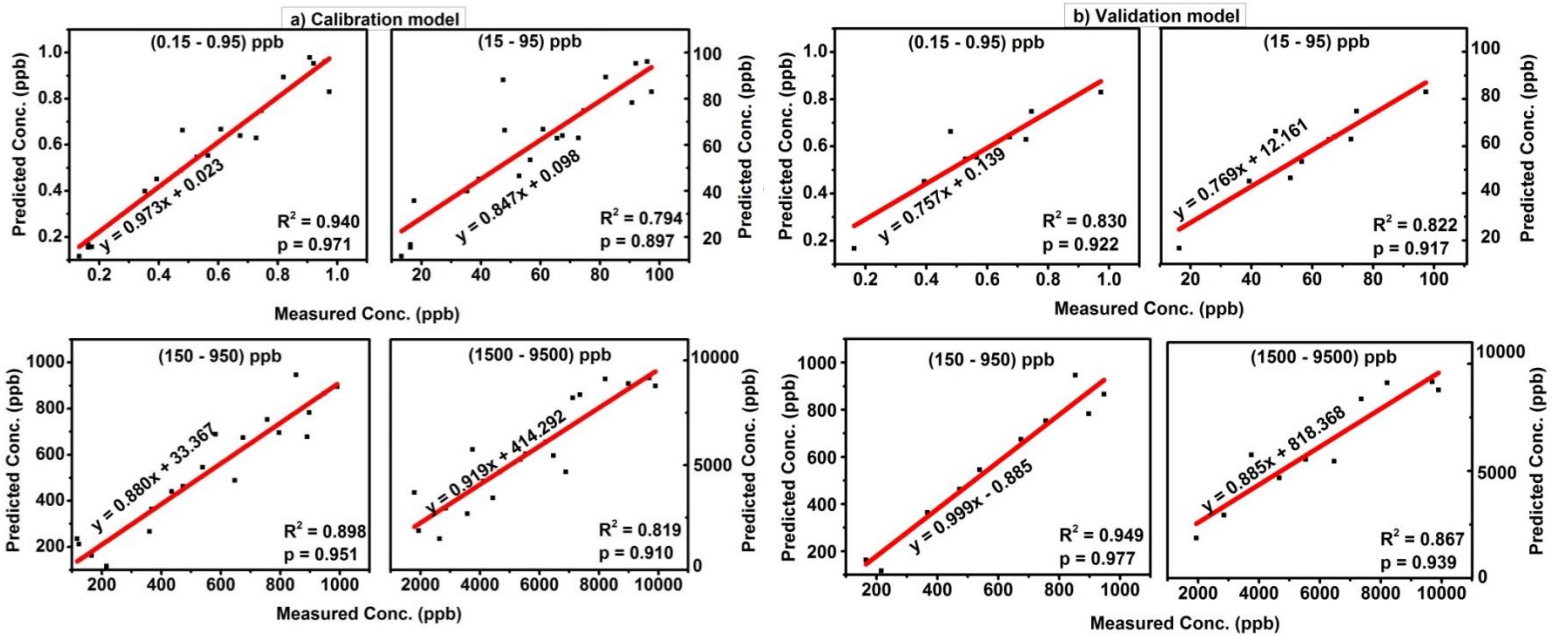

Figure 7.4: MLR calibration and validation models for flour samples at 785 nm excitation. The gradients of this models lower than those obtained from the same regression for kernel samples in Figure 7.3.

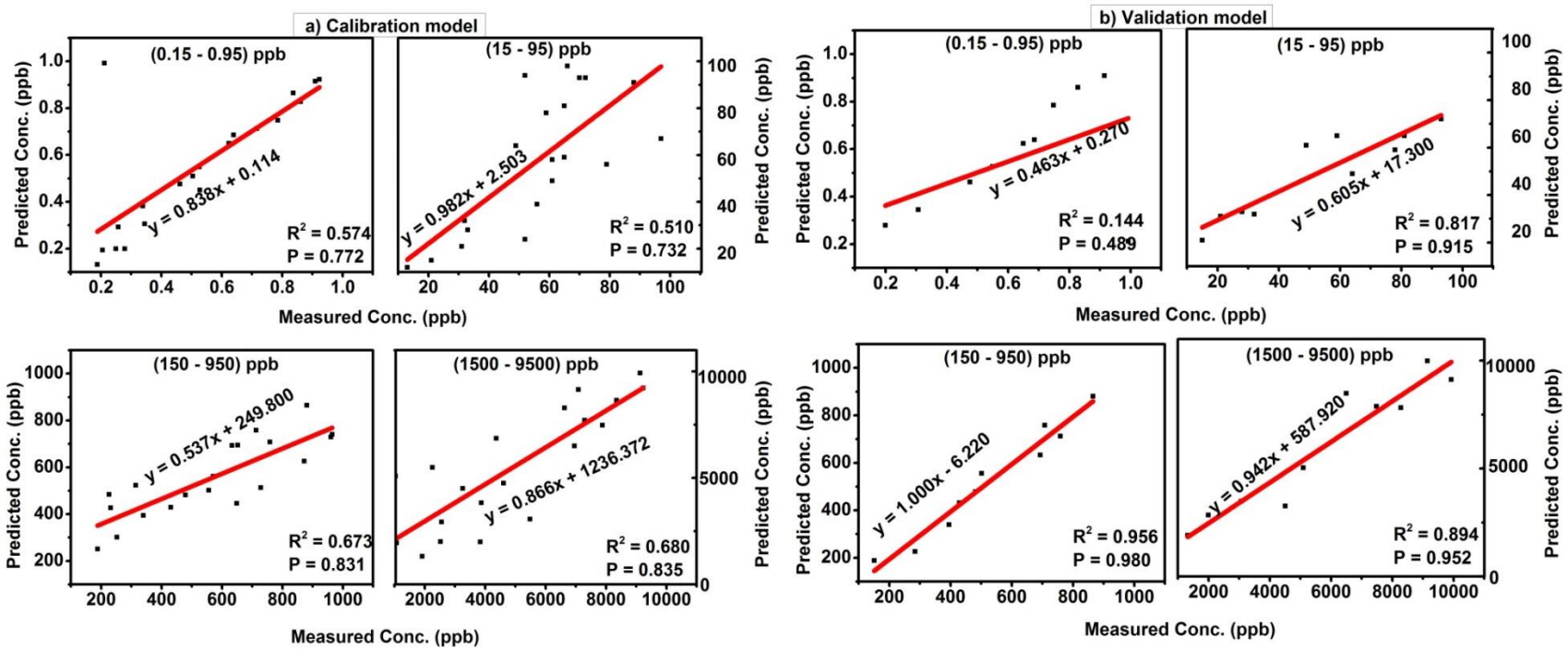

Figure 7.5: MLR calibration and validation models for maize kernels at 532 nm excitation. Just like in PLSR the calibration and Validation gradients of these models are lower than those derived from 785 nm excitation in Figures 7.3 and 7.4.

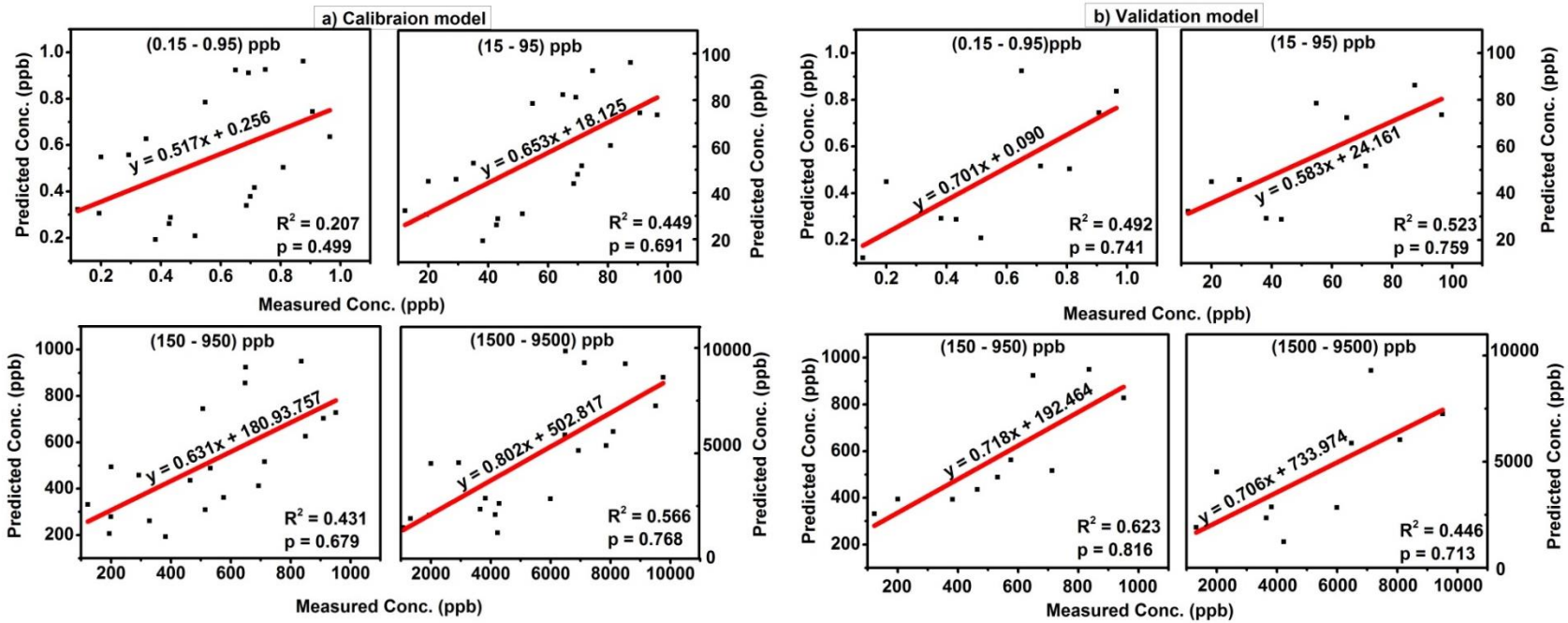

Figure 7.6: MLR calibration and validation models for flour samples at 532 nm excitation. This model displays the lowest gradients among all the models.

Table 7.2: The predicted concentrations in ppb for unsuspected samples with unknown concentrations. The samples were excited at 785 nm using PLSR model

Unsuspected samples															
Sample	M1	M2	M3	M4	M5	M6	M7	M8	M9	M10	M11	M12	M13	M14	M15
Predicted	666.83	687.98	791.91	12.053	26.591	808.94	19.283	719.89	91.589	28.297	814.54	818.00	654.17	677.95	281.16
Deviation	1.214	3.402	7.071	0.532	0.622	3.113	0.342	8.713	2.394	0.468	3.533	1.374	2.568	1.477	3.252
Sample	M16	M17	M18	M19	M20	M21	M22	M23	M24	M25	M26	M27	M28	M29	M30
Predicted	298.95	15.738	70.942	90.566	73.161	308.92	507.94	128.22	158.32	177.20	281.88	306.58	171.35	210.75	869.00
Deviation	9.858	0.017	2.113	1.112	0.604	7.154	5.241	5.310	5.446	6.503	2.614	19.996	9.508	2.826	4.085
Sample	M31	M32	M33	M34	M35	M36	M37	M38	M39	M40	M41	M42	M43	M44	M45
Predicted	194.03	187.34	151.31	168.36	356.10	556.46	560.59	641.83	711.54	220.14	325.69	717.44	838.01	650.72	803.18
Deviation	2.747	1.876	3.838	3.546	1.053	1.439	2.672	4.55	2.843	0.129	1.984	1.106	4.563	6.217	1.897
Sample	M46	M47	M48	M49	M50										
Predicted	768.36	659.99	708.67	51.156	161.08										
Deviation	1.146	3.013	1.868	2.129	3.085										

Suspected samples													
Sample	N1	N2	N3	N4	N5	N6	N7	N8	N9	N10	N11	N12	N13
Predicted Conc.	8.771E3	1.510E4	6.583E3	1.875E4	1.441E3	4.033E3	1.191E3	1.247E3	8.701E3	6.510E3	1.439E3	3.990E3	2.165E3
Deviation	20.204	31.558	27.408	38.761	26.449	22.943	26.196	21.581	21.445	23.747	21.433	26.595	10.166
Sample	N14	N15	N16	N17	N18	N19	N20						
Predicted Conc.	3.970E3	1.702E3	5.281E3	7.972E3	6.173E3	1.359E3	3.701E3						
Deviation	28.568	20.36	25.984	26.858	28.145	21.007	38.191						

Table7.3: The predicted concentrations in ppb for samples excited at 785 nm using MLR model

Unsuspected samples													
Sample	M1	M2	M3	M4	M5	M6	M7	M8	M9	M10	M11	M12	M13
Predicted Conc.	728.223	758.326	877.206	181.88	206.586	971.354	110.755	961.08	94.039	617.348	451.318	568.363	666.804
Deviation	11.31	5.446	11.503	12.614	19.996	29.508	12.826	28.085	29.747	11.876	13.838	12.546	38.214
Sample	M14	M15	M16	M17	M18	M19	M20	M21	M22	M23	M24	M25	M26
Predicted Conc.	680.84	591.919	380.922	156.102	196.466	654.173	677.954	781.163	273.161	295.738	198.959	215.738	109.424
Deviation	13.402	37.071	14.984	15.053	45.439	22.568	11.477	23.252	26.196	21.581	19.858	26.017	16.113
Sample	M27	M28	M29	M30	M31	M32	M33	M34	M35	M36	M37	M38	M39
Predicted Conc.	405.668	373.161	308.922	307.945	798.959	915.738	709.424	905.668	873.161	808.922	807.945	851.307	464.123
Deviation	20.11	23.604	27.154	25.241	19.858	23.252	26.196	21.581	19.858	26.017	22.568	21.407	28.292
Sample	M40	M41	M42	M43	M44	M45	M46	M47	M48	M49	M50		
Predicted Conc.	881.357	454.173	577.954	281.163	198.959	615.738	498.959	815.738	809.424	795.668	731.161		
Deviation	11.477	23.252	26.196	41.581	19.858	26.017	16.113	20.11	23.604	37.154	35.241		

Suspected samples										
Sample	N1	N2	N3	N4	N5	N6	N7	N8	N9	N10
Predicted Conc.	1.842E4	1.35E3	3.70E3	3.97E3	1.70E3	560.591	641.838	711.549	1.10E3	1.18E3
Deviation	100.872	82.365	85.225	83.568	109.36	99.672	44.55	52.843	106.129	101.984
Sample	N11	N12	N13	N14	N15	N16	N17	N18	N19	N20
Predicted Conc.	717.44	838.01	650.722	803.184	768.362	659.998	708.673	982.533	985.716	1992.912
Deviation	85.106	54.563	46.217	57.897	59.146	42.485	35.82	40.533	55.716	92.912

Appendix V

Spectrophotometer system

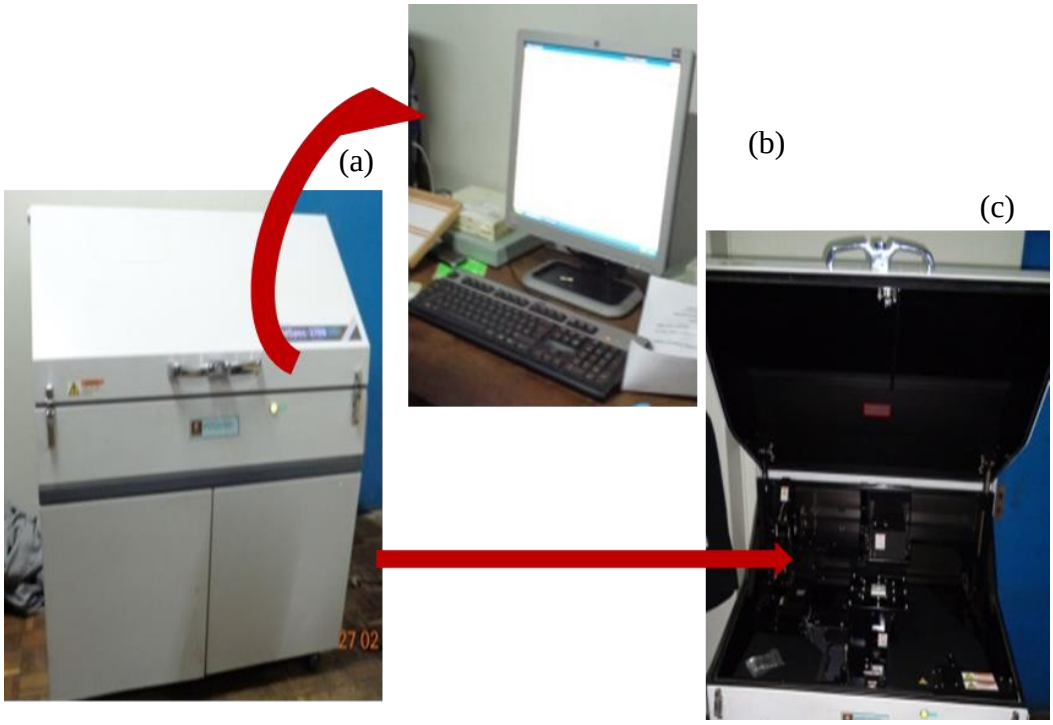

Figure 7.7: A picture image of spectrophotometer used to obtain fluorescence spectra of AFB1 (a). The computer is also attached to aid in data acquisition (b). Image c shows the optical part of the spnectrometer